This is to certify that the
dissertation entitled

The Frequency of Carbon-Enhanced Metal-Poor Stars and the
Origin of Carbon in the Universe

presented by

Brian Elliott Marsteller

has been accepted towards fulfillment
of the requirements for the

___Ph.D.___ degree in ___Physics and Astronomy___

_____
Major Professor's Signature

___7 / 3 1 / 0 7___
Date

PLACE IN RETURN BOX to remove this checkout from your record.
TO AVOID FINES return on or before date due.
MAY BE RECALLED with earlier due date if requested.

DATE DUE	DATE DUE	DATE DUE

THE FREQUENCY OF CARBON-ENHANCED METAL-POOR STARS AND THE ORIGIN OF CARBON IN THE UNIVERSE

By

Brian Elliott Marsteller

A DISSERTATION

Submitted to
Michigan State University
in partial fulfillment of the requirements
for the degree of

DOCTOR OF PHILOSOPHY

Department of Physics and Astronomy

2007

ABSTRACT

THE FREQUENCY OF CARBON-ENHANCED METAL-POOR STARS AND THE ORIGIN OF CARBON IN THE UNIVERSE

By

Brian Elliott Marsteller

In recent large surveys of metal-poor stars, such as the HK survey (Beers et al., 1985, 1992), the Hamburg/ESO survey (HES, Christlieb et al., 2001), and recently the stellar component of the Sloan Digital Sky Survey (SDSS, Stoughton et al., 2002), a curiously large fraction of stars which show enhanced carbon abundances have been observed. In fact, this fraction seems to increase as metallicity decreases. Since these stars, the Carbon-Enhanced Metal-Poor (CEMP) stars, then play a significant role in the formation and evolution of the earliest stellar generations, and thus all following generations, it is of vital importance to fully understand their true fraction, so that they can be properly understood, and properly accounted for in models of galactic and nucleosynthetic evolution.

In order to obtain this quantity, the frequency of carbon enhancement as a function of metallicity, a large quantity of metal-poor stars need to be analyzed to determine these important abundances. For this to occur from these large, pre-existing databases of low to medium resolution spectroscopy, an accurate method of quickly determining the metallicity and carbon abundance for a star is needed. Due to the limited data currently available in some of these extreme regions of parameter space, currently existing methods which rely on calibration samples do not prove sufficient. Thus, a new method, based solely on the physical properties of the stars and the information contained in their spectra, which is both relatively fast and accurate is needed.

Here we outline the development of such a technique which generates synthetic

spectra using the line index code MOOG, and automatically determines the required abundances. After verifying the validity of this technique using several samples, abundances are then determined for a large, unbiased sample of stars taken from SDSS.

From these abundances, the frequency of carbon enhancement is derived. Although a true frequency cannot be determined due to incompleteness stemming from the indetectability of carbon features in some of our stars, we are able to see a relatively low fraction of CEMP stars at higher metallicities, rising to much higher fractions at lower metallicities. Utilizing several statistical techniques to recover information from our incompleteness, we see that the fraction seems to get quite large at even moderately low metallicity, emphasizing the importance of these stars in chemically primitive environments.

We also see changes in these fractions brought about by the evolutionary state of the sample and their relative positions in the galaxy, corresponding to inclusion in different stellar populations. This latter fact has been noticed before (Frebel et al., 2006), and also agrees well with some current theories (Tumlinson, 2007).

With a more complete understanding of the relative fractions of stars which show enhancements in their carbon abundances over the span of galactic history, we can start to get a better understanding of the relative importance and efficiency of different mechanisms at given metallicities, in particular the nature of nucleosynthesis at the earliest times.

Dedicated to John and Terry,

without whom none of this would be possible

ACKNOWLEDGMENTS

First and foremost, I must acknowledge my advisor, Timothy Beers, whose enthusiasm for metal-poor stars made every project more interesting and exciting. Thanks to him, I was also able to travel the world – observing, attending conferences and meeting with a wide variety of Astronomers with similar interests in related fields. These activities would often renew my own excitement for my work, as I saw how much they were eagerly anticipated by our collaborators. Finally, I must thank Tim for, whether he was actually aware of it at the time, buying most of the alcohol consumed by numerous people at these conferences. I'm sure the bonds formed after four or five bottles of wine at a castle in Germany are sufficient to charge those to the grant.

I would also like to thank most wholeheartedly all of my fellow graduate students (and a couple of undergrads) – both those who came and went, and those who are still around – for occasionally entertaining me, and for helping me maintain some level of sanity. The days of board games, the nights of video games, and all the other activities made my time here that much easier. All the money I won in poker doesn't hurt either.

Individually, I would like to thank Chris "Topher" Waters for his considerable patience in answering my near infinite questions. I am a much more capable scientist today because of him, although he should still expect regular instant messages in the near future. Someday I'll be able to do statistics, I promise. I also would like to thank Chris for putting together the LaTeX class file used in the construction of this thesis.

I would also like to thank Aaron "Cluze" LaCluyzé and for his years of friendship. We had a lot of good meals, and even more good times. He did a lot to make graduate school much more bearable. I know I can count on him for anything should our paths

ever cross again. He also set an example which continues to inspire me.

In addition, I would like to thank Young Sun Lee for his continuing friendship and our many useful conversations. Whether it was trying to figure out exactly how to do something we needed to get done, or sharing a room at a conference, I always knew that we could count on each other. I'm sure we're both happy to get single rooms for a change, but I know we'll miss those trips.

Thanks to my family, especially my parents, for providing me with the skills I need to do my job, and being supportive of my lifelong education. I realize how lucky I am to have made it this far, and know that it wouldn't have been possible without them.

I would like to especially express my gratitude to a couple of very special people (who know who they are) for being in my life. They let me be who I am, and as a consequence, helped me find out who I am. They also helped me to figure out what it is that I want to do with all of this, which has made thoughts of the future much less frightening. Also, while my parents can be held responsible for getting me to graduate school, these individuals are in many ways responsible for me finishing, and for that I cannot begin to express my thanks. They truly are my inspiration.

TABLE OF CONTENTS

LIST OF TABLES

LIST OF FIGURES

CHAPTER 1:
INTRODUCTION

Humankind is fascinated by origins. People want to know where something came from, be it something as simple as how Spiderman got his powers or as profound as where humankind itself came from. There's a reason why the childhood homes of famous individuals, such as Abraham Lincoln, are historical monuments, and why dinosaurs are such a popular subject for kids. People want to see where these things came from so they can understand why they are what they are.

This is perhaps even more true in science, where investigation into the origin of things is common practice. In fact, all of science is really an investigation of the origin of some phenomenon. Often, this takes the form of an exploration of how something has changed over time, or a detailed analysis of what that thing is now. But all of these investigations are really just steps in exploring the ultimate origin of everything.

In astronomy, in particular, this is clearly the case. All research being carried out today is looking for the origin of something. Some areas are less overt, with the exploration of specific phenomena like the nature of variable stars or the morphology of galaxies. Others are more direct in their offerings, such as the study of cosmology and its exploration of the origin of the universe or the searches for extra-solar planets and its ultimate goal of understanding the origin of life on Earth.

In recent decades, the search for the earliest generations of stars, in an attempt to understand the origin of these fundamental cosmic ingredients, has yielded immense samples of stars more metal-poor than was thought possible to exist before the surveys

began. These samples have greatly changed our understanding of the early universe, and sparked many questions about the phenomena responsible for their creation.

Among these samples, new classes of stars have been discovered, and new understandings of old classes have been reached. In many cases, the significance of a class has been revealed in a new light, requiring further explorations. One such class, which we have studied in greater detail, are the very metal-poor stars which show enhanced carbon abundances.

Stars are generally referenced by their metal-content, often through the presence of iron through the quantity [Fe/H], defined as:

$$\left[\frac{\text{Fe}}{\text{H}} \right] \equiv \log_{10} \left(\frac{N_{\text{Fe}}}{N_{\text{H}}} \right) - \log_{10} \left(\frac{N_{\text{Fe}}}{N_{\text{H}}} \right)_{\odot} \qquad (1.1)$$

As the production of iron through time increases this quantity, the metallicity of a star is a rough estimate for the age of the star, and metal-poor stars are generally older stars.

In large surveys of metal-poor stars, such as the HK survey (Beers et al., 1985, 1992), the Hamburg/ESO survey (HES, Christlieb et al., 2001), and recently the stellar component of the Sloan Digital Sky Survey (SDSS, Stoughton et al., 2002), a surprisingly large fraction of stars show enhancements in their carbon abundances. Although stars with enhanced carbon abundances have been seen at all metallicities, they represent only a small fraction of stars at higher metallicities, and thus are not seen as anything more than an interesting subset. However, at the fractions seen at the lowest metallicities, reaching maybe 25% by [Fe/H] $\leq$ −2.5 (Marsteller et al., 2005), these stars fill an apparently significant role, and must be fully understood and accounted for in any studies of the Galaxy at these epochs.

In the following pages, an attempt will be made to better understand the origin of these stars through the exploration of their changing frequency at different metallicities as well as the changing fractions of individual subclasses contained within the

larger class.

To do this, we will first outline the basic processes involved in stellar nucleosynthesis and the production and destruction of elements in Chapter 2. This chapter will also cover other general astrophysical information which may be important to the formation of carbon-enhanced stars. A description of the carbon-enhanced stars themselves, as well as their major subclasses, are discussed in Chapter 3. In addition, a description of possible origin scenarios for the different subclasses are outlined.

In order to perform our analysis, a new technique to quickly and accurately determine abundances from low resolution spectra was developed. Based on currently existing methods and procedures, but written to automatically determine objective metallicities and abundances, autoMOOG fits individual spectra with customized synthetic spectra. The reasons for using this technique, and a more complete description of the technique itself, are outlined in Chapter 4. In §4.5, a detailed error analysis of this routine is performed.

Using several samples of stars which have existing low resolution and high resolution spectra, and therefore abundances, we are able to validate our abundance results in Chapter 5. Our low resolution abundances are also compared against the low resolution abundances determined using the line index method of Beers et al. (1999), as these methods have similar procedures but differing techniques. In addition, this comparison is being used to find problem spots in the calibration space of the line index method. Once these areas have been located, and the difficulties understood, the line index method can be recalibrated, improving its future performance.

Due to the occasional undetectability of carbon features in the spectra of our stars, the abundances of some stars in our sample were not determined. The nature of this incompleteness, and its ultimate effect on our results of the carbon enhanced frequency are discussed in §5.3.

A large, unbiased sample of stars obtained as part of the SDSS calibration efforts

are then used to determine the frequency of carbon-enhancement as a function of metallicity. This frequency is discussed fully in Chapter 6, as well as additional comments on the limitations of the results due to our incompleteness. Attempts to recover information from out of the incompleteness are performed in §6.2, and the recovered fractions and a discussion of the results in §6.3.

Finally, a full discussion of the meaning of all of our results in the context of the origin of carbon-enhanced stars will be given in Chapter 7. In addition, a description of future work that remains to be done in this study will be given, as well as what attempts are currently underway by myself and others in the field.

CHAPTER 2:
BACKGROUND

2.1 BIG BANG NUCLEOSYNTHESIS

A few minutes after the cosmic explosion known as the Big Bang, the universe had cooled to the point where protons and neutrons could exist, and could come together to make the first nuclei. Four protons came together, some becoming neutrons in the process, to form the first helium nuclei ($\sim 25\%$ by mass). Similarly, a trace amount of lithium was produced. The rest stayed as protons (or hydrogen, $\sim 75\%$ by mass). The universe then cooled too quickly for heavier elements to be produced. There was insufficient time for carbon to be produced through the triple-α process. The only limiting factor to the production of heavy elements was the short timescale of conditions hot enough to form heavier elements. All other elements in the universe had to wait to be produced in stars.

2.2 STELLAR NUCLEOSYNTHESIS

Any element that exists in the universe today that was not created shortly after the Big Bang was produced with the help of stars. Most of these elements were created in the interiors of stars over their lifetimes, and the rest were created during events related to their deaths.

Elements are created in the interiors of stars through fusion, which combines two light nuclei into a heavier nucleus. Due to the nature of the Coulomb barrier in atomic
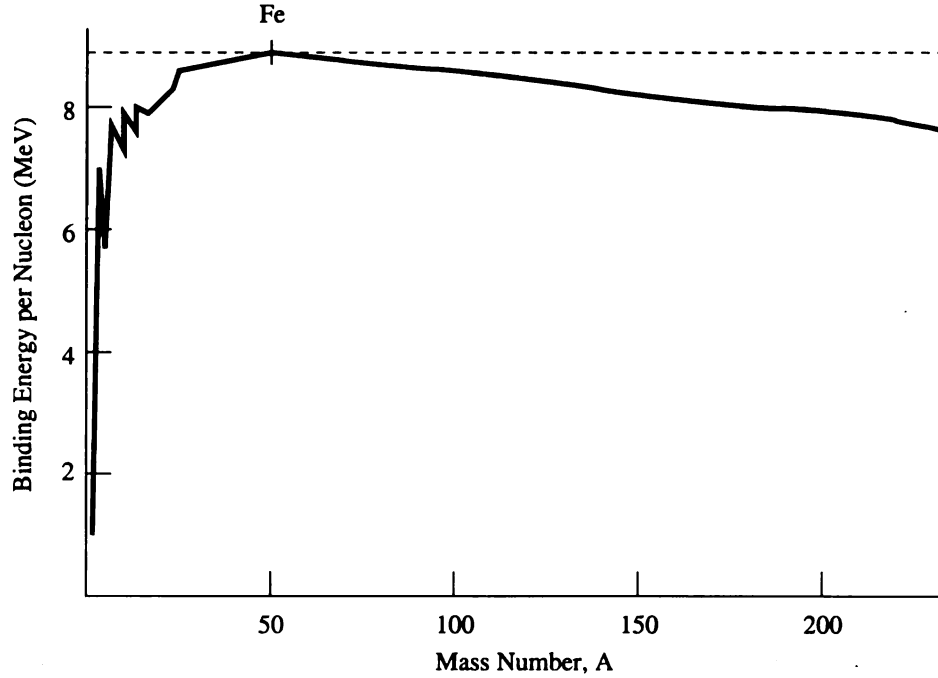
Figure 2.1 Binding energy per nucleon as a function of mass number.

nuclei (Figure 2.1), energy can only be gained through fusion for elements below iron. Massive stars (M $\gtrsim$ 10 M$_\odot$) are able to go through multiple stages of nuclear burning through fusion until iron is produced. Once iron is created, it cannot be burned, and the star quickly becomes unstable, ending its life as a supernova (Type II). Less massive stars never get hot enough to fuse heavier elements, and end their lives in a less explosive way, releasing their outer atmospheres and becoming a white dwarf.

Different mass stars produce a different yield of elemental abundances. Over the course of their lives, and especially at the end of it, they release these elements into the universe, to be the material out of which new generations of stars form. By studying the pattern of these elements, it is possible to reconstruct the nucleosynthetic origin of elements observed in the atmospheres of stars. In the following descriptions, emphasis will be placed on the nucleosynthetic products formed during the evolution of low and intermediate mass (0.8 - 8 M$_\odot$) stars. The evolution of high mass stars is more uncertain, but more importantly, is not as significant to the understanding of

6

Table 2.1. Nomenclature for stars of different metallicity, adopted from Beers & Christlieb (2005).

[Fe/H]	Term	Acronym
> +0.5	Super metal-rich	SMR
~ 0.0	Solar	–
< −1.0	Metal-poor	MP
< −2.0	Very metal-poor	VMP
< −3.0	Extremely metal-poor	EMP
< −4.0	Ultra metal-poor	UMP
< −5.0	Hyper metal-poor	HMP
< −6.0	Mega metal-poor	MMP
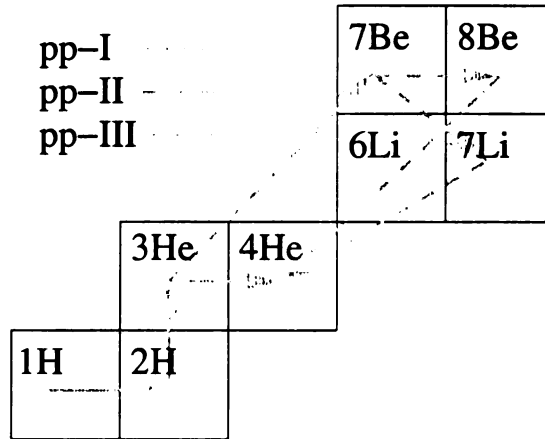
Figure 2.2 The path of the pp-chain in a chart of nuclides

the development of carbon and the presence of carbon-enhanced stars. Lower mass stars will not be followed, as their near infinite lifetimes mean they have little impact on nucleosynthetic history. Where appropriate, additional comments will be made to indicate processes in these stars which may be significant. To simplify the discussion of stars with a variety of metallicities, we adopt the classification scheme of Beers & Christlieb (2005).

Explosion
r-process

Log (Temperature, K)

10

9

8

7

s-process

He-burning

Core contraction

H-burning

9   6   3   0

Log (Time, years)
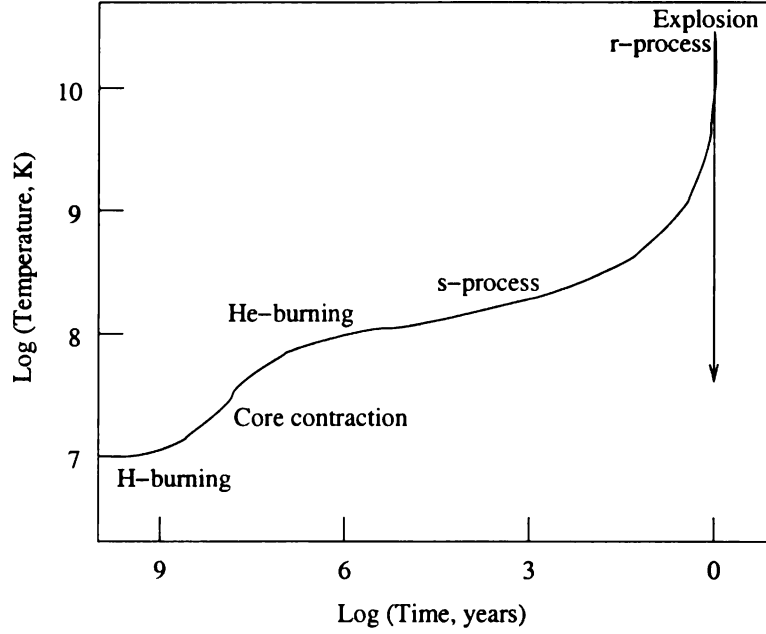
Figure 2.3 Timescales for important processes in the life of a star. After Burbidge et al. (1957)

2.2.1 HYDROGEN TO HELIUM

Throughout their lives, stars are composed mostly of hydrogen. Without nuclear burning to provide the energy for radiative support, stars would collapse due to gravity. In fact, stars are born through the gravitational collapse of a hydrogen cloud. It is only when the contraction of the gas has created sufficient temperatures at the core of the star to begin the fusion of hydrogen into helium that hydrostatic equilibrium is reached between gravity and radiation pressure, and the star becomes stable.

The cores of low mass (M $\lesssim$ 3.0 M$_\odot$) stars are cooler than more massive stars. As a result, low mass stars burn hydrogen through a different process than high mass stars. These stars turn hydrogen into helium through a process called the proton-proton (PP) chain, which depends only weakly on temperature ($\epsilon \propto T^4$, where ϵ is the energy generation rate). The PP chain is referred to as such because it requires only protons to proceed, as it combines them together to ultimately form helium.

8
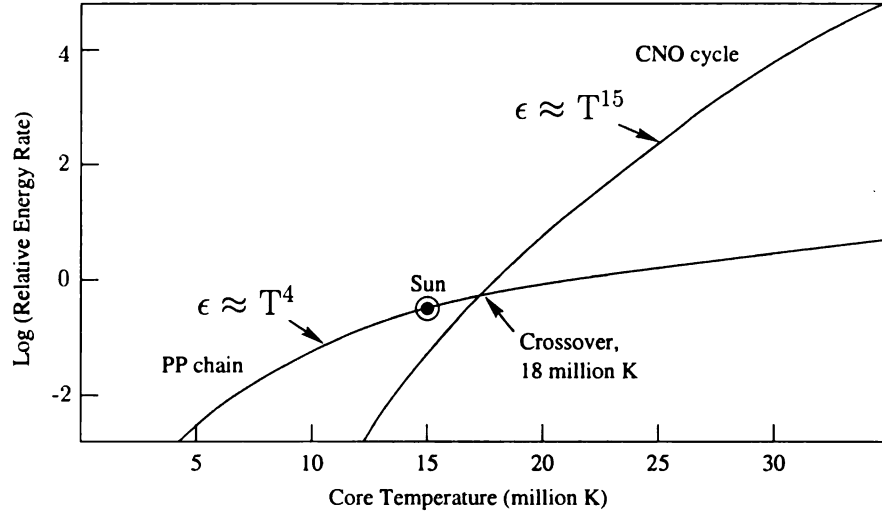
Figure 2.4 Energy production rates for the pp chain and the CNO cycle as a function of temperature. Each mechanism dominates in the region where its energy production rate is higher.

There are three paths to the PP chain, the PP-I chain, PP-II chain, and PP-III chain, whose paths are shown in Figure 2.2. Each subsequent chain in the series becomes less likely, with the PP-I chain dominating with a branching ratio of 69%, and nearly all the remaining 31% going to the PP-II chain. The first step in the process, which requires the conversion of a proton into a neutron through the weak force, is the slowest step in the process, and is responsible for the length of the hydrogen burning stages of stellar evolution, in particular the main sequence lifetime (Figure 2.3), and thus the longevity of stars.

The cores of massive stars are much warmer, and a different process, the carbon-nitrogen-oxygen (CNO) cycle, is responsible for the conversion of hydrogen into helium. The CNO cycle is very temperature sensitive ($\epsilon \propto T^{15}$), and it dominates the much warmer cores of massive stars. The relative importance of these two mechanisms as a function of temperature can be seen in Figure 2.4.

As its name might suggest, the CNO cycle cycles through carbon, nitrogen and oxygen, using them as catalysts, to convert four protons into one helium nucleus. The path of the CNO cycle can be seen in Figure 2.5. The cycle is generally viewed to

9
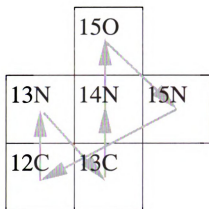
Figure 2.5 The path of the CNO cycle in the chart of nuclides. The path begins at ^{12}C.

start and stop at ^{12}C. Obviously, the presence of carbon is required for the activation of the CNO cycle.

Written out, the CNO cycle consists of the reactions:

$$
\begin{aligned}
^{12}\text{C} + {}^{1}\text{H} &\rightarrow {}^{13}\text{N} + \gamma \\
^{13}\text{N} &\rightarrow {}^{13}\text{C} + e^{+} + \nu_e \\
^{13}\text{C} + {}^{1}\text{H} &\rightarrow {}^{14}\text{N} + \gamma \\
^{14}\text{N} + {}^{1}\text{H} &\rightarrow {}^{15}\text{O} + \gamma \\
^{15}\text{O} &\rightarrow {}^{15}\text{N} + e^{+} + \nu_e \\
^{15}\text{N} + {}^{1}\text{H} &\rightarrow {}^{12}\text{C} + {}^{4}\text{He}
\end{aligned}
\tag{2.1}
$$
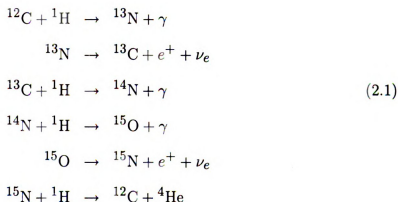
The bottleneck in this procedure, and thus the reaction which sets the lifetime of these stars, is the proton capture on ^{14}N. Since carbon, nitrogen and oxygen are catalysts in this process, the total number of these nuclei cannot change. However, their relative proportions can, and when the cycle is run to equilibrium, ^{14}N becomes the most numerous nucleus, and the ^{12}C/^{13}C ratio approaches 3.5. In fact, wherever hydrogen has been converted almost completely into helium, oxygen has been converted almost

completely into ^{14}N. Similarly, nearly all of the ^{12}C in the inner half of the star's mass has been converted into ^{14}N (Iben, 1967).

As hydrogen is depleted, the core must slowly contract to maintain hydrostatic equilibrium. This results in a gradual increase in luminosity over the duration of the main sequence. Once the core hydrogen has been converted into helium, core burning ceases. With the absense of radiation pressure to hold it back, gravitational collapse begins again, compressing the stellar core and increasing the temperature and density. At the same time, the convective envelope of the star deepens during a process called first dredge-up. First dredge-up results in a dilution of surface abundances, as many elements present on its surface are mixed down into the interior, while hydrogen and helium are brought to the surface. Also brought to the surface are the products of CNO equilibrium, so the ^{12}C/^{13}C and ^{12}C/^{14}N ratios will be lower for these stars than when they were on the main sequence. In fact, all such convective mixing episodes are responsible for bringing the products of nucleosynthesis to the surface, where they can be observed, or ejected into space by stellar winds (Herwig, 2005).

Eventually, the temperature has increased to the point where a shell of hydrogen just outside the helium core is able to ignite and hydrogen burning resumes. As this shell burns outwards, the star's luminosity increases and the star expands. By expanding, the outer envelope cools, and the star climbs the red giant branch (RGB). This is known as first ascent. During shell burning, the rate of nuclear energy production decreases with time as the hydrogen is used up. This causes continued contraction to maintain the temperatures necessary for hydrogen burning (Iben, 1967).

As the star ascends the RGB, convection reaches nearly to the hydrogen burning shell. As most of the ^{12}C has been converted into ^{14}N in this region, convection mixes the ^{14}N upward as it brings new ^{12}C down from the envelope. This process continues as the convective envelope grows, further lowering the surface ^{12}C/^{14}N.

If the convective envelope penetrates the burning hydrogen shell, it is able to mix

fresh hydrogen fuel from the outer layers of the star, making this hydrogen burning much more efficient. This process, known as Hot Bottom Burning (HBB; e.g. Scalo et al. (1975); McSaveney et al. (2007)), results in a higher temperature at the base of the convective envelope and a higher stellar luminosity. Also, through CN processing, HBB transforms dredged-up carbon into nitrogen.

Eventually, core temperatures become sufficient to begin the reactions:

$$
\begin{aligned}
^{14}\text{N} + \alpha &\rightarrow {}^{18}\text{F} + \gamma \\
^{18}\text{F} &\rightarrow {}^{18}\text{O} + \beta^+ + \nu_e
\end{aligned}
\tag{2.2}
$$
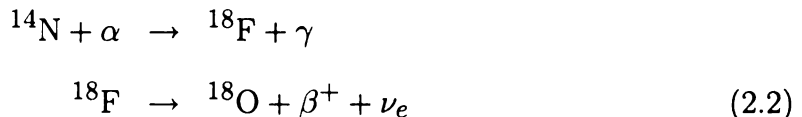
Within a small convective zone, ^{14}N is converted into ^{18}O. Thus, near the stellar center, almost all of the original ^{12}C, ^{14}N, and ^{16}O is converted into ^{18}O by the time the star reaches the tip of the RGB. This extra burning extends the RGB lifetime of the star (Iben, 1967).

2.2.2 HELIUM TO CARBON: THE TRIPLE-α PROCESS

The energy produced during hydrogen shell burning is insufficient for supporting the star against gravitational collapse. The core continues to contract, increasing its temperature, until eventually helium burning ignites in the core. For massive stars (M > 3 $M_\odot$), helium burning gradually turns on, while in low mass (M < 3 $M_\odot$) stars this occurs explosively and suddenly in a process known as helium flash.

Helium burning proceeds through a process known as the triple-α process, which converts three helium nuclei (α particles) into one carbon nucleus. The odds of three α's coming together at the same time is fairly remote, so in practice the mechanism proceeds through two steps, successive α-captures on a seed α particle, through the

reactions:

$$\alpha + \alpha \ \rightarrow \ {}^{8}\text{Be}$$
$${}^{8}\text{Be} + \alpha \ \rightarrow \ {}^{12}\text{C} + \gamma \qquad (2.3)$$

However, ^{8}Be is highly unstable, and will decay in 2.6 x 10^{-16} seconds without the third α. Therefore, the triple-α process only proceeds under conditions of high helium density. Under the right conditions, α-captures will not stop at carbon, and successive α-captures will produce the so-called α-elements – oxygen, neon, magnesium, silicon, sulfur, argon, and calcium. This can occur any time carbon and helium are present together. At the very least, an extra α-capture is likely to happen from time to time, resulting in a carbon-oxygen core, as opposed to a purely carbon core. Helium will also react with the ^{18}O in the core to form ^{22}Ne (Iben, 1967).

As the available helium in the core is depleted, central densities begin to drop and core helium burning ceases, causing the core to contract again. The star moves off of the horizontal branch and second dredge-up further increases the size of the convective zone, which had been reduced in size during core helium burning. Mixing then enriches the helium content of the entire convective envelope. The contracting core heats the stellar interior, eventually igniting a shell of helium just outside the core, and ultimately a shell of hydrogen just outside the helium shell. The star expands again, rising up the Asymptotic Giant Branch (AGB), increasing its luminosity. The convective shell continues to grow inward until it almost reaches the burning helium shell.

Helium burning within a thin shell is thermally unstable. Energy produced in the shell is trapped there, raising the temperature and thus increasing the rate of energy production in a process known as thermal runaway. This continues until enough energy has been stored to lift of the surrounding material, whose mass is

large compared to the shell, and allow the expanding shell to cool. Eventually, the matter above the shell falls back, compressing the shell until the process begins again. The time between pulses is ~10000 years, and the amplitude of each pulse is larger than the one before (Iben, 1967). During this time, the star becomes a thermally-pulsing asymptotic giant branch (TP-AGB) star.

A period of convective mixing is induced by each pulse, and the set of these convective periods are collectively known as third dredge-up. Third dredge-up brings primary nucleosynthesis products from combined H-shell and He-shell burning to the surface. In particular, these products include carbon, the slow neutron-capture process (s-process) elements, and helium. In extremely low metallicity stars, this convective envelope is deeper, resulting in surface enhancements of other elements, such as oxygen or neutron heavy species like sodium or magnesium.

Due to the thermal pulses and recurrent flash-burning events in the helium shell, AGB stars are able to provide a location for many key nucleosynthetic processes. This is due to their ability to expose nuclei to various episodes of hydrogen and helium burning. The abundances produced depend largely on metallicity and stellar mass.

The abundances of C and N produced by a single AGB star are inversely proportional, with either high carbon or nitrogen abundances, but never both. Stars which are enhanced in both elements are likely not produced by a single AGB. The mass of the star determines the appearance of HBB, which then determines whether carbon or nitrogen is enhanced. At [Fe/H] = −2.3, stars more massive than 3.5 $M_\odot$ have an efficient HBB that turns almost all dredged-up carbon and oxygen into nitrogen. Below this mass, this situation reverses (Herwig, 2005).

For all the nucleosynthesis that takes place within an AGB star, without the added features of large convective zones leading to high mass-loss rates, AGB stars would not be nearly as significant. Without the ability to pollute the ISM with the products of their nucleosynthesis, it wouldn't matter what AGB stars were capable of producing.

Table 2.2. Mass Loss Rates at various evolutions for a 1 $M_\odot$ star. Values taken from Lau et al. (2007).

	MS	RGB	AGB	AGB w/pulsations
Mass Loss Rate	10^{-17} $M_\odot$/yr	10^{-7} $M_\odot$/yr	10^{-6} $M_\odot$/yr	10^{-4} $M_\odot$/yr

And mass loss from an AGB star, especially during these thermal pulsations, is quite high, as seen in comparison with previous evolutionary stages in Table 2.2.

For low-mass stars, this is the beginning of the end. Never to reach the temperatures required to ignite their carbon cores, the continuing thermal pulses will eventually separate the outer layers from the carbon-oxygen core. This expanding gas will then cool, forming dust grains, which are propelled further outward by the radiation pressure from the hot core that is left behind. The core, fully exposed, emits ultraviolet radiation which ionizes the ejected gases, forming a planetary nebula. The core continues to collapse, eventually becoming electron degenerate, a white dwarf.

2.2.3 CARBON TO IRON

Although in general we are not discussing the evolution of massive stars, a brief description of carbon burning will be given due to its relevance to this overall discussion.

Massive stars are eventually able to contract their cores until they reach a temperature sufficient to ignite carbon burning. Carbon burning generally occurs by the following processes:

$$^{12}\text{C} + {}^{12}\text{C} \rightarrow \begin{cases} ^{16}\text{O} + {}^4\text{He} + {}^4\text{He} \\ ^{20}\text{Ne} + {}^4\text{He} \\ ^{23}\text{Na} + \text{p} \\ ^{23}\text{Mg} + \text{n} \\ ^{24}\text{Mg} + \gamma \end{cases} \tag{2.4}$$
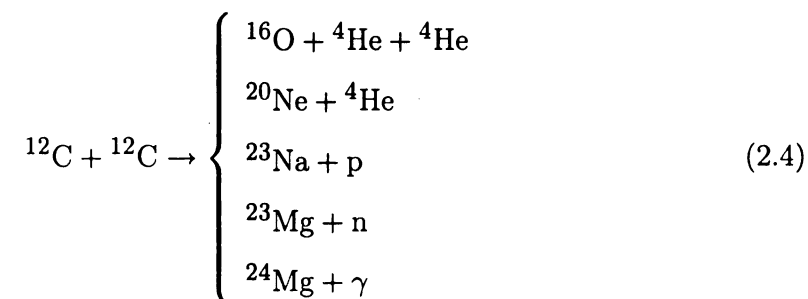
The path of carbon burning generally depends on the exact conditions at the core of a massive star and so the final products, as well as the particles freed in the process, are also determined by this factor.

2.3 BEYOND IRON: NEUTRON-CAPTURE NUCLEOSYNTHESIS

The nucleosynthetic processes that have so far been discussed have involved taking the very light elements produced during the Big Bang and fusing them together to form elements up to iron. This produces energy, and is the mechanism which powers stars and keeps them from gravitationally collapsing.

However, as can be seen in a plot of binding energy (Figure 2.1), fusion stops producing energy above iron. Instead, fission is energetically favorable for elements more massive than iron. That said, with a neutron source, these elements can still be produced.

There are two main processes that are responsible for the production of nearly all isotopes with $A \gtrsim 60$: the slow neutron capture process (s-process) and the rapid neutron capture process (r-process). As their names would suggest, the biggest difference between these two processes is an issue of time, specifically the relative lifetimes for neutron captures (τ_n) and β decays (τ_β).

Under conditions where $\tau_n > \tau_\beta$, only one or two neutron captures will occur before a β decay, so the path of neutron captures will be along the valley of β-stability, named because the isotopes in the valley are stable against β-decay, while those to either side are susceptible to β-decay. The neutron-rich side of the valley is the path of the s-process, as seen in Figure 2.6. The isotopes produced in the s-process, lying along the valley of β-stability, are generally more stable than those produced in the r-process.
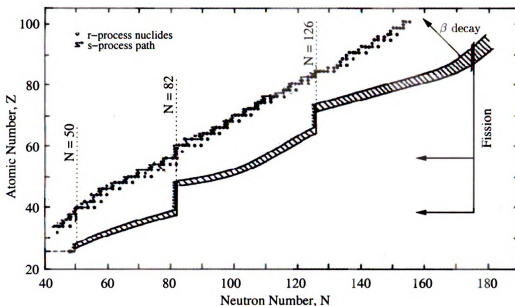
Figure 2.6 The path of the s-process and r-process in comparison with the valley of
β stability. Note also the influence of magic numbers on the patterns, especially for
the r-process. After Seeger et al. (1965).

On the other hand, if $\tau_n < \tau_\beta$, many neutron captures will occur before a single β
decay, so the path of neutron captures will occur near the neutron-drip line, far from
the valley of β-stability (see Figure 2.6). Once the source of neutrons has disappeared,
a large number of unstable nuclei have been produced, and they quickly begin to β-
decay towards the vally of β-stability. The resulting isotopes are the products of the
r-process.

Since the final elements produced by the r-process also lie along the valley of
stability, many elements heavier than iron are produced by both the r- and s-process.
However, the different paths taken result in different relative abundances, as seen by
the patterns of elements in Figure 2.7. The reason for this difference in patterns, in
particular the shift in the peaks of elements, has to do with the stability of nuclei
with so-called magic numbers.

Magic numbers are a number of nucleons, either protons or neutrons, such that
they are arranged into complete shells within the atomic nucleus. The currently
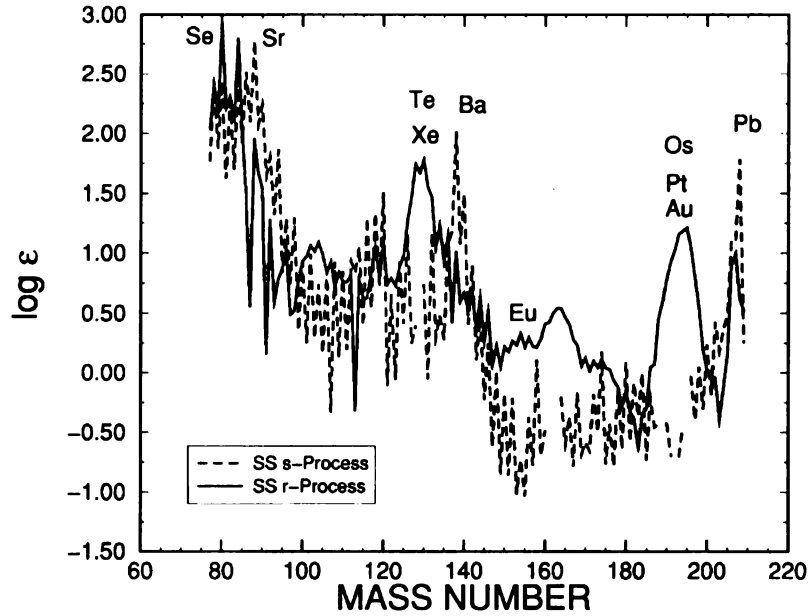
Figure 2.7 The solar r-process and s-process patterns. Figure adopted from Truran et al. (2002).

known magic numbers are 2, 8, 20, 28, 50, 82, and 126. Any nuclei consisting of a magic number of nucleons would have a higher average binding energy per nucleon as compared to those nuclei around them, and hence are less likely to undergo further neutron captures.

Due to the inherent stability of these nuclei, the number of these nuclei increase as the r- or s-process is in equilibrium, and nuclei accumulate in these positions (see Figure 2.6). Once these processes end, the s-process elements, lying already in the valley of stability, remain there, and peaks are seen in elements at or near magic numbers. Thus, elements cluster near the strontium peak, the barium peak, and the lead peak (see Figure 2.7). Indeed, these elements are commonly identified as the main s-process elements for this reason.

On the other hand, the r-process elements finish far from the valley of β-stability in magic numbers, but as they β-decay, they move away from these magic numbers, shifting to lower mass numbers by the time they reach the valley of β-stability. Thus, r-process elements end up at or near the tellurium peak, the europium peak, and the

18
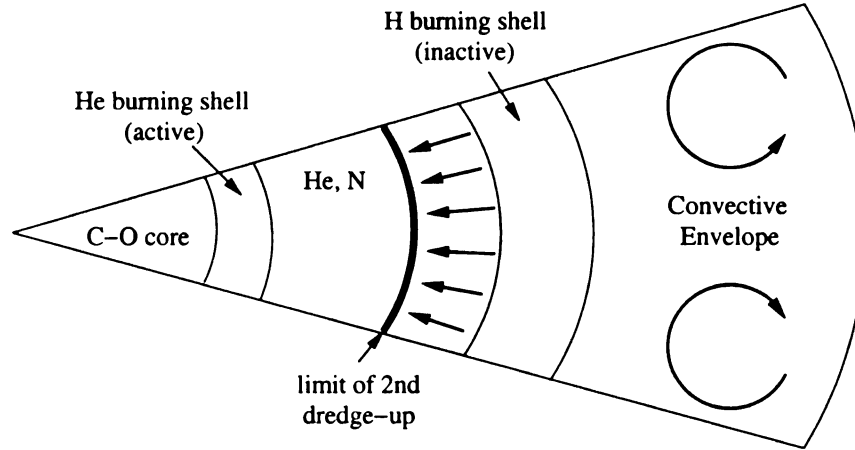
Figure 2.8 A schematic of the likely s-element production site.

osmium peak. Again, these elements are generally identified as proto-typical r-process elements.

While models detailing the paths of these two processes are fairly developed, lacking mainly certain reaction rates, the exact astrophysical site where they occur is less certain, especially for the r-process. The differences in values between τ_n and τ_β, and the resulting differences between the relative elemental abundances seen in the atmospheres of stars, can help determine the individual origins of these elements, which might then help constrain the astrophysical sites responsible for their production. Through various observations and stellar evolution models, certain sites have been suggested, as outlined below.

2.3.1 LIKELY SITES OF THE S-PROCESS

It has been identified that the s-process consists of (at least) a main component and a weak component. The heavier s-process elements ($A \gtrsim 90$) are primarily produced through the main s-process, whereas the weak s-process produces the elements up to $A \sim 90$.

The main s-process occurs in the thermally pulsing helium shells of asymptotic giant branch (TP-AGB) stars of 1-3 $M_\odot$. As schematically shown in Figure 2.8,

these stars consist of a degenerate carbon-oxygen core surrounded by burning shells of helium and hydrogen. Between the burning shells is a thin layer of non-burning helium, also enriched with high levels of ^{14}N from the products of CNO cycling.

During the thermal pulsation phase of the AGB, the partial mixing of protons from the envelope into the carbon-rich layers of the helium burning shell can intiate the production of ^{13}C (Herwig, 2005; Zhang et al., 2006). Such a pocket of ^{13}C in the helium rich shells can then produce the neutron source provided by the reaction:

$$^{13}C + \alpha \rightarrow {}^{16}O + n \tag{2.5}$$

These neutrons can then be captured by iron seed nuclei to initiate the s-process, producing elements up to lead and bismuth. At solar metallicity, lead is primarily produced through the s-process. At lower metallicities, there is some indication that lead may also be produced through the r-process, either directly or through the α-decays of the radioactive r-process elements uranium and thorium (Kratz et al., 2004).

The efficiency of the s-process in these regions may depend on a number of factors, including the size of the ^{13}C pocket and the availability of iron seed nuclei. In fact, at the lowest metallicities, with the limited supply of iron seed nuclei and thus the high neutron-to-iron seed nuclei ratio, it would be expected that an efficient s-process would produce an over-abundance of Pb, creating the so-called Lead Stars, which are in fact seen (Van Eck et al., 2001, 2003). However, the Pb stars are not the lowest metallicity s-process enhanced stars. Cui & Zhang (2006) have found that by varying the mass of the AGB star, they can account for the observed abundance patterns, with the lower mass (1.5 - 2.5 $M_{\odot}$) AGB stars being the source for the Pb stars.

There is also direct evidence for the s-process occuring in intermediate mass AGB stars through the presence of the radioactive element technetium (Tc). Technetium, which is made exclusively through the s-process, has a short enough half-life (2.1 x 10^5 years) that it can only be observed shortly after it is created, and must then be

observed where it was created. Technetium has been observed in the atmospheres of a few intermediate mass TP-AGB stars, which is the strongest direct evidence for the site of the production of any neutron-capture element.

Between thermal pulses, a new period of mixing, third dredge-up, brings the newly created s-process elements, and a good deal of carbon, to the surface of the star. During the AGB, the star will undergo many such thermal pulses followed by convective mixing, the total number dependent on the mass of the star. For stars at lower metallicity, the convective envelope is deeper, so third dredge-up also brings oxygen and more neutron-heavy species such as sodium and magnesium (Herwig, 2005). Strong winds from the stellar surface are also present at this time, sending material rich in these dredged-up elements into the ISM.

Since this process occurs in the later stages of evolution of low mass stars, which have lifetimes on the order of 10^9 years, it is also not expected that this process played a large roll in the oldest or most metal-poor stars, and in fact s-process enhancements in stars are not seen much below $[Fe/H] \sim -2.5$. The star with the lowest metallicity which still shows s-process enhancement is CS 22183-015 which has $[Fe/H] = -3.1$. The long life of these stars, and the lack of available iron seed nuclei both point to a more recent production mechanism. However, the nature of the s-process at low metallicities is still highly uncertain. The requirement for iron seed nuclei is not even assured.

In addition, at the lowest metallicities, the limited supply of elements from neon to calcium would have reduced the efficiency of the s-process, as these elements would have been competed for by a number of processes. This could also contribute to the decline of s-process elements in low metallicities stars.

The weak component of the s-process, on the other hand, occurs in an earlier stage of stellar evolution, during core helium burning, but only in more massive ($M \gtrsim 10$ $M_\odot$) stars. In this environment, temperatures are sufficiently high to facilitate addi-

tional α-captures on the carbon produced in the triple-α process, until the eventual α-capture on neon:

$$^{22}\text{Ne} + \alpha \rightarrow {}^{25}\text{Mg} + n \qquad (2.6)$$

which is the primary neutron source for the weak s-process.

Since this process occurs in an earlier stage of evolution, and in more massive stars which have shorter overall lifetimes, it is possible for the weak s-process to occur at much lower metallicities than the main s-component. In fact, one of the HMP stars shows evidence for strontium, primarily created by the weak s-process, but no evidence of barium, a product of the main s-process (Lau et al., 2007). This could indicate production via the weak s-process, or even the r-process. Either way, as we shall see, this indicates production within a massive star, consistent with the current understanding of the top-heavy IMF of the earliest stellar generations.

Stars which are enhanced in their s-process elements tend to have produced the s-elements in a way that matches a scaled solar s-process abundance pattern. This suggests that the s-process mechanism is metallicity independent, at least for those metallicities where it is possible. The absolute abundances likely vary with metallicity, due largely to the availability of iron seed nuclei, but the relative production of various elements is the same. This makes the ultimate analysis of the s-process and those stars enriched in its products much easier.

2.3.2 POSSIBLE SITES FOR THE R-PROCESS

Like the s-process, the r-process is expected to have a strong and weak component, with the strong component likely being responsible for the production of elements with $A \gtrsim 130\text{-}140$, while the weak would produce elements with $A \lesssim 130\text{-}140$. However, unlike the s-process, the sites for the r-process are not known. Observations of stars enhanced in r-process elements have helped to constrain possible sites (e.g. Sneden & Pilachowski, 1985; Gratton & Sneden, 1994; Ryan et al., 1996; Westin et al., 2000;

Christlieb et al., 2004; Barklem et al., 2005). Also, similar to how the lack of s-process elements at low metallicities suggests an s-process site associated with longer lived stars, r-process elements have been observed at low metallicity, indicating at least one site associated with rapidly evolving objects, such as massive stars. In fact, as we shall see, most r-process candidate sites are associated with Type II Supernovae, which occur only for massive stars.

One possible site, and possibly the most promising candidate at the moment, is within neutrino-driven winds or outflows that occur during Type II SNe (Woosley et al., 1994; Takahashi et al., 1994; Cowan & Thielemann, 2004; Goriely et al., 2005). However, these winds are not able to produce both the stong and weak component of the r-process, so another site is still necessary (Truran et al., 2002).

Another promising possibility for the formation of r-process elements is within the decompressed ejecta from a neutron star merger (Lattimer et al., 1977; Rosswog et al., 1999; Argast et al., 2004). Unfortunately, the frequency of such mergers is not expected to be sufficiently high to explain the observed levels of r-process elements (Qian, 2000).

Other scenarios which have been proposed and not yet eliminated, although clearly not as promising, are production within the magnetized jets of neutron-rich material ejected from collapsing stellar cores (LeBlanc & Wilson, 1970; Cameron, 2001), or from a burst of neutrons produced in the helium and carbon shells of massive stars undergoing Type II SNe (Truran et al., 1978; Thielemann et al., 1979; Blake et al., 1981). Through many of the same reactions which produce neutrons for the s-process, but with larger fluxes than seen there, this environment is theoretically able to produce the r-process elements. However, this mechanism seems unable to produce the heavier r-process elements, and the neutron flux may even be too low to produce the lighter elements.

The main uncertainty associated with the site of the r-process is the identification

of a site with the sufficiently large neutron fluxes and entropy required by the r-process. Thus, all of these proposed sites may prove insufficient.

However, all of these scenarios have one thing in common - association with Type II SNe, and thus the evolution, and ultimately the destruction, of massive (M $\gtrsim$ 8 $M_\odot$) stars. Such massive stars evolve quickly, on the order of 10^8 years, and thus are able to contribute to the nucleosynthesis of the early universe. In particular, r-process elements can be observed in stars with much lower metallicity than s-process elements. In fact, the detection of elements typically associated with the s-process at solar metallicity can likely be explained instead through r-process channels at the lowest metallicities. However, the true site of this process is still highly uncertain. It seems likely that the r-process will ultimately be associated with some sort of rapidly evolving environments, but at the moment this site is largely theoretical (Truran et al., 2002, and references therein).

2.4   EXPLOSIVE NUCLEOSYNTHESIS

Some nucleosynthesis occurs on very short timescales at the end of a stars life. These episodes tend to be very important for producing certain elements, in particular exotic, short-lived, elements heavier than iron, which aren't produced anywhere else.

One such process happens during Supernova Type Ia, which occurs after mass transfer across a binary system has pushed a white dwarf star over the Chandrasekhar mass of 1.4 $M_\odot$, breaking the core degeneracy and causing the star to explode.

As these explosions create iron as a main by-product, it is the timescale of SN Ia that set the iron enrichment of the universe. Since metallicity is typically defined based on the iron abundances of stars, this is generally a good indicator of time, for as time passes, more of these supernovae have had a chance to enrich the ISM. However, since they occur for intermediate mass stars, which have a lifetime on the order of 10^9 years, the appearance of iron in appreciable sums happens quite late

in the evolution of the universe. For stars with very low metallicities, below around [Fe/H] $= -2.5$, iron may then no longer be a good chronometer. This also indicates that the timescales associated with changes in metallicity are more sensitive at low metallicities, which may point to a flaw in using an iron-based metallicity indicator at the lowest metallicities.

There has been some speculation (see, for example, Umeda & Nomoto, 2002, 2005; Nomoto et al., 2006) that at low metallicities SNe Ia explode more violently, producing an order of magnitude more energy than a typical supernova. For this reason, they have been referred to as hypernovae, and have been invoked as a possible mechanism to produce the abundance patterns seen in the carbon-normal stars with [Fe/H] $\leq$ -3.5. A similar low metallicity version of a Type Ib supernova, which experiences additional mixing and fallback and is known as a "faint" supernova, has been suggested as the possible source of the large excesses of CNO elements seen in other metal-poor stars (Uméda & Nomoto, 2005).

An additional important type of supernovae is the Type II, which is believed to be associated with the activation of the r-process, and is discussed in greater detail below.

2.4.1 SUPERNOVA TYPE II

As a massive star reaches the end of its life, it has built up layers of heavier and heavier elements. Eventually, it has a hydrogen and helium layer over a shell of burning hydrogen, which is itself over a helium rich layer over a helium burning layer. This pattern of element rich layer over a burning layer of that element continues with levels of carbon, oxygen, and silicon. At the center is a core of burning silicon which produces elements near the iron peak.

As each burning episode is producing smaller and smaller amounts of energy per nucleon (see Figure 2.1) the timescales for each process are rapidly decreasing. For

a star of 20 $M_\odot$, core hydrogen burning on the main sequence lasts for around 10^7 years, core helium burning takes 10^6 years, core carbon burning only happens for around 300 years, core oxygen burning takes around 200 days, and silicon burning is complete after only 2 days (Carroll & Ostlie, 2006).

Once that time is up, and iron has been produced in the core, the core begins to collapse as usual. However, burning iron is not energetically favorable, so iron burning will not ignite. The core will continue to collapse, increasing its temperature until photodisintegration begins to break down the iron back into smaller components. This produces a large number of free electrons, which are then able to break the electron degeneracy of the core.

At this point, the core is able to contract very rapidly. The eventual densities reached (8 x 10^{14} g/cm^3) will turn the strong force into a repulsive force, through the Pauli exclusion principle applied to neutrons. This will send a shock wave back out into the star. This is sometimes referred to as the core bounce. It used to be thought that this shock would work its way through the outer core, dragging material along with it, until it reached a low enough opacity that the energy from the shock would be able to be released as photons. Now, it is thought that a massive release of neutrinos is responsible for the ejection of the envelope of the star (Baikov & Chechetkin, 2004). This is a Type II supernova. At some point during this process, or shortly thereafter, r-process elements may be created.

2.5 STELLAR POPULATIONS

As the Big Bang produced primarily hydrogen and helium, it follows that the production of heavier elements increased with time, such that stars produced early in the universe have a small fraction of metals, while stars produced more recently have a much larger fraction of metals. Historically, the metal-poor stars have been referred to as Population II and metal-rich stars are called Population I. More recently, Popu-

lation III has been used to describe the population of stars with zero metals, i.e. the first generation of stars to form in the universe before any nucleosynthetic processing had occurred.

These populations were not originally classified based on the abundance of metals, but rather on the kinematic properties of kinematically distinct groups within the Milky Way. Stars which have velocities similar to the Sun were classified as Population I, while stars with much larger velocities were classified as Population II. Eventually it was discovered that these populations varied also in location, with Population I stars lying mostly in the disk of our Galaxy, while Population II stars existed mostly outside the disk. With the addition of chemical differences, this enabled early astronomers to develop a picture of the formation and evolution of our galaxy, with a disk (Pop I) and a halo (Pop II).

In reality, there is a continuum of stellar populations, with all possible metallicities, representing a varied universe of stellar evolution and nucleosynthesis. Populations existing in the Milky Way, for instance the thin disk, thick disk, and halo, likely don't exist in the same way in other galaxies. However, due its more restrictive definition, a more recently defined population of stars needs a closer look, the Population III stars.

2.5.1 POP III

Zero metallicity stars, having only the elements produced during the Big Bang, are unable to process materials in the same way as their more metal-rich bretheren. In particular, the absence of carbon to act as a catalyst to the CNO cycle means that all Population III stars must process hydrogen through the PP chain. This requires higher temperatures than would be needed if CNO processing was available.

This situation doesn't last long, however, as the triple-α process can produce a small amount of carbon to enable the CNO cycle to commence. A carbon mass

fraction of only 10^{-10} is sufficient to switch to the CNO cycle, and all Pop III stars will be undergoing CNO cycling by the end of hydrogen core burning. In addition, Pop III stars, as well as massive, extremely metal-poor stars, do not have a first dredge-up (Herwig, 2005). However, by the AGB phase, a Pop III star will behave exactly like a metal-poor star, lacking only the iron and elements heavier than aluminum present in the other. The s-process can even still occur, although the lack of iron seed nuclei results in a seed nuclei with a lower mass number than iron, such as carbon.

2.6 BINARY MASS TRANSFER

The formation or non-formation of a binary system is largely an issue of angular momentum. With sufficient angular momentum, a bar-type instability arises in the star forming gas cloud and through the proceeding rapid transfer of angular momentum the cloud collapses to a single star. Without enough angular momentum, the collapsing cloud forms a rotationally supported disk, which continues to accrete material and can eventually undergo a ring instability and fragment into a binary.

Saigo et al. (2004) have studied the formation of Population III stars, and found that a vast majority of these stars are expected to form in binary systems, regardless of mass. This is in contrast with the ~50% of stars which form in binary systems today. An increasing binary fraction at low metallicities could have significant consequences in the study of the early galaxy.

Within a binary system, mass transfer may occur through several mechanisms, primarily through the operation of a stellar wind or by Roche Lobe overflow, usually dictated by the orbital separation of the two stars. All stars undergo mass loss through winds, although some evolutionary stages are more efficient at this than others (see Table 2.2). Thus, mass transfer through winds occurs at all times within a binary system. For stars with a sufficiently wide separation, this is the only mass transfer that happens, and it is such a wind which is believed to be the source of

the abundance patterns seen in the two HMP stars. With a closer separation, the initiation of a Roche Lobe overflow is possible. The amount of material transferred through such a scenario is vastly larger than the quantity transferred via wind, and in such situations the wind transferred material can be considered negligible.

For any binary system, there exists an equipotential surface in which there is a single point of contact at the center of mass of the system. This surface is known as the critical surface, and each half of the curve is known as a Roche Lobe. If either star expands outside of its Roche Lobe, it will then transfer material from its surface to the other star through the Inner Lagrangian, the point of contact between the two Roche Lobes.

The size of the Roche Lobes is dependent on the masses of the stars and their separation. These orbital parameters then determine at which evolutionary stage mass transfer may occur. For stars in a close binary, mass transfer may begin while the stars are on the main sequence, while for larger separations this may not occur until the RGB or AGB. As mass is transferred, the relative masses of the two stars changes, so the equipotential surface changes, and mass transfer may then proceed in the other direction, or do something entirely different (Lau et al., 2007). In addition, mass transfer tends to increase the separation between the two stars, which will also have consequences on the equipotential surfaces.

The importance of such mass transfer will be discussed in greater detail in §3.1.1.

Chapter 3:
Carbon-Enhanced Metal-Poor Stars

Since the time that the first spectra were taken of stars, it has been noticed that there is a subclass of stars which are more enhanced in their carbon abundances than the typical star. These stars were easily picked out due to the strong carbon features, specifically a strong CH G band at 4304 Å(see Figure 3.1), and were thus called carbon or CH stars. While these stars were recognized to exist, they always represented a fairly small portion of the full sample of stars.

Later, a small fraction of Population II stars were noticed to have overabundances of barium as well as carbon, and these stars became known as the barium stars (Bidelman & Keenan, 1951). But, again, these stars did not account for a significant fraction of the total stars, and were generally viewed as an oddity.

However, in recent large studies of metal-poor stars, such as the HK (Beers et al., 1985, 1992) and Hamburg/ESO surveys (HES; Christlieb et al., 2001), it has been noticed that a fairly large fraction of these stars show an enhancement in their carbon abundances. In fact, the fraction of these so-called Carbon-Enhanced Metal-Poor (CEMP; [C/Fe] $\geq$ +1.0) stars seems to increase with declining metallicity. If this trend holds true, it would suggest the existence of mechanisms effecient in the production of carbon existed at very low metallicities, and that the efficiency or frequency of these mechanisms is diminished at higher metallicities. CEMP stars seem to be a part of the same continuum as CH and barium stars, with the primary
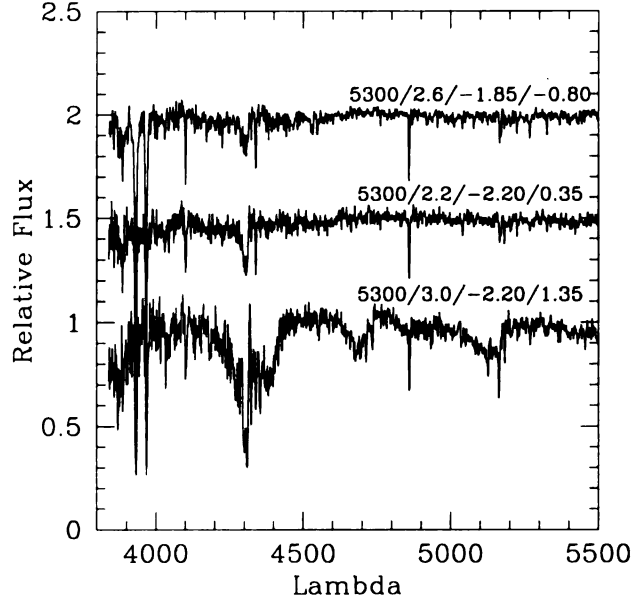
Figure 3.1 Example spectra of stars with similar stellar parameters, as indicated, but with increasing carbon abundances. Note the increasing strength of the G band at 4304 Å.

difference just being the metallicity range covered. However, with large samples, there is no clear distinction between these classes.

Carbon is an important element in the history of the universe. As a primary coolant, its presence is required to form low mass stars, and thus carbon influences the IMF (Bromm, 2005; Frebel et al., 2007). As a catalyst for the CNO cycle, it is required for effecient energy production in high mass stars. As the seed or neutron source for many nuclear reactions to create heavier elements, it is required for nearly all elements heavier than it.

The production of this carbon can generally be broken down into three possibilities – a primordial mechanism which pre-enriched the material the stars formed from, an intrinsic mechanism in which the carbon was produced in the same star where it is observed, or an extrinsic mechanism, where the star observed was polluted with carbon formed elsewhere. Due to the increasing fraction of such stars, it can be surmised that these mechanisms, whatever they may be, were more efficient at lower

Table 3.1. Definition of sub-classes of CEMP stars, from Beers & Christlieb (2005)

CEMP-r	[C/Fe] > +1.0 and [Eu/Fe] > +1.0
CEMP-s	[C/Fe] > +1.0, [Ba/Fe] > +1.0, and [Ba/Eu] > +0.5
CEMP-r/s	[C/Fe] > +1.0 and 0.0 < [Ba/Eu] > +0.5
CEMP-no	[C/Fe] > +1.0 and [Ba/Fe] < 0

metallicities.

There are also several subclasses of CEMP stars, as will be discussed shortly. The abundances of these different subclasses, as well as the relative frequency between them, can give us hints as to the relative importance of these production mechanisms.

3.1 SUBCLASSES

Since CEMP stars were first noticed in great abundance, it has been observed that the stars could be grouped into several subclasses, based on the patterns of neutron-capture elements present in their atmospheres (Norris et al., 1997a,b, 2002; Bonifacio et al., 1998; Hill et al., 2000; Aoki et al., 2002; Goswami et al., 2006; Aoki et al., 2007). For our current purposes, we shall adopt the classification scheme of Beers & Christlieb (2005), as seen in Table 3.1.

The origin of each subclass is about as well understood as the origin of the underlying neutron-capture processes by which they are enriched. The addition of carbon, and the detectability of the n-capture enriched material in stellar atmospheres, add additional constraints on their origin which may assist in further determining the sites of these processes. The relative fractions of the subclasses can perhaps give some additional constraints, as several proposed origin scenarios are expected to be statistically unlikely. Alternatively, these fractions may alter our view of the relative importance of such scenarios through the history of the universe. The currently

proposed scenarios for each subclass are outlined below.

3.1.1 CEMP-s

Easily the most common subclass of CEMP stars, comprising more than 80% of all CEMP stars (Aoki et al., 2007), and the one best understood, CEMP-s stars are those which are enhanced in both carbon and elements created by the s-process.

As we have seen, intermediate mass (3-8 $M_\odot$) stars undergo thermal pulsation while ascending the AGB. During these pulses, s-process elements are created in the carbon-rich, helium intershell. Following each pulse, during third dredge-up, material rich in carbon and s-process elements is brought to the surface. It is then possible to observe this star as a CEMP-s star, sometimes referred to as an intrinsic CEMP-s star, as it internally produced these elements and self-polluted.

However, that is not all there is to say about CEMP-s stars. The time a star spends producing s-process material is on the order of 10^3 to 10^5 years (Figure 2.3) and occurs near the end of the star's life. After a number of thermal pulsations of increasing strength, eventually one is able to permanently separate the collapsed core from the surrounding layers, producing a white dwarf and its planetary nebula. Such nebula should thus be enriched in carbon and s-process elements, which is indeed observed (for example, Sharpee et al., 2007).

In general, this material is then lost to the ISM, where it is quickly diluted and the overabundances disappear. If another star forms out of the still enriched gas, these elements would be spread over the whole volume of the star, and large enhancements would probably not be seen. A significant abundance of carbon and s-process elements would be needed if this new star were to be similarly observed to be a CEMP-s star. That said, such a star could still be observed to be mildly enhanced in these elements.

However, for a star in a binary system, with a less massive (and therefore longer lived) secondary, this s-process enriched material may have a different destiny. Due

to strong winds from the AGB star, or more likely the formation of a Roche-Lobe overflow leading to a mass transfer scenario, it is possible for the primary AGB to transfer this enriched material to the surface of the unevolved secondary companion.

Since carbon and s-process materials form during the AGB, we want a star to reach that stage and produce those elements before it starts to transfer material. Therefore, the stars which might produce CEMP-s stars are those with a sufficiently large binary separation, such that mass transfer does not proceed until the AGB phase of the primary star. However, even if mass transfer occurs prior to the second dredge-up, CNO isotopes can still be transferred because the CNO-rich H-burning shell is eventually exposed to the surface.

Mass transferred in this way releases around 100 times the mass of metals, and 1000 times the carbon, than a typical stellar wind. This is because the whole envelope of the primary is lost during such binary mass transfer, while only a small fraction is lost by the AGB wind (Lau et al., 2007).

If this secondary star is then observed, its surface will still show evidence of this s-process enrichment. Such a star is often referred to as an extrinsic CEMP-s star, as their enhancements come from an external source. For such an observed main sequence star, its s-process abundances will likely reflect the s-process production of the former primary, as no strong mixing episodes have yet occured in its atmosphere, mixing this material into deeper layers. Any gravitational settling which may have brought some of the heavier elements deeper into the star is expected to have minimal impact on these overall abundances.

However, the possibility has been pointed out (Stancliffe et al., 2007) that thermohaline mixing may be induced in the upper atmosphere of the secondary star as a result of this mass transfer. This mixing would cause dilution of this material by up to a factor of 100. If this does happen for all stars undergoing such a mass transfer, then even a main sequence star would show significantly lower abundances of material

than were created by the former primary. The abundances observed then represent a small fraction of these true abundances, which would then be much larger than is currently estimated.

If this former secondary is observed as a giant star, it has undergone at least one episode of deep mixing and dredge-up, which will bring the enriched material into the interior of the star and deposit normal carbon levels on its surface. Such a star may still appear to be carbon-enhanced, but with abundances reduced significantly compared to before such mixing. In fact, Komiya et al. (2007) have argued that CEMP giants exhibit a wide range down to low [C/H] values due to dilution by a factor of up to $\sim$100, a factor corresponding to the difference in the depth of the surface convective zone of giants and dwarfs.

The amount of mixing, which is thus important to fully understand the enhancement scenarios, can be determined by measuring ratios of elements (e.g. [C+N/Fe], [C/N]) and isotopes (e.g. ^{12}C/^{13}C), as these ratios indicate the amount of CN processing which has occurred.

In order for this scenario to be valid, all CEMP-s stars observed must be observed to be members of binary systems. Direct detection of the white dwarf companion is rarely possible, and radial velocity variations are not always detected due to limited temporal coverage and due to the orientation of the system relative to the line of sight. However, a recent statistical work by Lucatello et al. (2005) have shown that all CEMP-s stars observed are consistent with membership in a binary system. Thus, for the moment at least, no additional scenarios are required to explain the origin of CEMP-s stars.

3.1.2 CEMP-r/s

CEMP-r/s stars show enhancements of both r-process elements and s-process elements (Cohen et al., 2003; Barbuy et al., 2005; Jonsell et al., 2006). Due to this

double enhancement, CEMP-r/s stars might help to identify possible sites for the r-process, since the existence of such stars constrains possible environments. In addition, all known stars showing enhancements of r- and s-process elements also show enhancements in carbon, in agreement with the understanding of the link between s-process elements and carbon (Jonsell et al., 2006).

The suggested formation scenarios for these stars can generally be separated into two categories – independent r- and s-process enhancements, through two distinct mechanisms, or a single scenario which causes both enhancements.

The independent formation scenarios just mix the possible sites for the r-process with the site of the s-process. In other words, you have an s-process scenario occur in material pre-enriched in r-process material, possibly by a nearby supernova. This could be an intrinsic s-process enhanced star (Hill et al., 2000; Cohen et al., 2003), all on its own, or an extrinisically enhanced star in a binary system.

These independent scenarios have a number of problems however. Most CEMP-r/s stars are observed to be near the turn-off, while intrinsically enhanced stars must be on the giant branch. Also, if these processes occur in truly independent scenarios, then the probability of finding stars enhanced by both mechanisms would be the product of the probabilities of the individual mechanisms, so such stars would be rarer than observed. In addition, the chemical homogeneity of the r/s stars argue against independent scenarios. The [Eu/Fe] ratios are also higher for r/s stars than for r stars, suggesting that if the scenarios are independent, the additional europium must have been produced by the s-process, which may not even be possible. If these stars formed out of material enriched in r-process elements, as opposed to being polluted by them at some later stage, then those enhancements would exist througout the whole volume of the star, as opposed to just the surface. In order to produce the enhancements seen, a much larger amount of r-process material would have to have been produced. Finally, all r-enhanced stars are giants, while most r/s stars are

turn-off stars. If the common giant status for r stars is an indication of a formation scenaro, then r/s stars must have formed through a different mechanism (although they could have been the binary companions to the r stars with transferred material). These facts suggest that a single scenario which is able to account for both r- and s-process enhancements is much more plausible for the formation of these stars.

Due to our understanding of the site of the s-process, it is expected that any scenario used to explain the production of CEMP-r/s stars involves binarity. Not all CEMP-r/s stars are known to have binary companions, but this is likely for the same reasons that not all CEMP-s stars are observed to be in binary systems. In addition, due to the much larger enhancements of r-process enhancements needed for stars forming out of such material versus the amount needed for a surface enhancement, possibly coming from a binary mass transfer scenario, it can be assumed that a binary system is required for the r-process enhancements as well.

In addition, the chemical homogeneity of the r/s stars suggests that a single scenario should be able to account for all r/s stars. Therefore, scenarios which are plausible, but infrequent in occurance, can be generally discounted. Similarly discounted, for reasons stated previously, are scenarios in which stars formed from pre-enriched materials.

The first scenario of this type is actually just a slight variation of our independent scenario. A supernova goes off near a molecular cloud, triggering star formation in the now r-process rich material. Later s-process enhancements proceed as usual (Gallino et al., 2005; Ivans et al., 2005). It is unclear, however, how common such a scenario might be, and the formation of the star in pre-enriched material is still a major problem.

The remaining scenarios all take place in an isolated star system. The first idea here is the evolution of a triple system, where one star explodes as a supernova, enriching the other two in r-process elements. The remaining two stars then form

the usual s-process scenario (Cohen et al., 2003). The system surviving the initial supernova, and the specific orbital parameters required for this scenario suggest that this scnerario could not easily produce all known r/s stars (Jonsell et al., 2006).

The main two scenarios which are generally considered for the presence of CEMP-r/s stars involve only a binary system. In the first scenario, the secondary is polluted by s-process elements by the primary in the usual way. If the primary undergoes little mass loss, it may be possible for the core of the star to exceed the Chandrasekhar limit, and undergo a Type I.5 supernova, which has been proposed as a possible site for the r-process. This is a possibility due to the metallicity dependence of mass loss from an AGB, with lower metallicity stars undergoing less mass loss (Zijlstra, 2004). It is unclear how this reduced level of transferred mass might affect the observed abundances.

A similar scenario begins with the same s-process material transferred to the secondary. Eventually the secondary evolves and transfers material back to the primary, which undergoes accretion induced collapse (AIC) from a white dwarf to a neutron star. AIC creates a neutrino-driven wind, in which r-process elements may be created. These elements then pollute the secondary star (Qian & Wasserburg, 2003). Again, it is unclear how this re-transfer of material back to the primary might affect the ultimate s-process abundances, although one might then expect the r/s stars to show less s-process enhancement than is seen in s-only stars. This is not seen at least in measurements of [Ba/Fe], although there could be an additional r-process contribution for the r/s stars. However, this scenario also requires that the observed star be a giant, which is also genarally not true.

3.1.3   CEMP-NO

Stars which have enhanced levels of carbon, but show no enhancements of neutron-capture elements, are known as CEMP-no stars. Using a limited sample of such
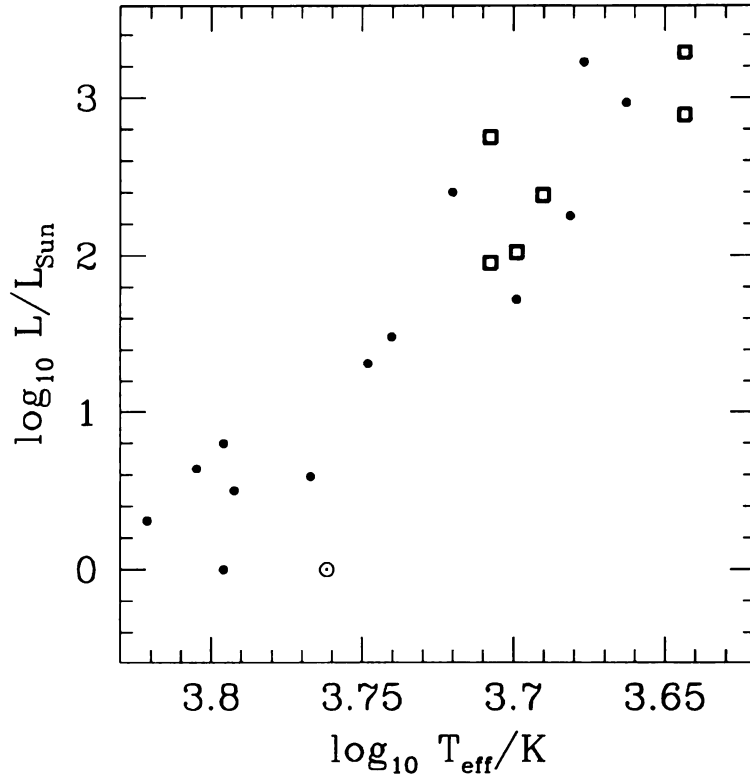
Figure 3.2 An H-R diagram showing samples of CEMP-no (squares) and CEMP-s (circles) stars. Figure after Ryan et al. (2005).

stars, Ryan et al. (2005) noticed that, unlike CEMP-s stars, which are seen at all stages of evolution, CEMP-no stars are only ever seen high up on the first-ascent giant branch (Figure 3.2). They also tended to have $^{13}C/^{14}N$ ratios which were close to the value expected assuming CN equilibrium. They attributed this finding to the dilution of s-process enhanced materials in the giant stars which then re-classified them as CEMP-no stars rather than CEMP-s stars.

A more recent study by Aoki et al. (2006), using a much larger sample of CEMP stars, has found that CEMP-no stars are in fact present at all evolutionary stages and the dilution of these materials is less significant than assumed by Ryan et al. (2005). Aoki et al. (2006) also note that a small sample of CEMP stars could easily be biased towards giants due to the comparative ease of detecting carbon features in cooler

stars (see our discussion of this topic in §5). In addition, stars which show enhanced barium abundances tend to have a higher absolute carbon abundance, which would make them easier to detect at a given temperature. Thus, smaller samples of CEMP stars which contain CEMP-no stars will likely only detect CEMP-no stars as giants, while CEMP-s stars will be detected at all evolutionary stages.

In stars of low metallicity, a process called Helium-Flash Driven Deep Mixing (He-FDDM; Fujimoto et al., 1990, 2000) can occur to stars on the RGB tip, triggered by helium core flash. In many ways, this is similar to the helium shell flashes that initiate third dredge-up. During the flash, carbon and s-process elements are created. A mixing episode then begins, dredging material to the surface. However, this newly made material is much deeper during He-FDDM than it is during third dredge-up. The mixing is unable to bring all of these materials to the surface. The convective region generally penetrates into the carbon rich layers, but does not go as deep as the layers of s-process rich material.

In nearly all ways, these stars operate exactly like typical low-mass non-CEMP stars. Only their carbon abundances, and by extension oxygen and α abundances, are different from a standard star, and this can be explained by the material out of which they formed. These stars should not appear to have a binary frequency any different than non-CEMP stars, and in fact should have many properties similar to non-CEMP stars.

Komiya et al. (2007) have recently looked at the mass and metallicity range of stars to deduce the likely origin of CEMP-no stars. They found that if the star is greater than $\sim$3.5 M$_{\odot}$, or more metal-rich than [Fe/H] $= -2.5$, carbon and s-process enhancement proceeds as expected, arising from convective mixing brought about by the third dredge-up. However, for very metal-poor, [Fe/H] < -2.5, lower-mass (0.8$\leq$M$\leq$3.5M$_{\odot}$) stars, He-FDDM may operate during the RGB helium flash, producing an additional source for the production of carbon and s-process elements, although

a large production of nitrogen is also expected, producing a N/C ratio of between 1/5 and 1. In addition, for the lowest mass (M$\lesssim$1.2 M$_\odot$), lowest metallicity ([Fe/H]$\lesssim$-4) stars, the production of s-process elements occurs, but are not convectively mixed to the surface, producing CEMP-no stars with a large nitrogen abundance.

3.1.4 CEMP-R

A number of stars show enhancements of their r-process elements, but at the moment only one star, CS 22892-052 (Sneden et al., 1994, 2003), also shows carbon enhancements. Due to this, and due to the r-process not generally being associated with carbon production, it is assumed that the presence of these elements is due to independent mechanisms. With only one known star, CEMP-r stars are not yet truly a CEMP subclass, but rather an oddity, and a full analysis of an origin may not be possible without the discovery of additional such stars.

The general thought to explain CEMP-r stars is that they are essentially CEMP-no stars which happen to be r-process enhanced, just as a non-CEMP star might be. Through some mechanism that produces r-process material, these CEMP-no stars, which self-polluted with carbon due to He-FDDM, were enriched in r-process material.

3.2 FREQUENCY

The frequency of occurance of different phenomenon can often reveal the nature of that phenomenon. For example, CEMP-s stars appear to have a binary fraction of 1, which leads us to think that binarity should be important for producing CEMP-s stars. Once we find out that the s-process operates in soon-to-die intermediate/low mass AGB stars, we then understand that for this material to be observed, the doomed AGB must pass it along to a different star in the prime of its life. The importance of binarity then becomes obvious, and we have a good understanding of this whole process.

Relative fractions of assorted phenomenon is thus a powerful tool to deducing the nature of astrophysical phenomenon. It is not alone in this task, but its importance is undeniable.

The fraction of stars at a given epoch (e.g. as traced by [Fe/H]) which are enhanced in their carbon abundances can help us identify the sources of this carbon enhancement. In addition, once the mechanisms are better understood, these fractions can help define important astrophysical quantities at different epochs, such as the binary fraction or the IMF, which are of vital importance to the understanding of galactic and nucleosynthetic models of the universe.

The total fraction of CEMP stars has recently been an issue of great debate, variously reported as ~10% (Frebel et al., 2006), ~15% (Cohen et al., 2005) or ~20% (Lucatello et al., 2006) of stars with [Fe/H] $\leq$ -2.0; ~25% of stars with [Fe/H] $\leq$ -2.5 (Marsteller et al., 2005); or nearly 40% of stars with [Fe/H] $\leq$ -3.5 (Beers & Christlieb, 2005). However, these values are not mutually exclusive. The fraction of CEMP stars is expected to increase with declining metallicity, which is illustrated very well with these results. Only the results of Frebel et al. (2006), Cohen et al. (2005), and Lucatello et al. (2006) seem to contradict each other, but even this can be understood in terms of the evolution of their samples.

Both Frebel et al. (2006) and Cohen et al. (2005) have looked exclusively at giant stars, while Lucatello et al. (2006) looked at a mixture of evolutionary stages. As we have seen, as stars move off the main sequence and up the giant branch, they undergo first dredge-up as their convective envelopes penetrate deeper into their interiors. Stars similarly experience extra mixing as they move off the RGB bump. These periods of mixing have the effect of diluting the surface carbon abundance in favor of nitrogen. This can be seen especially when looking at the combined abundances of C and N, which remains constant as C is converted into N (Spite et al., 2006; Lucatello et al., 2006). This dilution would decrease the observed C abundance by

~0.3 to 0.6 dex. As a result, stars which had been enhanced in carbon to just over the [C/Fe] = 1.0 limit will now no longer be classified as CEMP. Samples of giant stars will therefore show a lower CEMP fraction, which is what is seen in these results. Presumably, a sample of only dwarf stars would show an even higher CEMP fraction than is seen in Lucatello et al. (2006).

The samples studied to date have also been relatively small, and, as a result, the only values which have been determined are the cumulative fraction of CEMP stars below some limiting metallicity. Also, as was just discussed, the effect of evolutionary states has not been studied in great detail. Clearly, the true value of interest would be a detailed frequency of carbon enhancement as a function of metallicity for different evolutionary stages. The frequency alone should be able to indicate something about the nature of the galactic IMF and the nucleosynthetic history of the Milky Way. How that frequency changes for samples of different evolutionary stages would allow for a greater understanding of precise convection and mixing parameters, especially amongst stars of varying metallicity.

Also of importance are the relative fractions of the subclasses of CEMP stars. CEMP-s stars appear to comprise more than 80% of all CEMP stars (Aoki et al., 2007), emphasizing the ease of producing CEMP stars through this mechanism. The presumably changing fractions of each subclass with declining metallicity might better identify the sites of these processes, and the relative importance of them to galactic nucleosynthesis.

An increasing fraction of CEMP stars at lower metallicities might indicate that the mechanisms which produce these carbon overabundances were more common or more efficient at lower metallicities. If the relative fractions of the assorted subclasses are the same, with a majority of stars in the CEMP-s class, that could suggest a higher binary fraction or more favorable conditions for mass transfer, with regard to orbital parameters or the rate of mass loss.

In reality, the unavailability of the s-process at low metallicity, and the metallicity dependence of many of the mechanisms responsible for the other subclasses, such as He-FDDM or Type 1.5 SNe, would suggest dominance by these subclasses over CEMP-s stars at the lowest metallicities. If this is not observed, then these mechanisms, or our understanding of them, may be flawed. But it's these ratios which help to unravel the true nature of the origin of these stars and these elements.

CHAPTER 4:
AUTOMATIC ABUNDANCE
DETERMINATIONS

4.1 ASSUMPTIONS FROM THE LINE INDEX METHOD

In order to study the elemental abundance patterns of stars, those abundances need to be determined. Some basic information, the stellar parameters - the effective temperature, T_{eff}, the surface gravity, $\log g$, and the metallicity, [Fe/H] - need to be obtained before abundances can be determined.

Following the prescription of Beers et al. (1999), the effective temperature can be estimated from the color (namely B-V) of a star. Surface gravities can be determined by assuming a rough evolutionary stage for a star. Although the color of a star is directly connected to the temperature of a star, and indirectly to the surface gravity, this technique is largely possible due to calibration with a number of stars of known temperature and gravity. Despite this, determination of these parameters from photometry alone is a powerful tool for quickly obtaining this information for a large sample of stars.

In order to determine metallicity, however, Beers et al. (1999) only require low to medium(1-2 Å) resolution spectroscopy. This is much easier and less time consuming to obtain than high resolution spectroscopy. However, at these resolutions it is often difficult to measure iron lines directly. As a result, a line which traces the metallicity, [Fe/H], of a star, but is readily detectable at low resolution is needed. In optical

spectra, the only lines which are semi-consistently strong and visible in all stars are the Balmer lines, which do not trace metallicity, and the CaII H and K lines, which do.

Due to the proximity of the Hϵ line (at 3970 Å) to the Ca H line (at 3969 Å), the Ca H line can not be consistently used to measure metallicity, and the uncertainty in the contribution of the hydrogen line to the strength of the calcium feature eliminates the usefulness of the Ca H line in metallicity determinations. The Ca K line (at 3934 Å) does not suffer this problem and therefore makes an excellent metallicity indicator.

Even so, calcium is an α-element, and so does not always trace the iron abundance directly. In metal-poor stars, an α-enhancement exists which must be properly accounted for to truly obtain the metallicity of a star. Again, following Beers et al. (1999), we use an α-enhancement of:

$$[\alpha/\text{Fe}] = \begin{cases} 0 & \text{if } [\text{Fe/H}] \geq 0 \\ -0.267 * [\text{Fe/H}] & \text{if} -1.5 \leq [\text{Fe/H}] < 0 \\ 0.4 & \text{if } [\text{Fe/H}] < -1.5 \end{cases} \qquad (4.1)$$

To obtain the strength of the Ca K line to be used to determine metallicity, Beers et al. (1999) measure the KP index, a pseudo-equivalent width estimator for the line. The KP index is then a numerical value corresponding to the overall strength of the Ca K line, with no information as to its specific shape. Using calibration stars of known metallicity to calculate a regression, the KP index is used with the B-V color of the star to yield a measurement of the stellar metallicity. Thus, from just the B-V color and the KP index, these stellar parameters may be obtained. This is known as the Line Index method.

In stars with enhanced carbon abundances, like CEMP stars, strong carbon features contaminate the measurement of many other lines. Most noticeable of these carbon features is the G band, a CH molecular feature centered near 4304 Å, al-

though numerous C_2 features are often apparent as well. In fact, many CEMP stars were noted as "strong G-band" stars in the HK survey (Beers et al., 1992).

The abundance of carbon in the atmosphere of a star absorbs much of the optical light. Some observed colors, in particular B, are affected fairly strongly by this. Thus the calibration of Beers et al. (1999) with B-V colors will yield invalid results for carbon-enhanced stars. Rossi et al. (2005) attempted to correct for this effect by re-calibrating the line index method using J-K colors instead, as there is very little carbon contamination present in the infrared.

In addition, Rossi et al. (2005) used the GP index, similar to the KP index but for the G band rather than the Ca K line, as an estimator of the carbon abundance, [C/Fe], of a star. The new calibrated line index method requires the KP index and J-K colors to determine metallicity, but only the KP and GP indices to obtain [C/Fe].

However, they note that they continue to have problems for very cool stars, or those with especially large carbon abundances, due to the presence of especially strong molecular carbon lines in the sidebands of the GP index, which effects the placement of their continuum. Cohen et al. (2005) have noticed a similar effect may contaminate the measurement of the KP index as well (see Figure 4.1).

Both Beers et al. (1999) and Rossi et al. (2005) note that the line index method is only applicable for stars with [Fe/H] < -1.0, due to issues with saturation of the KP index for more metal-rich stars. So, while the line index method is an useful, and, importantly, rapid method for determining stellar parameters and carbon abundances, there are several known areas of parameter space where it is not applicable. In addition, since it is a calibration-driven technique, it requires large pre-existing data sets of stars with known parameters. It is thus more prone to problems in regions of poorly sampled parameter space. With increasingly large sets of data being produced (such as the Sloan Digital Sky Survey), the calibrations are steadily improving, and it should soon be possible to better constrain the behavior of the KP and GP indices
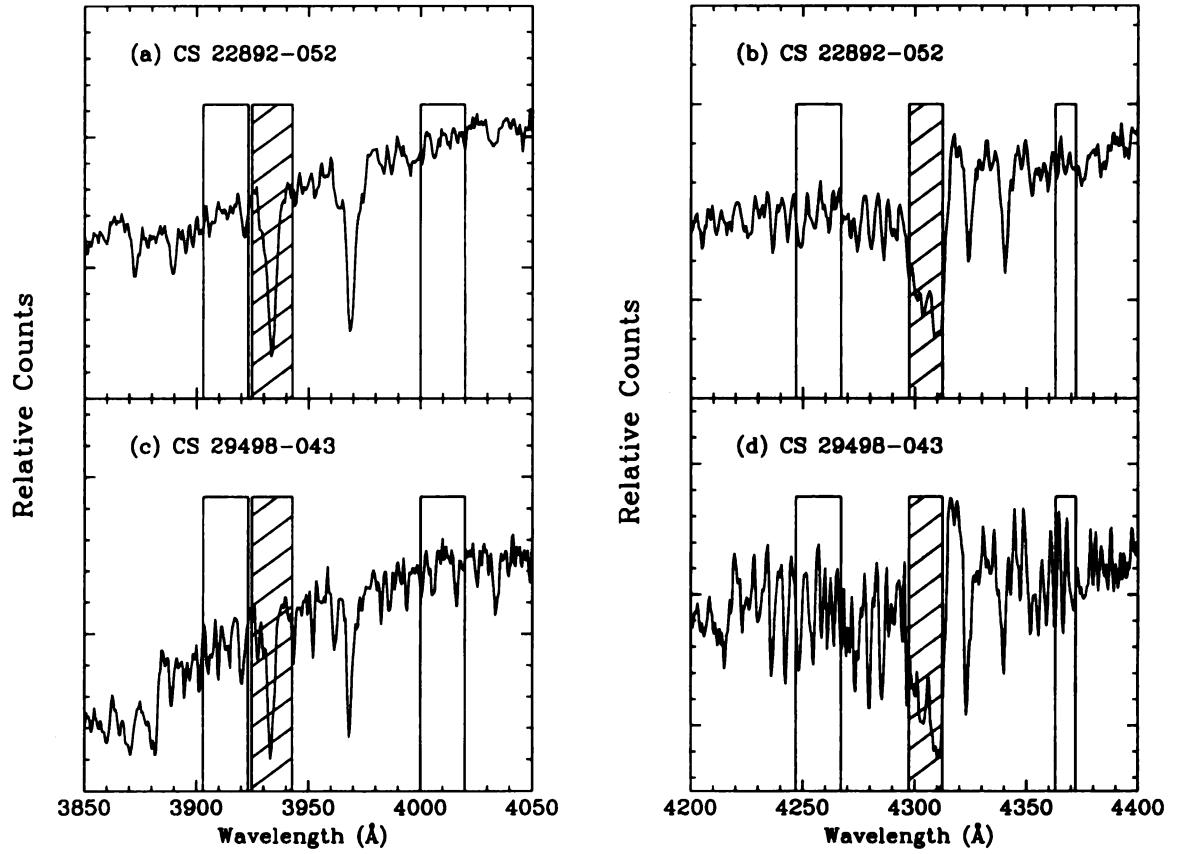
Figure 4.1 Locations of the line indices KP and GP (hatched rectangles) and the sidebands used for continuum placement (open rectangles). Figure courtesy Rossi et al. (2005)

at very low metallicities and very high carbon abundances. Nevertheless, there will undoubtedly still be problematic areas for the line index method. In these regions, spectral synthesis should do a better job.

4.2 SPECTRAL SYNTHESIS

By utilizing models of stellar atmospheres in conjunction with atomic and molecular linelists, it is possible to create synthetic spectra which can then be compared against data to determine abundances. Using the 2002 version of the line analysis code MOOG (Sneden, 1973), synthetic spectra are generated. As inputs, a grid of ATLAS9 1D, LTE stellar atmosphere models (Castelli & Kurucz, 2003) and atomic and molecular linelists which include numerous molecular carbon features[1] are used. The current grid of models used has spacing of 100 K in T_{eff}, 0.2 in log g, and 0.5 in [M/H], or overall solar-scaled metallicity, for the majority of the grid coverage. The density of models decreases towards the edges of the grid.

There are some possible concerns to using only 1D, LTE model atmospheres. Due to their respective sizes, giants are adequately modeled by 1D models, while dwarfs are more appropriately modeled by 3D models. Similarly, based on the respective densities of their photospheres, dwarfs are reasonably modeled assuming LTE, whereas giants should really be represented using NLTE. 3D and NLTE models are currently being developed (for example, Collet et al., 2006), but for now 1D, LTE models must prove sufficient. Adopting 1D, LTE atmospheres is not truly appropriate. The scale of the corrections these models would have are in general comparable to the uncertainties in the measurements or the quality of the data. These corrections are more of a concern for high-resolution analyses.

---

[1]http://kurucz.harvard.edu/linelists.html

4.3 Spectral Synthesis with MOOG

MOOG is a line analysis code which uses input stellar atmosphere models and atomic and molecular linelists to generate synthetic spectra. While it is capable of performing other tasks as well, it is this functionality which is most useful in this analysis.

To run MOOG, all relevant information can either be directly supplied or provided through a parameter file. The relevant information for this discussion that is supplied includes the name of the stellar atmosphere model to use as well as the names of the linelists, including a list of strong lines such as the Balmer lines and the Ca H and K lines. In addition, any atoms to vary from the model metallicity, as well as any appropriate isotopic ratios to use, must be specified. The wavelength region to synthesize over, the resolution and smoothing of the synthesized spectra and, if plotting, the wavelength region to plot must also be indicated. If determining abundances from data, the location of that file is also necessary. Since the spectra generated are flattened and normalized, the input data must be comparable. This task is performed using a set of routines written in IDL (Y. S. Lee, private communication) which fit polynomials to the spectra.

MOOG then generates the synthetic spectra and plots them against the data. A number of plotting parameters, including the relative positions of the data and the synthetic spectra may then be manipulated, or individual abundances changed until a reasonable fit is reached. MOOG can also plot both the spectra and a residual of the fit with the data, to assist in abundance determinations.

In this way, individual abundances may be varied until a reasonable fit is reached. However, MOOG is used to generate and display the synthetic spectra, not to determine a best fit. So, the fit must be done by hand (see Figures 4.2 and 4.3), which is a relatively slow process. For high-resolution analyses, with relatively small sample sizes, this method is reasonable. However, in order to determine abundances using spectral synthesis for increasingly large samples of low and medium resolution spectra,
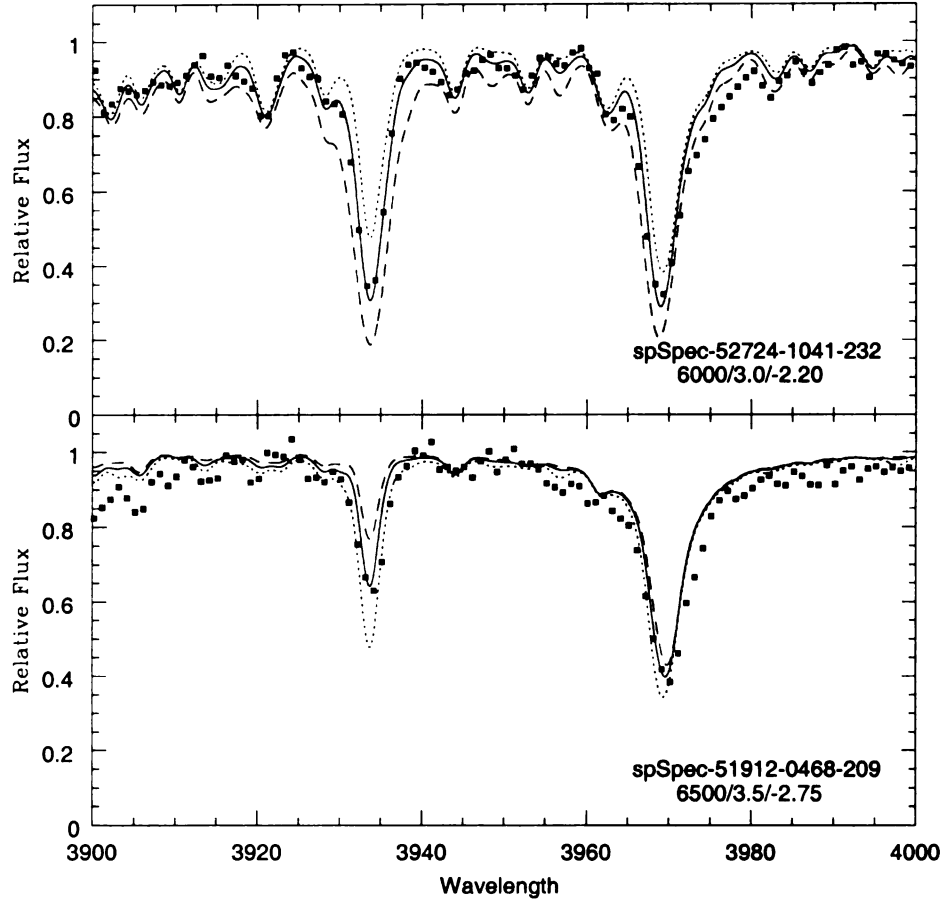
Figure 4.2 Fits of the Ca K line at 3933 Åfor stars with different metallicities but similar temperatures and surface gravities. The solid line represents the best fit, as determined by hand, while the dashed lines correspond to the best fit ±0.5. Note the weaker calcium line for the star with lower metallicity.
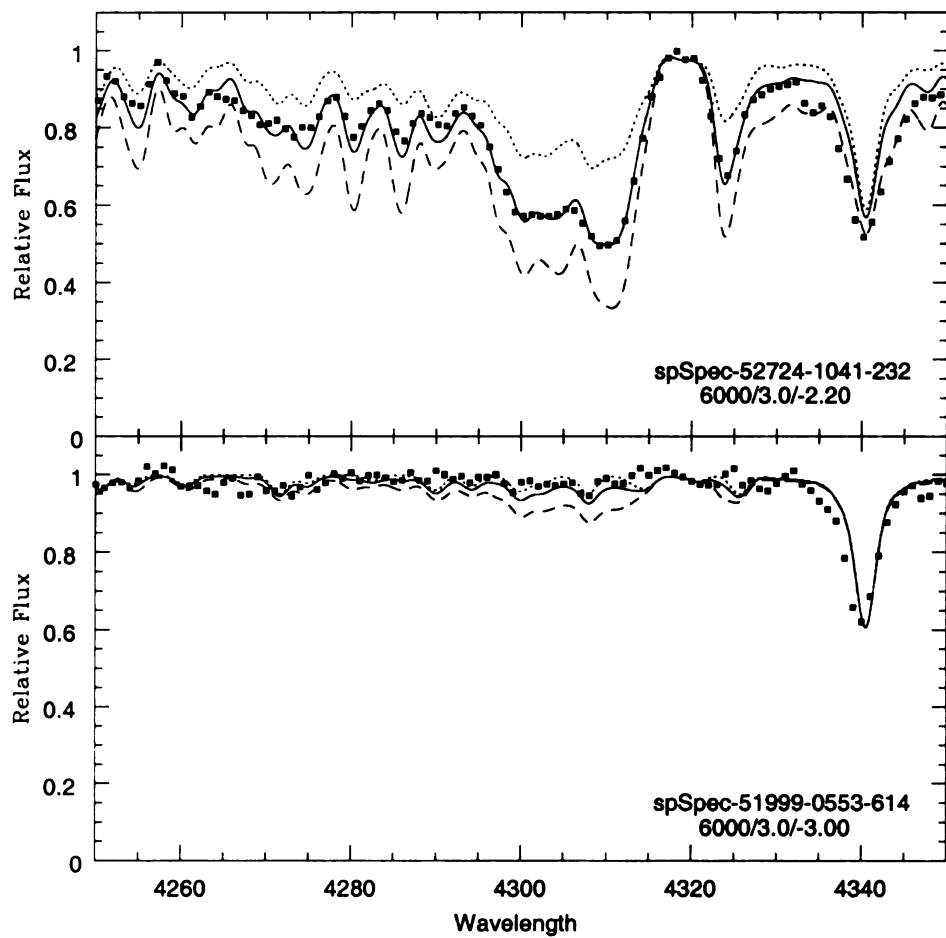
Figure 4.3 Same as Figure 4.2 but for the G band near 4304 Å. The lower plot shows the location of the upper limit that is used for this star.

a faster alternative is needed.

In addition, despite the MOOG based residual calculation, the abundance selected might vary from user to user as different users tend focus on different aspects of the fit, or even for a single user depending on familiarity with a given spectral region.

Thus, to determine abundances for large sets of data in a reasonable amount of time, and to generate scientifically valid (i.e. reproduceable and objective) results, a single technique using a quality factor, such as χ^2, must be implemented. For this to proceed quickly, automation is required at some level.

4.4 AUTOMATING MOOG

There is no need to write an automatic spectral synthesizer, as MOOG is a sufficiently useful spectral synthesizer which can be fairly easily used in an automatic way. The program autoMOOG has been developed for exactly this purpose. Below is a description of those tasks which are performed by autoMOOG in the processing of stellar spectroscopy.

First, the parameter files for each star need to be generated. As much of the information will remain the same, a template parameter file can be used and simply updated with the relevant values for each star. Since the effective temperature and surface gravity to use can not be easily determined, the values as determined via external means are adopted. From the grid of models, the model which most closely matches these starting parameters is selected. The models used also assume a microturbulence velocity of 2 km/s, which Rossi et al. (2005) have shown their abundance determinations to be relatively insensitive to. For similar reasons, a $^{12}C/^{13}C$ ratio of 10 is adopted even though this is not necessarily applicable to all stars in this analysis.

Based on the line being fit, appropriate wavelength regions and the abundance to vary can be specified. All abundances are currently fit to the nearest 0.05 dex.

That said, MOOG is capable of simultaneously generating spectra with up to five abundances, so for the first pass, an input, starting abundance rounded to the nearest 0.05 is used, as well as the set of two abundances just above and below this initial abundance. If a star does not have an initial abundance, which is often the case, the model metallicity scaled abundance is used to start. If this is not a reasonable starting point, only a little extra time is required, but the ultimate derived abundance is no different.

The resolution of the synthetic spectra is chosen to be less than, although appropriate to, the resolution of the data. The synthetic spectra is then smoothed using a gaussian smooth, with a full-width at half-maximum (FWHM) appropriate to the data. The FWHM used, selected by the user and thus not fit, is a relatively stable variable which will not significantly alter abundance determinations. The location of the data no longer needs to be specified in the parameter file, as it will now only be used outside of MOOG.

Once this parameter file is prepared, MOOG is run, and five synthetic spectra are produced. These now need to be compared to our input data. First, using a cross-correlation technique for the region around Ca K, a non-heliocentric corrected radial velocity to apply to the data is calculated. The velocity resolution is directly related to the resolution of the synthetic spectra, and is thus typically $\lesssim$ 10 km/s. While this is less robust than fitting over a large spectral range with multiple strong lines, it ensures the best possible fit at the Ca K line, and this velocity is generally appropriate for any other feature as well. Since flattened, normalized spectra have already been produced, a slight shift to align the local continuum of the data and the model at the positions of the lines being fit is all that is needed to properly align the two spectra.

The χ^2 value for each synthetic spectra is then calculated, and the minimum from our initial five abundances is identified. If the minimum is at either end of

the initial set, spectra for the next five abundances in that direction are generated and compared against the previous minimum. This procedure continues until a true minimum is reached. Examples of the fits acheived by autoMOOG for a variety of stellar parameters can be seen in Appendix A.

Similar to the line index approach, this fit is first performed for the Ca K line, although any metallicity dependent feature will work. However, unlike the line index method which calibrates the strength of the KP index against the metallicity, the Ca K line is fit to get a calcium abundance, and then the α-enhancement values from equation 4.1 are used to derive [Fe/H]. An initial guess for [C/Fe] is also included in the metallicity fit to address the possible effect pointed out by Cohen et al. (2005), in which strong carbon features may contaminate the metallicity dependent lines. Once the metallicity has been determined, any other line can be fit. Following the line index method, the G band is fit to determine [C/Fe].

While generally not true for the Ca K line, often lines are indistinguishable from the continuum, or are hidden in noise. In these cases, an abundance can not be determined. Instead, an upper limit on the abundance can be calculated. Such an upper limit should be calculated from the flattening of χ^2 space as abundances are reduced. Unfortunately, this procedure has not yet been implemented, so an alternative is used instead.

For now, a G band is considered detectable if its deflection from the continuum is at least 5% the value of the continuum at that position. The upper limit values were determined by varying abundances of synthetic spectra and comparing their strengths against an essentially "zero" abundance spectra which was used as the continuum level. A surface in T_{eff}-log g space was then fit to these values. Stars with carbon abundances below this surface were reassigned with the value of the upper limit at that position. These stars are then appropriately flagged as being upper limits rather than true fits.

Until a proper upper limit determination is implemented, any lines to be fit would have to separately be defined in this way. Obviously, this is not practical, so for now only carbon fits at the G band will yield a proper upper limit determination where appropriate. An artificial threshold of [X/H] = −3.0, where X is the element to be fit, is used for all other upper limit determinations.

Although not shown here, autoMOOG is capable of fitting any element from any detectable line. Thus, it would be possible to, for instance, measure the abundance (or an upper limit) of s-process elements such as barium (4554 Å) or strontium (4078 Å), expected to be enhanced for many CEMP stars. In this way, CEMP stars could be roughly separated into the CEMP-s and CEMP-no classes. Radial velocities, determined automatically for the fit, can also be used for kinematic studies of the halo.

4.5 ERROR ANALYSIS

In order to estimate the errors on the abundances, a set of noiseless synthetic spectra across the grid of parameters was generated. Since these spectra had known parameters, the abundance determinations could be directly compared with the proper values. These spectra were first run through autoMOOG to determine any intrinsic scatter in the estimates. These errors are listed in Table 4.1. All of the errors are calculated as the quadrature sum of the 1σ scatter of the differences and the offset from zero of the distribution. In all cases, the scatter, rather than any offset, dominates this error determination. Also, the minimum errors are limited by the resolution of the abundance determinations, namely 0.05 dex.

Since the line index values for T_{eff} and log g are adopted in choosing a model, the line index errors in these parameters (150 K in T_{eff} and 0.51 in log g; Rossi et al. (2005)) need to be translated into errors on the abundances. Since [Fe/H] and [C/Fe] are fit internally, using the line index values only as a starting point, the line

Table 4.1. Errors in abundances from various sources

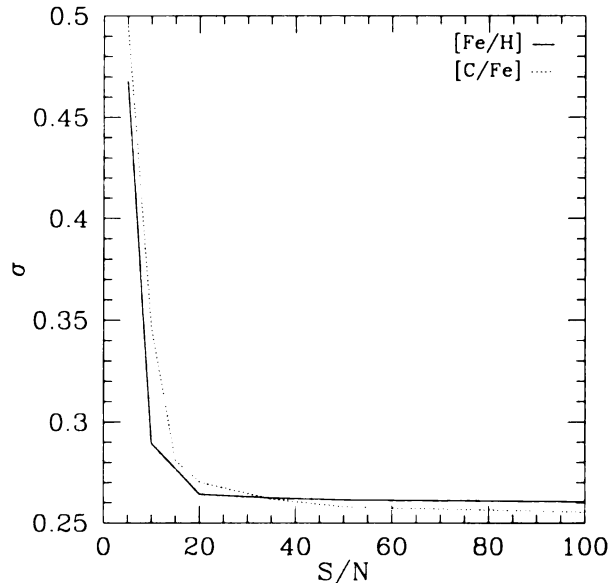|	Intrinsic	T_{eff}	log g	Total
[Fe/H]	0.090	0.232	0.065	0.257
[C/Fe]	0.101	0.152	0.168	0.249

Figure 4.4 The total error for [Fe/H] (solid line) and [C/Fe] (dotted line) versus Signal-to-Noise.

index errors for these parameters do not need to be considered.

To translate these errors, the same synthetic spectra used to determine the intrinsic error will be refit, with incorrect stellar parameters, corresponding to the line index errors and related to the spacing of the grid of models (i.e. ±100, ±200 K in T_{eff} and ±0.2, ±0.4 in log g), being provided to the routine. The resulting errors for [Fe/H] and [C/Fe] based on the uncertainties in these parameters are shown in Table 4.1.

What is seen is that [Fe/H] is fairly strongly dependent on temperature, but has virtually no dependence on surface gravity, whereas [C/Fe] is weakly dependent on

both. Overall, though, both values have nearly the same total error, $\sigma \sim 0.25$.

The error in the abundances due to the changing signal-to-noise of the data also needs to be considered. To determine this, varying amounts of noise were injected into the essentially infinite S/N synthetic spectra and they were run through autoMOOG again. This error combined with the previous errors can be seen in Figure 4.4. The total errors are then less than 0.30 for S/N $\gtrsim$ 10 for both [Fe/H] and [C/Fe].

CHAPTER 5:
VALIDATION

In order to truly test autoMOOG, it needs to be run on actual data, preferrably data for which high resolution spectroscopy has been obtained. A comparison of these results with other methods designed for lower resolution spectra, such as the line index method, which is particularly useful as it looks at the same features, would also be valuable. These comparisons are performed for two sets of data, as outlined below.

5.1   THE DATA

One set of data which was analyzed are the sample of stars observed by Bidelman & MacConnell (1973, hereafter BM), selected to be a collection of the most metal-poor stars found to date. This sample ranges from around [Fe/H] = −2.0 up to solar metallicity, and thus represents a modestly metal-poor, and carbon-normal, sample for our analysis. The high resolution results used in this study come from Cayrel de Strobel et al. (2001). The medium resolution spectra that are being fit were obtained by Norris et al (in preparation).

The other set of data are a sample of CEMP stars observed as part of the Hamburg/ESO R-Process Enhanced Star survey (HERES; Christlieb et al., 2004). Initially selected from the full Hamburg/ESO and HK survey, the HERES project attempted to obtain moderate resolution ($\sim$ 2Å) follow-up spectroscopy for metal-poor giant candidates. For bright stars confirmed to have [Fe/H] < −2.5, higher resolution

(R=20,000) spectroscopy was obtained. Their goal was to identify the 2-3% of these stars which showed large enhancements of r-process elements, so that investigations into the nature of these stars could be conducted.

As a consequence of these observations, several hundred metal-poor stars, many of them carbon-enhanced, were observed at moderate and high resolution. This then makes the perfect sample for the present analysis, as the medium resolution data can be run through our routine, and the high resolution results are available for the purposes of comparison.

5.2   RESULTS

Due to the high quality of the majority of the data, metallicities and carbon abundances were determined for nearly all the stars in the samples. A total of 913 stars were fit, including 529 from the BM sample and an additional 384 from the HERES sample. Comparisons of the results versus the line index estimates and high resolution results are plotted versus [Fe/H] and [C/Fe] in Figures 5.1 and 5.3, respectively. In some cases, stars had no metallicity or carbon abundance determination available from the line index method. In addition, many of the BM stars lacked high resolution metallicities, and almost none had high resolution carbon abundances. In all of these cases, abundances were obtained using autoMOOG, but obviously no comparison was possible and so these points are not plotted.

In addition, the temperatures used were determined by the line index method. At times, the parameters adopted for the high resolution analysis vary from these values, occasionally up to a difference of nearly 1000 K, although generally only by a few hundred K. As seen in Section 3.5, offsets in temperature by a few hundred K could lead to offsets in metallicity of $\sim$0.2 dex, and $\sim$0.15 in [C/Fe]. Due to the inconsistent nature of these offsets, this could lead to enhanced scatter or a general offset in any of the comparisons to high resolution.
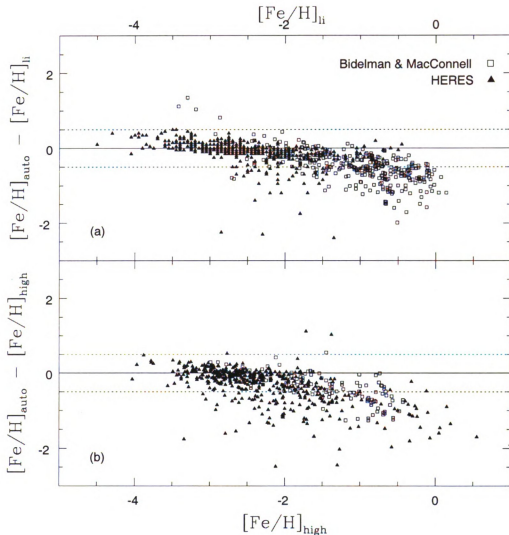
Figure 5.1 Comparisons of metallicity between our routine and the values as determined from (a) the line index method and (b) high resolution analysis. In both cases, the higher metallicity, carbon-normal BM stars are plotted as open squares, while the more metal-poor, carbon-rich HERES stars are plotted as filled triangles. The solid line corresponds to agreement with the various abundances. The dashed lines to either side correspond to a difference of ±0.5 dex.

When comparing results for metallicity with the line index estimates and the high resolution analysis (Figure 5.1), it can be seen that there exists a generally good agreement at low metallicities, with a small scatter and no appreciable offset. There appears to be a small slope in the comparison with the line index values, although this is not present in the high resolution comparison. This would suggest that the problem actually lies within the line index method, and indeed, it is already a known issue with this method.

At higher metallicities, in particular for stars with [Fe/H] > -2.0, the scatter increases and the offset is a little larger. Overall, however, the slope remains largely the same. In fact, it appears that the generally good agreement at the lowest metallicities seems to deviate more and more as higher metallicities are reached, increasing both the overall scatter and the deviation from agreement.

These are the same stars which are problematic for the line index method. As the metallicity of a star increases, the strength of the Ca K line continues to grow, and its profile changes as its wings broaden. In addition, numerous other lines which were very weak at low metallicity have also gained in strength, and contribute to an overall dampening of the local apparent continuum. The overall effect of this is that the area of the Ca K line with respect to the apparent continuum, the KP index, approaches some fixed value, the KP saturation value. For these high metallicity stars, different approaches are then implemented as part of the line index method to determine the metallicity of the star. This is why the line index values in this comparison seem to agree fairly well with the high resolution abundances, at least in how they both compare with the autoMOOG results.

Spectral synthesis, however, should be robust enough to account for this high metallicity effect. Even so, a quick glance at Figure 5.1 reveals that this does not appear to be the case. However, the fault lies not with the synthetic spectra, which properly reproduces the apparent continuum and the Ca K profile, but rather with

the flattened, normalized spectra used to compare against.

When a continuum is fit to a spectra to produce a flattened, normalized spectra, it is placed along the apparent continuum level of the star. At low metallicity, the absence of strong features means that the apparent continuum is close to the position of the true continuum. As the metallicity increases, especially for $[Fe/H] \gtrsim -1.5$, the apparent continuum gets farther and farther from the true continuum. Continuing to fit the apparent continuum will thus yield larger and larger scaling inconsistencies in the normalized data, producing things which are further and further from the true shape of the spectra.

In order to properly explain this problem, synthetic spectra of various metallicities need to be examined. Plotted in Figure 5.2 are the synthetic spectra of a star with $T_{eff} = 4800$ K and $\log g = 2.2$ with possible metallicities of $[Fe/H] = -1.75$ (dashed line) and $[Fe/H] = -0.60$ (solid line), exactly as they came out of MOOG. It is immediately apparent that the large central feature of the Ca K line is much broader for the higher metallicity than the lower. In addition, the apparent continuum for the higher metallicity spectrum is much lower (at ~ 0.5) than the lower metallicity (at ~ 0.7). These two spectra are clearly different from each other, and there should be no confusion when selecting one of these based on the observations of a star.

Overplotted on these synthetic spectra are the data from star CD-57 949, taken from the BM sample. The filled triangles correspond to the flattened, normalized spectra as produced from the continuum fit to the data. The open triangles, on the other hand, are the exact same data after application of a scaling factor selected to best match the higher metallicity synthetic spectra. Based on the input, filled triangle spectra, autoMOOG appropriately selected a metallicity of $[Fe/H] = -1.75$ for this star. The fit is far from perfect, but is at least reasonable based on the appearance of the data. The filled triangle data is clearly better matched by the lower metallicity spectrum than it is by the higher metallicity.
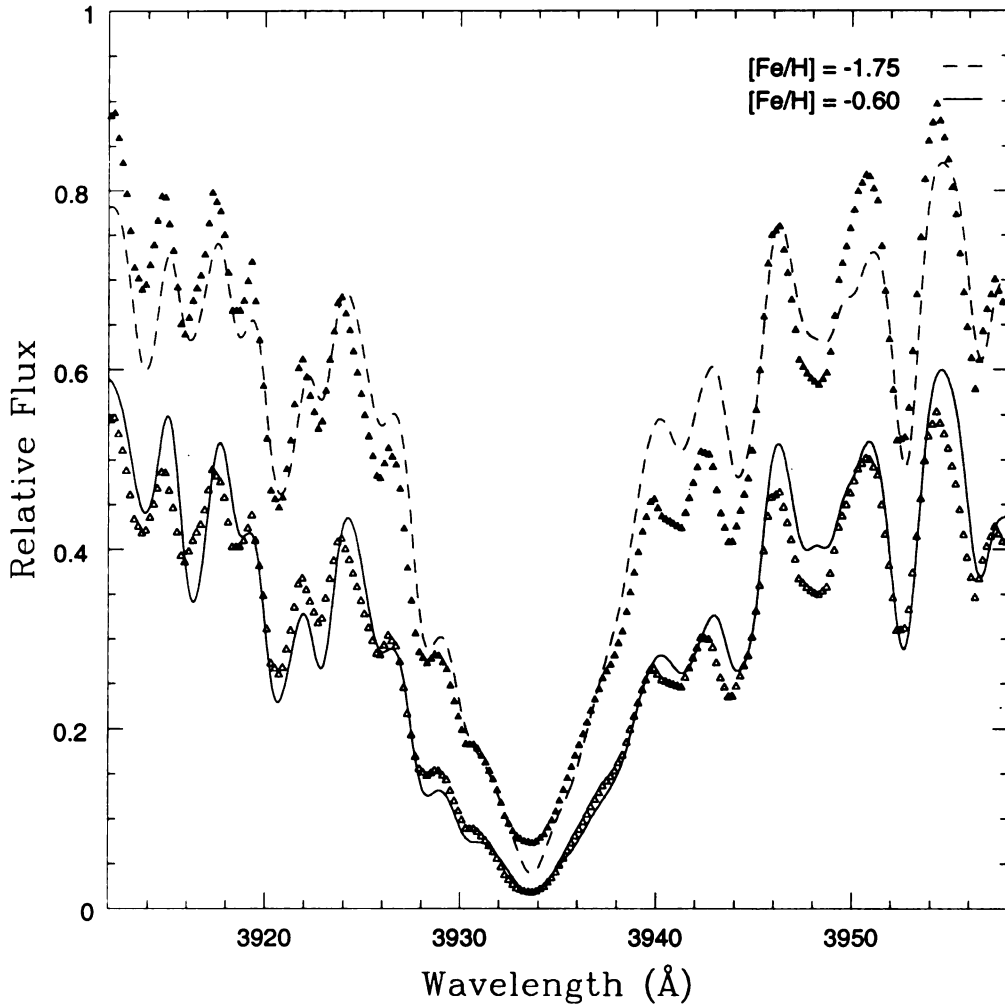
Figure 5.2 Synthetic spectra near the CaII K line assuming [Fe/H] = -1.75 (dashed line) and [Fe/H] = -0.60 (solid line) for a star of T_{eff} = 4800, $\log g$ = 2.2. Overplotted are points corresponding to data from a star in the BM sample, using the data created after the continuum fit (filled triangles) and that same data scaled (open triangles). Note the apparent continuum levels at around 0.7 for the metal-poor spectra, and around 0.5 for the metal-rich.

However, the higher metallicity synthetic spectra, at [Fe/H] = -0.60, is close to the actual metallicity of CD-57 949. If the data were appropriately scaled, like it is with the open triangles, it would much better match this spectra. Even in this rough simulation, it is fairly clear that the open triangles match the higher metallicity synthetic spectra much better than the filled triangles match the lower metallicity. Unfortunately, since the input data is scaled as the filled triangles, an incorrect, and always lower metallicity, synthetic spectra is chosen as the best fit. This problem becomes more and more severe at higher and higher metallicities as the apparent continuum is further and further surpressed relative to the true continuum, resulting in larger deviations to lower selected metallicities.

This then is the reason behind the difficulties at high metallicities. Until a proper scaling is used, possibly just by better locating the true continuum, this will continue to be a problem. There is currently no solution in place to account for this problem. Until this happens, autoMOOG will not properly determine metallicities for stars with [Fe/H] $\gtrsim$ -1.0. However, as the goal of this work is to study phenomenon at the lowest metallicities, this is not an immediate concern, as the lower metallicities seem to be properly recovered.

Turning now to an analysis of the fits on carbon, [C/Fe], compared to the line index and high resolution abundances (Figure 5.3), a good agreement is seen all around. With no appreciable slope or offset, a reasonable scatter is all that is apparent. Plotted are only those stars for which fits as opposed to upper limits were obtained, and those stars which had line index or high resolution abundances. Obviously, very few of the BM sample had high resolution carbon abundances available. The concentration of BM stars right at [C/Fe] = 0 is also clearly noticeable, while the HERES sample is spread over the full range of carbon.

It might seem as though the [C/Fe] fits would be dependent on the quality of the [Fe/H] fits, and would thus exhibit the same sort of behavior. While some of the larger
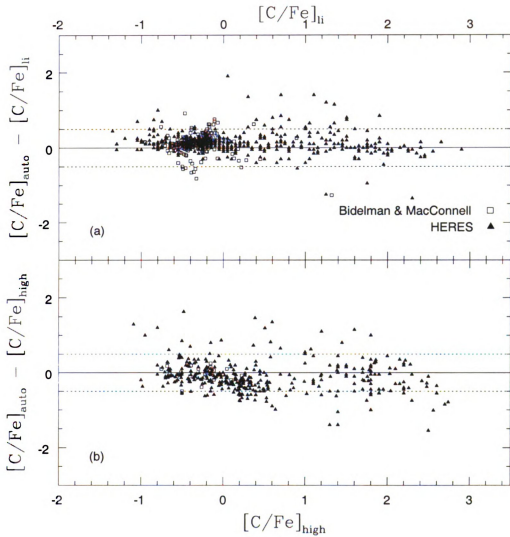
Figure 5.3 The same as Figure 5.1, except for [C/Fe]. Only stars which have carbon fits are plotted, not those with only upper limits.

scatter may in fact be due to this, overall this is not really the case. The reason for this is that the carbon fits are primarily a fit of [C/M], where M is the scaled model abundance. So, when fitting the G band, it is neither [C/Fe] nor [C/H] that is being fit, but rather this model dependent carbon. To ultimately derive [C/Fe], this carbon value needs to be offset by the deviation of iron from the model. It is during this step that the metallicity difficulties may be applied to the carbon fit. However, this offset is generally small relative to the overall fit, and likely results in nothing more than some additional scatter.

It is also possible to use these results to perform an internal consistency check on the method. Since a number of stars from the BM sample have been observed mulitple times, the abundances determined for each individual spectra can then be compared to each other to see if autoMOOG determines the same relative abundances for a given star, regardless of the spectra used. For each star, an average metallicity and carbon abundance are calculated from the available data, and then the residuals between each individual abundance and the average are calculated.

For both metallicity and carbon abundance, a very small scatter around zero of around 0.02 dex is observed, consistent with the intrinsic errors (Table 4.1). The scatter for [Fe/H] at high metallicities may be slightly larger than elsewhere. This is assumed to be a result of the exact continuum fit used for each spectra, and is thus associated with the general high metallicity difficulties. Even so, this scatter is still quite small, increasing by no more than 0.01 dex.

5.3 UPPER LIMITS

When the G band can be properly fit, the correct [C/Fe] is generally produced. It would, however, be worthwhile to also find out under what conditions only an upper limit is obtained. The detectability of the G band relative to temperature and metallicity is analyzed in Figures 5.4 and 5.5, respectively.
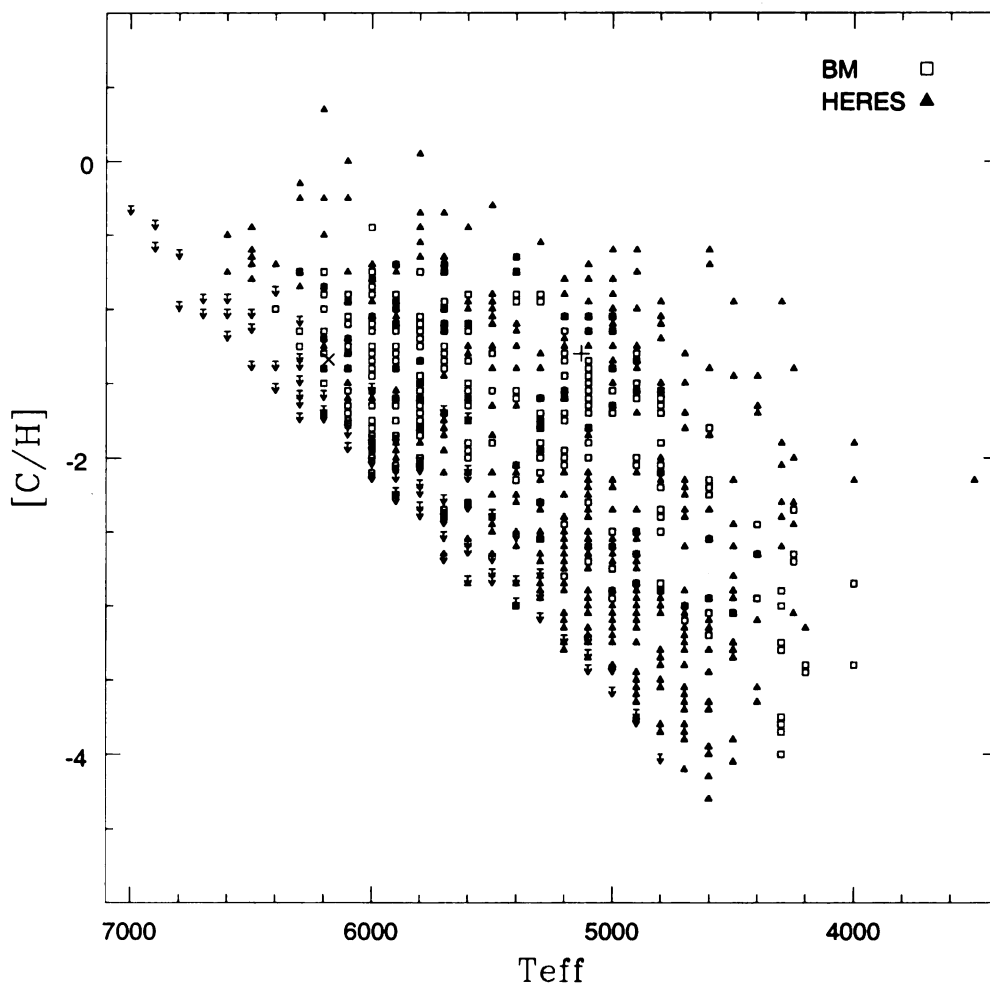
Figure 5.4 Carbon abundances ([C/H]) plotted versus effective temperature. Plotted are the abundances for the BM sample (open squares) and the HERES sample (filled triangles). All upper limits are denoted with an arrow. The HMP stars HE 1327-2326 and HE 0107-5240, not studied here, are displayed as the x and +, respectively.

In Figure 5.4, the carbon abundance, [C/H], is plotted versus effective temperature using the values from autoMOOG. The stars in these samples cover a fairly wide range of temperatures, from 4000 K to 7000 K. Both samples of stars seem to cover about the same temperature range.

The G band is a molecular line, which will, for the same abundance of carbon, be stronger at lower temperatures. As you increase in temperature, the G band weakens until it is no longer detectable. The point where this happens is obviously dependent on the level of carbon enhancement, [C/H], and is easily seen in the plot. [C/H] is used for this analysis as it is solely a measure of the carbon abundance, without any implicit assumptions about overall metallicity, which, along with the temperature, is all the strength of the G band depends on. From the line of detectability, it can be seen that for cool stars, the G band can essentially always be detected. However, for warm stars, those especially above 6000 K, carbon abundances must be fairly high to be detected. Indeed, for temperatures above 7000 K, it seems unlikely that carbon could be measured at all, regardless of the quantity of carbon. In part, this is due to the apparent upper limit on [C/H].

Although there are a handful of stars with slightly higher carbon abundances, a general limit to the allowed carbon abundances falling at [C/H] $\sim$ -0.5 can be seen, which is higher than some have found (Ryan, 2003; Frebel et al., 2006), while lower than others (Cohen et al., 2005; Lucatello et al., 2005). It is highly likely that the true location of this upper limit is temperature dependent, with cooler stars exhibiting a lower value, and warmer stars higher. This may be seen in this data, and could further be supported by the previously mentioned results, and is presumeably due to evolutionary effects.

In any magnitude-limited survey, such as SDSS, a sample of cool stars will tend to consist primarily of giant stars rather than dwarf stars, due to the higher luminosities of giants at a given temperature. As such, the coolest stars in these samples are

probably giants while the warmer stars are more likely to be dwarfs. As discussed previously, surface carbon abundances are diluted during convective mixing episodes during giant branch ascent. In this way, the observed [C/H] of a star may decrease by maybe 0.3 to 0.6 dex. Obviously, this means that dwarf stars will reach a higher [C/H] limit than will giant stars. Although the evidence is not strong in Figure 5.4, a slight trend is noted and is on the order of these dilution effects. As shall be seen, this evolutionary effect should also play a role in the definition, and thus frequency, of carbon enhancement.

Although abundances are diluted in giant stars, molecular carbon features are easier to detect due to their cooler temperatures. As a result, samples of CEMP stars which are selected based on colors or the detection of strong carbon features in their spectra will be biased towards giant stars. Any such sample will produce a lower CEMP fraction than a sample of just dwarfs or even a sample with an even mixture of evolutionary states, like an intermediate age globular cluster. Careful analysis of evolution is thus necessary for any determination of CEMP frequency.

Although the two samples do not fully complement each other, as seen in their combined MDF (Figure 5.5), their results can still be used to analyze the detectability of the G band with respect to metallicity. Plotted in Figure 5.5 is the MDF of the full samples of stars, and the MDF of stars with only a determined upper limit.

This second set of stars overall traces the shape of the full MDF, although accounting for slightly larger percentages of stars as metallicity is decreased. This is not surprising, as metal-poor stars have, by definition, low abundances and weak lines. However, due to the high quality of these samples, carbon abundances are able to be determined for a significant fraction of stars, even at the lowest metallicities.

For the G band to be detected, a fairly large amount of carbon is needed. For a [Fe/H] = -3.0 star, even a CEMP star with [C/Fe] = 1.0 only has [C/H] = -2, which, according to Figure 5.4, would only be detectable for a star cooler than $\sim$5500 K.
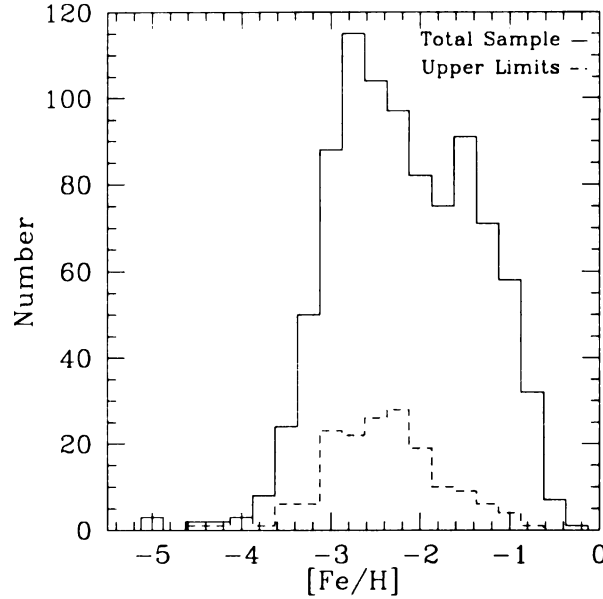
Figure 5.5 Metallicity distribution function for the full HERES and BM sample (solid line) and those stars for which only an upper limit on carbon have been determined (dashed line).

Therefore, it can also be said that for stars with [Fe/H] < -3.0, the G band is likely not detectable without a substantial [C/H] (not [C/Fe]), depending again on T_{eff}. At these low metallicities, [C/Fe] seems less a measure of carbon enhancement as it does iron deficiency. While this could merely point to a flaw in using the G band to determine C abundance in certain T_{eff}-log g regimes, it might also be suggestive that a definition of carbon enhancement based on [C/Fe] may not be ideal.

As a further example, the Hyper Metal-Poor (HMP; [Fe/H] ≤ -5.0 as in Beers & Christlieb (2005)) stars HE 1327-2326 (T_{eff} = 6180, [Fe/H] = -5.6, and [C/Fe] = 4.26; Aoki et al. (2006)) and HE 0107-5240 (T_{eff} = 5130, [Fe/H] = -5.3, and [C/Fe] = 4.0; Christlieb et al. (2004)) can be examined. These stars have [C/H] = -1.34 and -1.40 and are indicated as the "x" and "+", respectively, in Figure 5.4. Even with similar values of [C/H], HE 1327-2326 falls very close to the line of detectability, while HE 0107-5240 falls well above.

This is largely due to HE 0107-5240 being a giant star, while HE 1327-2326 is

a sub-giant star. Thus, evolutionary state needs to be taken into account when determining carbon enhancement, as has been done recently by Aoki et al. (2006) and Lucatello et al. (2006), although they continue to define carbon enhancement based on [C/Fe]. However, if a star with [C/Fe] $\geq$ 4.0, well above the [C/Fe] $\geq$ 1.0 criteria for CEMP inclusion, may or may not have detectable carbon features at medium resolution, it probably should not be considered to be *very* enhanced in carbon, if it is even included as a CEMP star. Even [C/H] does not seem to be an ideal solution, although it would be less affected by iron deficiencies. Ultimately, a definition of carbon enhancement which is physically motivated is needed. Until theory has produced such a discriminator, the observational definitions must prove sufficient.

5.4 DISCUSSION

The two validation samples span nearly the full range of known metallicities, and sample an assortment of carbon abundances. By covering this much parameter space, it can be seen exactly where autoMOOG is appropriately used and is unlikely to come across any stars which do not behave in a well understood way.

For stars with [Fe/H] $\leq$ -2.0, both the metallicity, [Fe/H], and carbon abundance, [C/Fe], are able to be successfully recovered for the majority of the stars in the samples. Despite the known problems with their metallicities, the carbon abundances for the more metal-rich stars are similarly recovered.

From Figure 5.4 it can be seen that both the carbon-normal and carbon-enhanced samples span nearly the same range of temperature and [C/H]. Indeed, from these two parameters, there is no way to discern which sample is the carbon-enhanced sample. Only by looking at [C/Fe], and thus metallicity, do these samples separate in any reasonable way.

Looking at a plot of [C/H] (or alternatively [C/Fe]) versus metallicity (Figure 5.6,
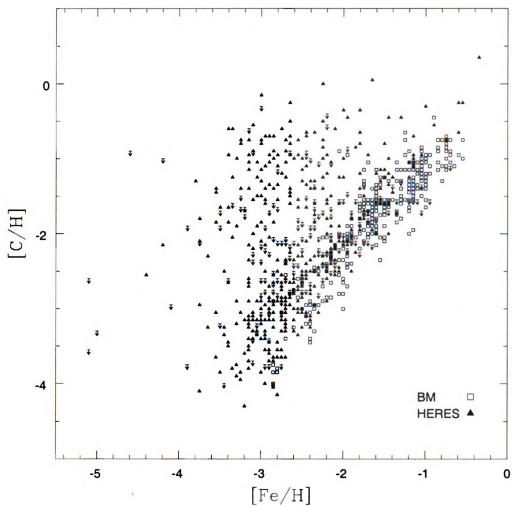
Figure 5.6 The same as for Figure 5.4, but for [C/H] versus [Fe/H].

a few very distinct patterns can be immediately noticed. First, the bulk of stars fall on a diagonal line which shows increased [C/H] as metallicity increases. Above this line is nothing but scattered points, stretching from this line to the upper limits of [C/H] near -0.5. These scattered stars all have carbon abundances higher than those along the main line, and are thus known as carbon-enhanced stars, as opposed to the carbon-normal stars which fall on this line.

Looking at it like this, the two samples once again behave as expected, with almost all of the carbon-normal BM stars falling indeed along the line of normalcy. The HERES sample, which has been denoted the carbon-enhanced sample, also falls mostly along this line of carbon normalcy. However, nearly every star in these samples which exhibit enhanced carbon abundances comes from this sample, earning it that moniker.

Although no stars are seen below this carbon-normal line, it is unclear whether this is a detectability issue, or a real lack of stars. If this truly represents a lower limit to the carbon levels as a function of metallicity (this line corresponds to a value of [C/Fe] $= 0$), then this is telling us something interesting. This suggests that the bulk of stars undergo some process which produces a relative level of carbon and iron exactly as seen in the Sun. This might also correspond to some sort of carbon-iron equilibrium that more carbon enhanced stars may not pass as they accumulate higher iron abundances. This could be the natural consequence of a metallicity dependence on carbon production.

The remainder of the stars, those not falling on this line, the so-called carbon-enhanced stars, clearly show evidence of something else. Due to the general scatter and lack of noticeable pattern, this suggests that these stars have likely undergone some process which are less tightly constrained and more prone to large fluctuations. Alternatively, the carbon and iron seen in their atmospheres may be produced in uncorrelated mechanisms.

It is possible that the fraction of stars classified as carbon-enhanced increases as metallicity is decreased due primarily to the increased room between the line of carbon-normalcy and the carbon upper limit as metallicity decreases. Since the scatter of carbon-enhanced stars is essentially uniform, the 3 to 4 dex to work in, versus maybe a single dex at [Fe/H] = -2.0, means that that many more carbon-enhanced stars must exist at the lowest metallicities. Naively, this would seem to suggest that the fraction of carbon-enhanced stars with [Fe/H] = -3.0 should be approximately two times the fraction of carbon-enhanced stars with [Fe/H] = -2.0. Clearly then, this fraction increases rapidly with declining metallicity.

Although the mechanisms which produced either set of stars can not be specified from this plot, the slope of the carbon-normal line, and the existence of an absolute maximum carbon abundance, can predict the relative fractions of carbon-enhancement as a function of metallicity.

The frequency of carbon-enhancement below a given metallicity, the typical value calculated due to the small sample sizes at low metallicity, is also dependent on these factors, but add the complexity of the MDF into the calculation. As MDF's are largely empirical, such a frequency calculation is less clear and concrete.

CHAPTER 6:
THE FREQUENCY OF CARBON
ENHANCEMENT

Now that we have developed a technique to quickly calculate metallicities and carbon abundances, and have checked the quality of the results using available samples with high resolution results, we may address the issue of the frequency of carbon enhancement as a function of metallicity. To do this, a large sample of stars will be needed, selected in such a way that they should show no bias for or against any of the physical traits we are attempting to analyze. This data should also be of relatively high quality, in terms of signal-to-noise, although the resolution of the data is not a strict constraint.

As part of the calibration efforts for the Sloan Digital Sky Survey, eight targets on each spectroscopic plug plate were assigned as spectrophotometric standard stars (PHO), and eight were chosen as reddening estimation stars (RED) (Stoughton et al., 2002). These stars were selected, using color cuts of $0 \leq g - r \leq 0.6$, to be F type near turn-off stars, due to the generally clean nature of such spectra, containing primarily just Balmer lines and Ca H & K. The samples are separated in apparent magnitude, with $15.5 < g < 17$ for the PHO sample, and $17 < g < 18.5$ for the RED sample. Through the end of the fifth data release (DR5; Adelman-McCarthy et al. (2007)), both calibration samples together accounted for the observations of 24,368 such stars.

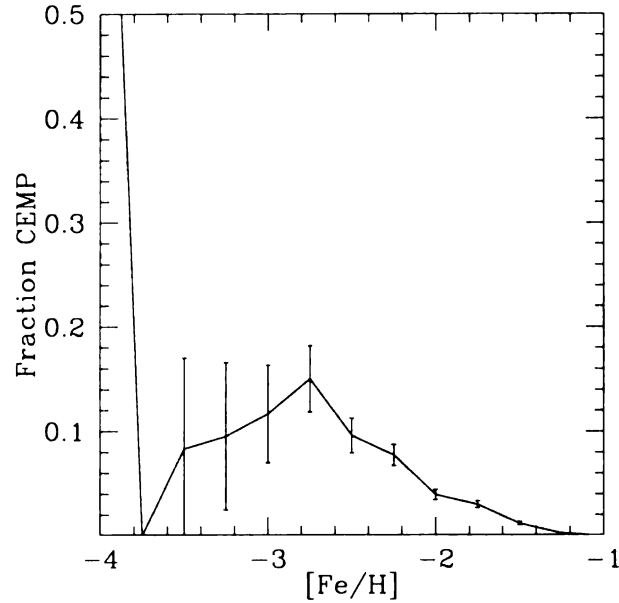Thus, these stars were not selected based on metallicity or carbon enhancement,

Figure 6.1 The frequency of carbon enhancement at a given metallicity for the combined PHO and RED samples.

and make an excellent sample for this analysis. However, due to the cleanliness of their spectra, and the generally warm temperatures of F type stars, the ability to detect a G band and thus determine a carbon abundance may be severely limited. If carbon could be measured in all of these stars, it would make an ideal unbiased sample of stars from which to calculate the frequency of carbon-enhancement. As it is, it should still begin to reveal the shape of carbon-enhancement in an unprecedented way.

6.1 FREQUENCY OF CEMP STARS

From the determinations of metallicity and carbon abundance, the frequency of carbon enhancement as a function of metallicity was determined (Figure 6.1). Due to the selection of the PHO and RED samples, each sample, as well as the combined samples, can be looked at independently when addressing the issue of frequency. However, each individual sample yields essentially the same results, and are well represented by the

combined samples, so our analysis will focus solely on that. A very low frequency at high metallicities ($[Fe/H] > -1.0$) is seen, gradually increasing at lower metallicities. This fraction goes from around 5-7% of stars with $[Fe/H] = -2.0$ to around 15% of stars with $[Fe/H] = -3.0$.

Due to the lack of stars, specifically those with detectable carbon features, with $[Fe/H] < -3.0$, it is difficult to say if this trend of increasing frequency continues to the lowest metallicities. Even if it does, it is difficult to say what the shape of this quantity would look like – whether it would continue to steadily increase, reach some plateau, or increase faster and faster.

Although the general frequency of carbon enhancement at any metallicity is worth determining, the recent interest in this quantity has largely been in its value at the lowest metallicities, especially below $[Fe/H] = -3.0$. Unfortunately, this is exactly where this data starts to break down, and where no results are immediately available.

Due to the relatively small samples of stars with $[Fe/H] \leq -3.0$, the usual thing done in this sort of analysis is to look rather at the frequency of carbon enhancement below a given metallicity, or a cumulative carbon fraction, as this allows for an artificial inflation of the sample sizes. This will also make it possible to directly compare our results to those of others.

Figure 6.2 is then the cumulative fraction of CEMP stars below a given metallicity. Again, the same behavior of an increasing fraction of CEMP stars at lower metallicities is seen until around $[Fe/H] = -2.5$. At this point, the curve turns over and starts to descend. However, this again is not the true behavior of the carbon fraction, but rather the effect caused by our incomplete knowledge of the carbon abundances of the sample, especially at low metallicities.

For comparison purposes, several CEMP fractions from the literature have been included in Figure 6.2. Except for the low metallicity turn-over, these results best match the results of Frebel et al. (2006), and are below the remainder of results.
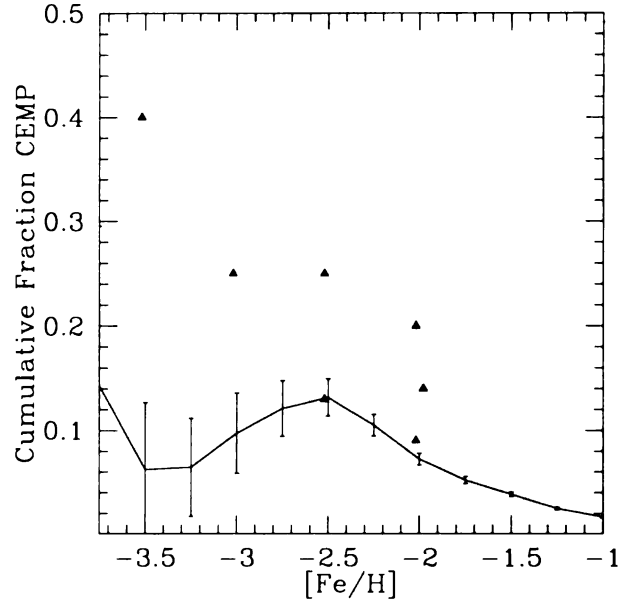
Figure 6.2 The frequency of carbon enhancement below a given metallicity for the combined PHO and RED samples (solid line) and values as reported in the literature (filled triangles).

This could suggest that this sample is primarily composed of giants rather than true turn-off stars. This would actually make some sense, as the color cuts used to select the F type stars were made assuming solar metallicity stars. Lower metallicity stars are bluer than this, and thus these same color cuts would sample a larger fraction of giant stars, which are redder, than would be expected.

The more metal-poor we get, the more we're looking at the fraction of CEMP giants rather than CEMP dwarfs. As has been discussed previously, this will yield a lower CEMP fraction due to dilution of surface carbon abundances during giant branch ascent.

However, this is not the only cause for these results. Due to the undetectablity of the G band for regions of the sample, all of these fractions actually correspond to lower limits. Since only stars with detected G bands which qualify as CEMP are included in the numerator, but all stars regardless of G band detectability in the denominator, these fractions actually correspond to hard lower limits, so the true
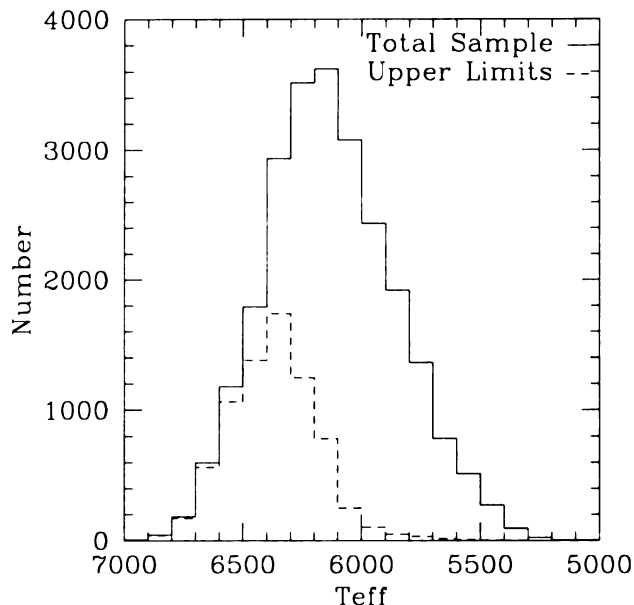
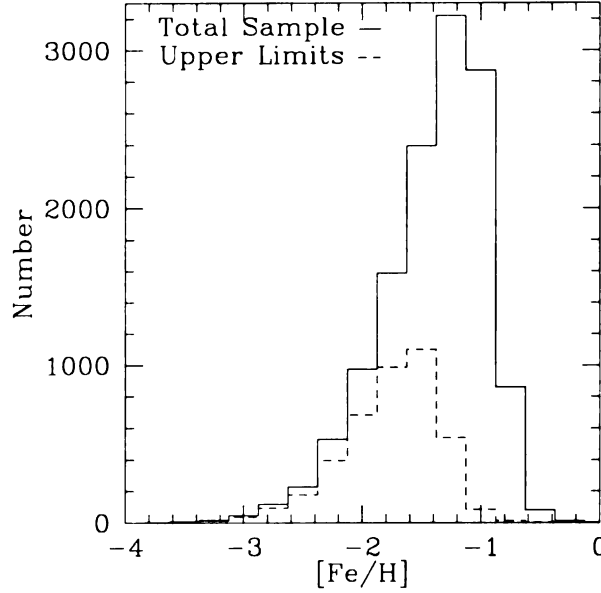Figure 6.3 The temperature distribution functions for the full sample (solid line) and the stars without detectable G bands (dashed line).

fraction for this sample must lie above these values, to within the error.

So, while the other literature values seem much higher than these results, especially at the lowest metallicities, the true fraction contained in this sample could easily be in agreement with any of these other values. In order to truly compare these results, the incompleteness of this sample must be studied in greater detail, and then several techniques to attempt to recover some of this lost information from the data will be used.

6.1.1 AREAS OF INCOMPLETENESS

With this new sample of data, the completeness of the data will be looked at again in terms of a detectable G band with respect to temperature and metallicity.

When looking at the distribution of our full sample and the sample of stars which lack detectable G bands as a function of temperature (Figure 6.3), a clear sign that detectability is lost at warm temperatures is seen. Since the G band is a molecular

Figure 6.4 The metallicity distribution functions for the full sample (solid line) and the stars without detectable G bands (dashed line).

feature, and is thus less stable at higher temperatures, this comes as no surprise. Almost all stars with $T_{eff} > 6500$ K are lost, but larger numbers are retained as the temperature is decreased. For stars with $T_{eff} < 6000$ K, the sample is nearly complete. This fact will be important during our recovery attempts.

When looking instead at the distribution versus metallicity (Figure 6.4), we see, like in Figure 5.5, an overall tracking of the MDF, with stars at all metallicity being lost at some level. However, due to the generally warmer stars in this sample, a much larger portion of weak-lined metal-poor stars are being lost than previously. Indeed, the incompleteness is fairly severe for [Fe/H] < −2.0, and below −3.0 hardly any stars survive.

With this information in mind, let's look again at the cumulative fractions (Figure 6.2). What was seen as a turning over in the fraction at [Fe/H] = −2.5 is then due to the severe incompleteness below this level. However, this incompleteness is still fairly strong above this threshold, and indeed continues at some level for the full range

of metallicity plotted. This means that not only might the fractions at the lowest metallicities, below this turning over, be much larger and more in agreement with previous results, but the whole set of fractions could easily increase.

6.2 RECOVERING FROM THE INCOMPLETENESS

In order to get a rough idea for what the true fraction of carbon enhancement in this sample may be, an attempt at several independent techniques to recover information from the data will be made based on various noticeable trends. Hopefully these techniques yield similar results and represent a closer-to-true frequency.

6.2.1 ATTEMPT ONE: SIMPLE DENSITY ARGUMENTS

As was briefly discussed in §5.4, one possible reason for the increase in the fraction of CEMP stars at low metallicity may be due to the increasing size of available carbon abundance parameter space. In other words, at low metallicity, the area between the upper threshold of [C/H] and the line of carbon-normalcy increases.

If the distribution of stars above the carbon-normal line is random, then a simple density of states argument can be made to infer the relative fractions of CEMP stars at various metallicities. A proper analysis should be done which verified the randomness of this sample, but for the moment a rough treatment of this issue will suffice. For the moment, a random distribution will be assumed.

Then, if an approximate area between the upper threshold at [C/H] $= -0.5$ and the line of normal carbon is determined, and normalized to the area at [Fe/H] $= -2.0$, then we have relative factors of 2 for [Fe/H] $= -3.0$, 3 for [Fe/H] $= -4.0$, and 0.25 for [Fe/H] $= -1.0$. In other words, the fraction of CEMP stars at [Fe/H] $= -4.0$ is roughly three times the fraction at [Fe/H] $= -2.0$. Thus, this fraction increases quite rapidly, but seems to do so in a linear fashion.

It should also be noted that this only indicates the relative fractions of CEMP

stars at a given metallicity, not the cumulative fractions that we have been working with. To determine these cumulative fractions, an assumption must be made about the shape of the MDF of the sample. However, for the sort of back of envelope calculation being made here, an assumption that this fraction and the cumulative fraction are approximately equal will be made. If this method proves reasonable, a full treatment can be performed as part of a future analysis.

In order to recover information using this method, a metallicity which is roughly complete is needed. Looking at Figure 6.4, it can be seen that the sample is approximately complete at $[Fe/H] = -1.0$, but not at any lower metallicities. We can use the fraction at this metallicity to roughly calculate the fractions at lower metallicities.

Using these scaling factors, the fractions listed in Table 6.1 are recovered. The new fraction at $[Fe/H] = -2.0$ is very nearly the same as it was initially, suggesting that this sample may in fact be mostly complete at this metallicity. The new fractions at $[Fe/H] = -3.0$ and -4.0 increase considerably, although they are still quite a bit lower than the literature values at these metallicities.

6.2.2 ATTEMPT TWO: SHAPE OF CARBON DISTRIBUTION

For the second attempt, we're going to assume that the shape of the carbon ($[C/Fe]$) distribution function (CDF) is the same for any subsample of stars. In particular, we assume that the high carbon tail of the curve is the same, specifically the curve of $[C/Fe] \geq +1.0$. Based on the distribution of $[C/Fe]$ with metallicity, this is not really a valid assumption when applied to subsamples of stars selected on the basis of metallicity. However, it should be mostly valid for subsamples based on temperature.

With the exception of the evolutionary effect on the carbon abundance of a star, different subsamples of stars with different temperatures should have similar distributions of carbon. The evolutionary effects would tend to just shift the whole distribution, without changing its overall shape.

We also assume that those stars which are dropping out of our results due to carbon undetectability are those with a smaller carbon abundance. In other words, CEMP candidates with [C/Fe] just over the 1.0 threshold are more likely lost than those with [C/Fe] = 3.0. Thus, if we match up the tail of the CDF curve for [C/Fe] $\gtrsim$ 2.0 for individual temperature subsamples, we can deduce the approximate number of stars that should exist as CEMP stars in the lower portion of the curve.

In order to do this, the shape of the high end tail of the CDF needs to be determined using a more complete sample. For this purpose, we will make use of the sample of stars observed as part of the HERES program, which have previously been used as part of our validation efforts (§5.1).

For this recovery attempt, we can only look at the cumulative fraction of CEMP stars, as we can separately analyze our CDF tail only for samples of stars selected to have a given metallicity or below. Due to the relatively small sample sizes, this technique is only usable as an integrative method, and can not be used to recover true fractions at a given metallicity. This will, however, match the previous results.

Figure 6.5 looks at the tail of the CDF for stars with [Fe/H] $\leq$ −2.0, both for the HERES sample and for our incomplete SDSS sample. Clearly, in a curve such as this, the incompleteness of the sample is smoothed out of the results, so a global recovery of this sort is not possible. Individual temperature bins should still be feasible.

The shape of this tail for these two curves is surprisingly similar. Despite the deviation just above [C/Fe] = 1.50, the global shapes are nearly the same, and come out quite naturally just by normalizing each sample based on the total number of CEMP stars in that sample. This is a very encouraging result which lends weight to the usefulness of this technique, and its presumed applicability.

In order to maintain reasonable numbers of stars, the full sample was broken into subsamples based on effective temperature with a $\Delta T = 200$ K. For the coolest subsamples of stars, due to their near completeness, we would not expect to recover
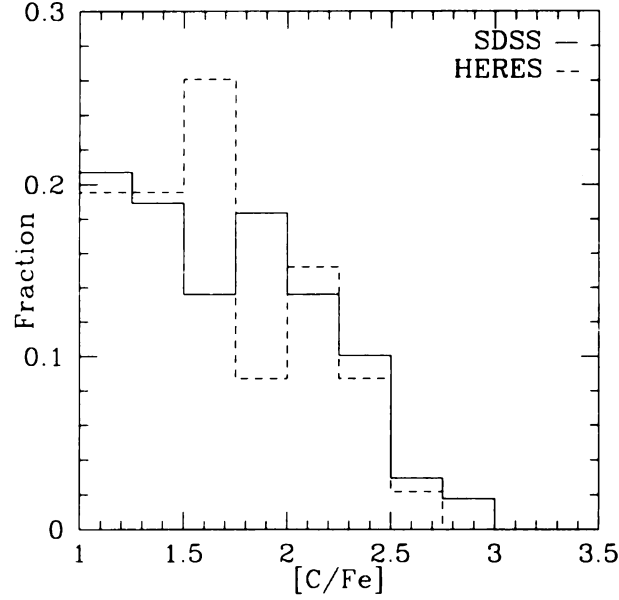
Figure 6.5 The high end tail of the carbon distribution function for the HERES sample (dashed line) and the SDSS stars (solid line).

anything using this method, and indeed that proves to be the case. In fact, for some of these samples, they did not extend to the highest values of [C/Fe], but well matched the lower regions of the curve. This, again, is likely due to our evolutionary effects, as many of these cooler stars are giants. Unfortunately, this may point to a potential flaw in this technique and might suggest that a temperature based selection is not, for this sample at least, a truly unbiased criteria. Even so, this analysis will continue in the hopes that some useful information might still be gathered.

To better illustrate this technique, an intermediate temperature bin ($6150 \leq T_{eff} < 6350$) is plotted against the curve for the two full samples (Figure 6.6). Clearly missing are around half of the stars with $+1 \leq$ [C/Fe] $\leq +1.5$, which can then be recovered as presumably being true CEMP stars. This is then done for each temperature bin, until a full set of recovered CEMP stars can be added to the known CEMP stars, and a new frequency can be calculated. This was also done looking at the curves for all stars with [Fe/H] ≤ -1.5 and [Fe/H] ≤ -2.5. The recovered
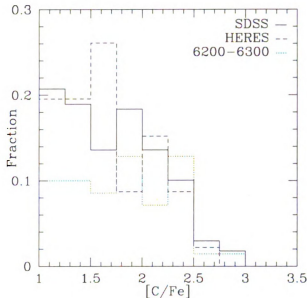
Figure 6.6 Same as Figure 6.5, but with an additional curve corresponding to an intermediate temperature bin included to illustrate the technique.

fractions are listed in Table 6.1.

6.2.3 ATTEMPT THREE: COMPLETE SUB-SAMPLES

Based on the completeness curve with respect to temperature (Figure 6.3), it can be seen that a sample of stars selected to have $5500 \leq T_{eff} \leq 5900$ will be a fairly complete sample, and just about the largest sample that can be put together that would be that complete. Unfortunately, as it is fairly cool, it will primarily consist of giant stars, so the fractions calculated will be the CEMP fraction of giants below given metallicities. However, since it seems that any fraction calculated with this sample is essentially a fraction of giants, this just means that our results will be lower than the fraction of dwarfs, and this evolutionary difference will be discussed further in the next section.

Looking then only at this subsample of stars, a cumulative frequency of carbon enhancement as a function of metallicity (Figure 6.7) can again be caluclated. Also
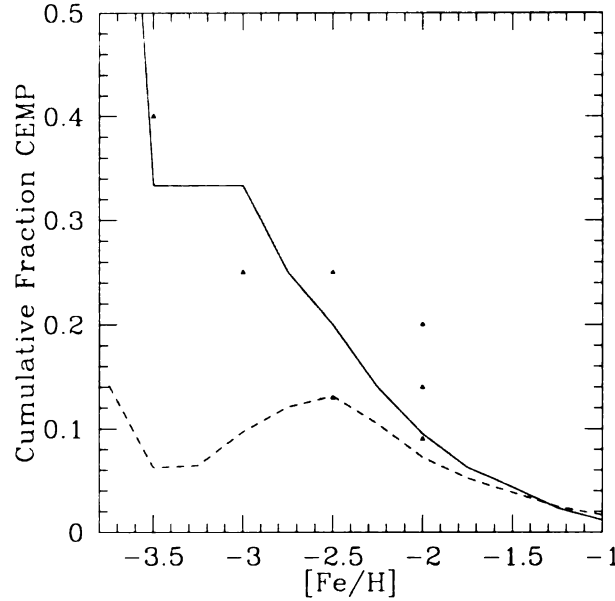
Figure 6.7 The cumulative fraction of CEMP stars as a function of metallicity for the cool subsample of stars (solid line) and the full sample (dashed line). Also plotted are various values from the literature.

plotted are the frequencies for the full sample and the values from the literature.

It can be seen that the same low, asymptotic value is recovered at high metallicities of only a few percent. As metallicity is decreased, these two curves begin to diverge, with the cool sample separating above the full sample. The cool sample continues rising below [Fe/H] = −2.5, where the full sample turns over, and ultimately plateaus at [Fe/H] = −3.0 with a frequency of over 30%. This plateau is likely not a real feature, but actually corresponds to where the frequency meets the completeness curve. In other words, at this point, every star with a detectable carbon feature is classified as carbon-enhanced.

Interestingly, this curve seems to suggest an accelerating rate at which the frequency is increasing at low metallicities, and that larger fractions are being reached quicker. If this curve continued rather than artificially plateauing, it would indicate that half of all stars with [Fe/H] ≤ −3.5 are carbon-enhanced, surpassing even the lofty estimate of Beers & Christlieb (2005).

87

Table 6.1. Recovered fractions at different metallicities from our various techniques.

[Fe/H]	Initial	Method 1	Method 2	Method 3
−1.0	0.021	0.021	—	0.012
−1.5	0.045	—	0.062	0.044
−2.0	0.085	0.084	0.108	0.095
−2.5	0.139	—	0.214	0.200
−3.0	0.098	0.168	—	0.333
−4.0	—	0.252	—	—

This rapid increase has other implications as well. While these fractions still best match the relatively low values of Frebel et al. (2006) at [Fe/H] ≤ −2.0, they rise quickly to almost recover the Marsteller et al. (2005) results at [Fe/H] ≤ −2.5, then surpass the Frebel et al. (2006) results at [Fe/H] ≤ −3.0 and likely the Beers & Christlieb (2005) results at [Fe/H] ≤ −3.5. Importantly, however, while matching the low 9% Frebel et al. (2006) result at [Fe/H] ≤ −2.0, the fraction rises to nearly the 20% Lucatello et al. (2005) result by [Fe/H] ≤ −2.5. A large increase in the fraction over only a half dex in metallicity. And this is nearly the same scale as our errors in metallicity. The point here is that the three seemingly discrepant results at [Fe/H] ≤ −2.0 may be more consistent than previously thought. Evolutionary effects may not even be needed to explain these differences; they could be fully accounted for by measurement uncertainties and the rapid increase in carbon fractions. In other words, these three results actually agree quite well.

6.3 DISCUSSION

Upon application of several different techniques to recover information from our incomplete sample, we start to get a better idea as to the shape of the frequency of CEMP stars as a function of metallicity. Unlike the initial, incomplete frequencies

which turn over at some critical metallicity, all of the recovered fractions continue to rise as metallicity is decreased, although the rate at which they rise varies slightly.

Our second and third recovery methods yield surprisingly similar results, suggesting that these values may in fact be tracing the true frequency. Although still relatively low (~10%) at [Fe/H] ≤ -2.0, these results rapidly increase to a fairly substantial fraction of CEMP stars at a slightly reduced metallicity.

Our first method, on the other hand, yields much lower fractions at all metallicities. This method is probably not tracing the true carbon frequencies, but is rather limited by faulty assumptions made during this analysis. For one thing, it looks at discrete carbon fractions, rather than cumulative fractions. A quick comparison of Figures 6.1 and 6.2 will show that discrete fractions are inherently the lower of the two, so these recovery results are not surprising. In addition, a full analysis of the distribution of points above the carbon-normal line is required to truly measure these quantities. The assumption of random scatter may not have been reasonable, leading to larger deviations at lower metallicities, where this assumption may have been most invalid.

When comparing the results from just the cool subsample of stars, in which the fewest assumptions are made in calculating a cumulative fraction, with the values from the literature (Figure 6.8), it can be seen that the literature values are all consistent with the results obtained in this analysis. In fact, these points largely appear to be scattered around our frequency curve, suggesting that these varied results may not in fact represent disagreements, and the current controversy with regards to this parameter may be largely unfounded. The local scatter of these points, while likely not truly significant, could be due to any of a number of factors.

Any errors or offsets in measurements of metallicity could shift portions of the curve up or down or even just smooth and average things together. Due to the rapid changes in frequency versus metallicity seen here, even small offsets could yield
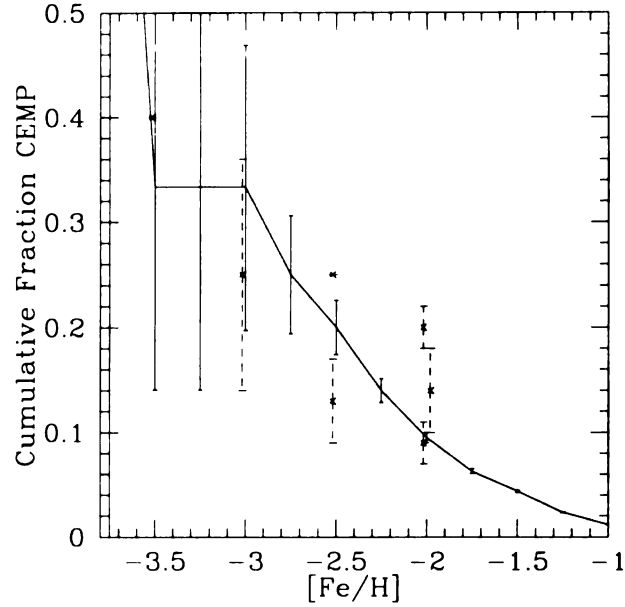
Figure 6.8 The cumulative fraction of CEMP stars as a function of metallicity for the cool subsample of stars. Also plotted are various values from the literature, offset slightly in metallicity to easily distinguish the error bars for the samples.

significant frequency differences. The fact that the literature values actually agree so well is an encouraging fact, rather than a source of contention.

As has been previously discussed, the impact of evolution may also contribute to any deviations. To analyze this impact more quantitatively, the frequency of carbon enhancement will be determined assuming a threshold for carbon enhancement at $[C/Fe] = +0.7$ rather than $[C/Fe] = +1.0$. This value is chosen in part as it has in fact been used as a threshold by some (Aoki et al., 2006) already. In addition, a shift in carbon abundances by 0.3 is around what might be expected due to dilution by convective mixing during stellar evolution.

Assuming our sample to consist entirely of giants, lowering the carbon enhancement threshold has the effect of reversing the effects of evolution and approximately determining the frequency of our sample when it was dwarfs. In practice, this sample likely consists of both giants and dwarfs, but this analysis is still useful to give a sense of the magnitude of the shift which might be expected.
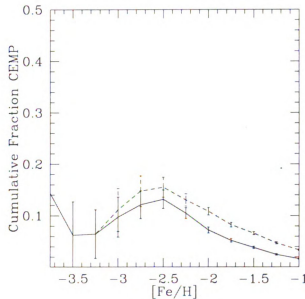
Figure 6.9 The frequency of carbon enhancement below a given metallicity for the combined PHO and RED samples (solid line) and the frequency assuming a [C/Fe] ≥ 0.7 cut-off (dashed line).

Plotted in Figure 6.9 is the frequency of carbon enhancement as a function of metallicity assuming a cut-off of [C/Fe] = 1.0 and [C/Fe] = 0.7. There is essentially a fixed offset between these two curves of around 3%, with the frequency of [C/Fe] ≥ 0.7 stars lying above the other. This offset may seem small, and in fact is likely reduced in size by the incompleteness issues, but it still represents an important factor that should be taken into consideration.

Recent work by Frebel et al. (2006) has also shown that the frequency changes as one gets further from the galactic plane, suggesting that different stellar populations yield different CEMP frequencies. In other words, the thin disk shows a different frequency than does the thick disk, or the halo. Their analysis showed that the distribution of frequencies is higher as you increase Z, the vertical height above the galactic plane. This is not an effect of lowered metallicity, but a seemingly fundamental difference between stars of these different populations.

In another work, Tumlinson (2007) see a similarly changing frequency for different

stellar populations. From a purely theoretical standpoint, and based on a characteristic mass dependent on the temperature of the CMB at a given epoch, they are able to produce a curve of the frequency of CEMP stars as a function of metallicity. This curve is surprisingly similar to our own observational curve, featuring the same quadratic shape, although displaced to higher values than seen here.

Thus, the offset in values is due to this locational effect and the general shape is due to the evolution of carbon in the galaxy. The fact that theory and observation yield the same result for this curve suggest that the true cause for these stars is beginning to be understood. Hopefully the theory continues to improve, and more complete observations are able to confirm this pattern as well. Until then, the limited evidence we have at the moment suggests a promising future in the understanding of these vital stars.

CHAPTER 7:
CONCLUSIONS AND FUTURE WORK

Due to the observed large fractions of such stars observed among samples of metal-poor stars, CEMP stars clearly occupy a key position in the nucleosynthetic history of the early galaxy. Thus, to truly understand this nucleosynthetic history, it is first necessary to understand the true contribution of these stars to that history. We must see how the fraction of these stars changes over time. It is also important to understand the origin of these stars and the mechanisms responsible for their production.

To ultimately determine the frequency of carbon enhancement as a function of metallicity, we first had to develop a new routine which was capable of quickly and accurately determining metallicities and carbon abundances for a large sample of low resolution spectra. By combining the general procedure of the line index method – using the Ca K line as a proxy for metallicity and the G band as a measurement of the carbon abundance – with the technique of determining abundances using synthetic spectra as calculated by MOOG, and automating the whole thing, we are able to quickly and objectively calculate abundances from low resolution spectroscopy without relying on the availability of calibration data. We lose the empirical nature of the line index method, but keep its speed and applicability to lower resolution data. Similarly, we lose the somewhat slow, not always objective nature of spectral synthesis, but keep its foundation in physical descriptions of stars through the use of stellar atmosphere models and atomic and molecular linelists.

7.1 The Quality of the Method

With this procedure developed, we can then start to determine metallicities and abundances for stars with available low or medium resolution spectra. Before we do this, however, we need to ensure the quality and consistency of our results.

To test our consistency, and also determine our intrinsic error, synthetic spectra with known parameters were run through autoMOOG. We were also able to use multiple observations of the same star to check our consistency. Overall, we found excellent agreement between these results or with known parameters, to generally less than a tenth of a dex.

For the quality of our results, stars which had observations taken at low resolution so they could be processed through autoMOOG but which also had metallicities and abundances determined from high resolution spectroscopy were needed. This comparison would test not only our ability to reproduce these results in general, but would also further verify the applicability of this procedure, specifically using the Ca K line as a proxy for metallicity, as metallicity at high resolution is generally measured directly from iron lines. So, we are testing not only our ability to fit the calcium line but also our assumption of an α-to-iron ratio.

As was seen, there is currently a problem in our metallicity determination for stars with [Fe/H] $\geq$ 1.5, likely due to an inability at the moment to correctly determine the placement of the continuum for these stars. However, there could also be an issue related to the assumed α-to-iron ratio, especially if these stars are associated with different populations. If this effect is indeed present, however, it is expected to be small and not the primary reason for these discrepencies.

As for the primary concern, the continuum placement, work is currently underway to resolve this problem. An analysis of flux calibrated data, which should be immune to this effect, would indicate if the poor continuum placement is indeed the cause of this deviation. If it is, the flux calibrated data would then indicate the quality of the

resultant fits in these metallicity ranges that should be expected after resolving this issue.

In order to account for this effect if it does exist, we are currently exploring the possibility of auto-rescaling the data to fit the models. As we saw in Figure 5.2, the scaled data fit the high metallicity model much better than the unscaled data fit the low metallicity model. Comparing the χ^2 values for these two models should identify the higher metallicity model as the better fit. Thus, rescaled data compared to models should uniquely identify a best fit which should be appropriate.

In the low metallicity regime, where fits of metallicity are already reasonable, this scaling should have very little impact, as the apparent continuum levels will not significantly change and any scaling factor will be small. Thus, calculating and applying this scaling can be done for all data, not just those stars above some critical metallicity, and should yield reasonable results.

At higher metallicities, where the scaling factor will be more significant, our preliminary studies have shown that this technique often does exactly as expected, choosing a best fit metallicity that is very similar to that determined from high resolution analysis. Unfortunately, for the moment, it is fairly inconsistent in its success. When it doesn't work, it very obviously does not work, selecting a supersolar metallicity, often up to several dex over solar, which is easily identifiable as incorrect.

At such high metallicities, the numerous strong lines wipe out nearly all of the stellar flux, yielding a flat and smooth spectra with a very low relative flux. Scaling almost any data to this level of flux produces a similar looking spectra, with most lines present being smoothed out. Thus, any data which is not selected to have an appropriate metallicity will be artificially selected to have these supersolar metallicities. The preliminary tests we have performed to sort out the continuum issue suffer from this problem, but a more detailed correction to autoMOOG should not similarly be hampered by this effect.

At low metallicities, where we are in fact most concerned with the quality of our results, the absense of many strong lines, or any lines in general, results in a well defined continuum with a fairly high relative flux. Thus, for these stars, we have no similar difficulties when determining metallicites, and this is seen in a comparison of our results with high resolution determinations, where a generally good agreement is seen, with a reasonable amount of scatter, consistent with our errors. The possibility of using an incorrect or inconsistent α-to-iron ratio is still present, although again would only be responsible for fairly small discrepensies, so is not an immediate concern.

Our results for carbon do not seem to suffer from the same sorts of problems, with fairly well fit continua for even large carbon abundances. As a result, our abundances well match those results obtained through high resolution analyses. However, due to a multitude of stars which had weak or undetectable carbon lines, especially those at lower metallicities or warmer temperatures, abundances were not able to be determined for all of the stars in our samples. Instead, upper limits, calculated in advance using synthetic spectra, were determined for these stars.

We are currently exploring a new technique for the determination of upper limits, based on the changing shape of χ^2 space, as opposed to being defined based on a pre-defined curve calculated from synthetic spectra. This has the distinct advantage of allowing autoMOOG to be significantly more flexible when fitting different lines, without the need to determine this threshold for every line in advance. In addition, switching to this method may solve our rescaling problem when calculating metallicities, as it should identify a saturating feature as well as an absent one. Looking at this shape of χ^2 space should also yield more appropriate, and data specific, estimates of the error on an abundance, as opposed to the more global errors we are using at the moment. So, this technique will contain several improvements over the existing architecture. At the moent, however, this is only in the early development stages.

7.2 Application of the Method

Using the current version of autoMOOG, we determined metallicities and carbon abundances for a large, unbiased sample of stars observed as part of the SDSS calibration efforts. With these abundances, we attempted to calculate the frequency of carbon enhancement as a function of metallicity. As seen in previous studies, we note that the frequency increases at the lowest metallicities, and our values agree fairly well with those determined previously.

At the lowest metallicities, our fractions suffer fairly heavily from our known incompleteness, leading to the calculation of hard lower limits on the true fractions. At its peak, our fractions reach ~14% of stars which are carbon-enhanced with [Fe/H] ≤ -2.5. As the fraction of such stars at the lowest metallicities is the value most sought, our fractions, due to our incompleteness, are not able to significantly add to the discussion. Thus, to contribute to the topic, we perform a few simple calculations to try and recover a value closer to the true fraction contained within our sample.

Making a few general assumptions about the behavior of the stars in our sample, we statistically recover lost CEMP stars through various methods. Our first approach, just using the appearance of available parameter space, relied too heavily on untested assumptions which may not have been valid. Even so, we saw an increasing fraction of CEMP stars down to the lowest metallicities. Although the fractions themselves were not as large as we were expecting, they still indicated that a significant fraction (more than a quarter) of stars at the lowest metallicities show enhancements in their carbon abundances relative to iron.

Our second and third attempts – using the shape of the tail of the CDF and a nearly complete subsample of stars – yielded very similar results, which were larger than our first attempt, and in good agreement with the values collected from the literature. This suggests that we are measuring a similar physical property as these other, more complete, studies. However, these previous analyses generally only obtain

a single point along this curve, and were thus unable to say much about the global behavior of this quantity. With this recovered information, we can say much more along these lines.

From these results we see that not only does the fraction of CEMP stars increase at lower metallicities, it seems to be accelerating. In fact, we find that maybe half of stars with [Fe/H] ≤ -3.5 seem to be carbon-enhanced. It would not be unreasonable to suppose that a majority of the earliest generations of stars were carbon-enhanced.

7.3 THE MEANING OF THE RESULTS

With this fraction, and its behavior relative to metallicity, we now need to consider the meaning behind these results. The nonlinear behavior of the curve could just point to the nonlinear age-metallicity relation. Since each small bin at the low end of metallicity represents a small fraction of the amount of time passing during a small bin at high metallicity, the general quadratic nature of our curve could be simply an issue of elapsed time. It is possible that we would see a more linear curve if we plotted the carbon fraction versus time as opposed to metallicity, but that is not a parameter we currently have available. However, this might make for an interesting future study.

In terms of the increasing nature of the carbon fraction itself, this could just lie in the simple CEMP definition of [C/Fe] $\geq +1.0$. Processes available in the most chemically primitive environments seem to be generally more efficient at producing carbon than they were at producing iron. Thus, this increasing fraction seems to be a very natural consequence of metallicity-dependent nucleosynthesis. If this is true, the increasing fraction has more to do with our current definition of carbon enhancement than it does with any physical circumstance in the early universe.

However, looking at plots of carbon (either [C/Fe] or [C/H]) versus metallicity, there is a clear grouping of stars along a line of carbon-normalcy (namely [C/Fe]

= 0). For these stars, which represent a majority for all well-sampled metallicities, carbon and iron are produced at the same relative rate, corresponding to the relative abundances seen in the Sun. Thus, for these stars at least, where carbon and iron production seem to be correlated, it is not just a matter of how carbon enhancement is defined.

As we saw with our first recovery attempt, there exists an upper limit on [C/H] for all metallicities. While this value does seem to depend on some property, likely an evolutionary one, for a given sample it seems to be fairly well defined. For our sample, this limit is at [C/H] = −0.5. We also noted that there was likely some correlation between the increasing fraction of CEMP stars at lower metallicities and the increasing parameter space between this upper limit and the line of carbon normalcy. The question is then why this parameter space exists, or more generally, why there exists this fixed upper limit, as opposed to an upper limit that changes with metallicity.

Overall, this suggests that there are two primary mechanisms which produce carbon in stars. The first we have already seen produces iron and carbon in the same relative proportions and is responsible for the carbon-normal stars. The second is capable of producing a wider range of carbon abundances, up to the level of our upper limit. Over time, these stars then accumulate iron from additional sources, maintaining the same [C/H] while reducing their [C/Fe]. These mechanisms, whatever they are, seem to be largely metallicity independent, with the changing iron abundances due to nothing more than the passage of time.

To identify what these mechanisms are we must look at these stars in greater detail. The changing overall fraction of CEMP stars gives us our first insights into the nature of these stars and their origin. The quadratic shape of this curve, and its increasing at lower metallicities, are fairly well understood properties. However, the level of this fraction also contains information we need to discover and understand.

For one thing, this level changes depending on certain properties of the stars.

Dwarf stars will sit at a slightly higher level than giant stars, and this is understood to be due to dilution of atmospheric abundances during mixing episodes of stellar evolution. In part, this is then due to the simplistic definition of carbon enhancement at a fixed value of [C/Fe] for all stars. In reality, this definition should take into account the evolutionary state of the observed star, so that a more robust frequency can be calculated, regardless of the sample used.

For the moment, however, this definition is an empirical determination, and not even fully agreed upon within the community as to its exact value. It is also unclear exactly how much dilution of carbon can occur in the atmosphere of a giant star, and how much star-to-star variation might exist. Until these uncertainties are given more consideration, a new definition of carbon enhancement may be premature. In addition, although carbon, at a given abundance, may be much easier to observe in giant stars, any study of this frequency should be conducted using samples consisting entirely of dwarf stars, if possible, to avoid this uncertain effect of dilution. While a sample of giants will give a rough idea as to the nature of this curve, as seen for example in this analysis, these uncertainties when dealing with giants will result in much larger uncertainties when determining the carbon fraction.

There also appears to be a variation in the level of the frequency depending on the stellar population of a sample. In the Milky Way, the halo would then exhibit a different frequency than the thin disk, although both should still show the same general increasing, quadratic shape. This can best be seen by looking at the changing carbon fractions amongst samples of differing heights above or below the plane of the disk (Frebel et al., 2006). From our sample, rough photometric distances were calculated to see if we could identify this behavior as well. Unfortunately, it was discovered that these stars all fell relatively close to the galactic plane, and were likely members of the thick disk. A recent kinematic study of these stars (Carollo et al, in preparation) may help identify the various populations contained within this

sample and allow for a fuller treatment of this possible effect in future analyses.

This behavior has also been noticed in the theoretical work of Tumlinson (2007), whose calculations of the shape of the frequency curve are based on an IMF which is influenced by the local CMB. The general idea is that the CMB sets a minimum temperature in a star-forming gas, which determines the characteristic fragmentation scale of the gas, which then sets the IMF of the forming stars.

From this, they find a CEMP fraction which rises quickly below $[Fe/H] = -1.0$, similar to what is seen here. However, their curve plateaus just below $[Fe/H] = -2.0$, at a modest $\sim 30\%$ of stars being carbon-enhanced. While our data also seemed to plateau around 30% in our third recovery attempt, this was believed to be due to the limitations of our incompleteness rather than a physical property of our sample. For now, we can only say that our results are consistent with these theoretical results, although the existence of this plateau remains an open question.

Another interesting observation in these results is the variation in the carbon fraction with location in the galaxy, which they attribute to the age of the stars in a region, with the oldest stars being concentrated in the most central regions. These older central regions then formed with a higher CMB temperature, and thus a higher characteristic mass. This higher characteristic mass then reduces the likelihood of forming a binary system with an intermediate and low mass star, which is likely required for the formation of CEMP stars. Thus, the fraction of CEMP stars closer to the plane will be lower than further out, where the characteristic mass is smaller.

At the same time, older populations of stars probably formed under a more top-heavy IMF than did younger populations. This means that there would in general be fewer of the less massive stars required to be in binary systems to form CEMP stars in older populations. This would also suggest a smaller CEMP fraction to exist in older populations.

These factors seem to explain the positional variation of the CEMP fraction within

a galaxy, but they raise some concerns about the overall shape of our fraction. As an older population evolves, the more massive stars, which dominate these populations, evolve themselves onto the giant branch, or even beyond. Eventually, you would form CEMP stars through the mass transfer from intermediate mass to low mass stars. At this point, the majority of stars in the population would no longer be detectable, having moved past the giant branches. Of the remaining observable stars, CEMP stars would be dominant, even though they only actually represent the tail of the IMF. Thus, you would see a fairly large CEMP fraction from such a sample, and this may in fact help explain the increasing fraction of such stars at low metallicity.

However, for an older population, these low mass stars may reach first ascent, and dilute their surface abudances, reducing the derived carbon fraction. From this standpoint alone, an older population should show a lower fraction than a younger one. Such a population would still need to be fairly old, such that subsolar mass stars have evolved to the giant branch, so in practice this effect may not be seen.

This all yields a natural situation where the fraction of carbon stars increases at low metallicities, and the fraction at a given metallicity will tend to be higher the further from the center of a stellar halo you look, as is indeed seen in recent observations. Unfortunately, this work only looks at the formation of stars in subhalos, without the added complication of stellar disks. Given such a subhalo, and the distribution of stars within it, all of these arguments would hold true, and this problem would seem to be essentially solved.

In reality, the Milky Way has at least two disks, and while they do lie towards the center of the galactic halo, and do seem to show lower carbon fractions at a given metallicity than is seen further out, they are comprised of materials that are in fact younger than those which make up the halo. And while there are likely old halo stars in these regions, they are overwhelmingly dominated by thin and thick disk stars, so it can not even be claimed that these observations are catching the older stellar

populations of the halo in these regions, which might actually exhibit these observed characteristics.

This analysis also assumed the formation of the majority of CEMP stars through binary mass transfer scenarios, a completely reasonable assumption considering that ~80% of CEMP stars are CEMP-s stars, which are reasonably well understood to have formed as the less massive star in a binary system. The measurement of the CEMP fraction is then seemingly a measurement of the binary fraction, which is directly related to the IMF.

Globally, 80% of CEMP stars are CEMP-s stars and this argument seems valid. However, at low metallicities, the efficiency, or availability, of the s-process is severely diminshed and s-process enhancements are not seen below [Fe/H] = -3.0. This indicates that there is likely to be a changing relative fraction of the assorted subclasses of CEMP stars with changing metallicity, so assuming a fixed global fraction of CEMP-s stars is probably not reasonable.

Thus, looking at the changing relative fractions of the individual subclasses of CEMP stars is just as vital as the global CEMP fraction. To study this further, we can select all the stars from our sample of SDSS calibration stars which have been identified as carbon-enhanced, and attempt to measure lines of barium or strontium in their spectra to classify them as CEMP-s stars. This sample will clearly be hampered by our incompleteness and thus will not give a true measure of these changing fractions, but even a general analysis may easily yield interesting information about this topic.

7.4 ONGOING WORK: HESCAR

We are also in the process of analyzing a sample of stars selected from the Hamburg/ESO survey based on their carbon-enhancements, the HESCAR stars (Christlieb et al., 2001). Based on the strengths of the C_2 and CN bands, calculated through the

use of line indices, these stars were automatically selected from the large database of HES spectra. These stars were easily identifiable even at HES resolutions ($\sim$15Å) due to the high signal-to-noise of the data and the intrinsic strength of these features.

These stars were initially selected to be used as tracers of the potential of the Milky Way halo, due to their intrinsically high luminosities. However, these stars have other uses as well. Since it has been realized that large fractions of the most metal-poor stars are also carbon-enhanced, it follows that a sample of stars selected based on strong carbon-enhancements is likely to contain a number of metal-poor stars. In fact, stars of all metallicities will be observed as part of a survey targeting carbon-rich stars. Due to the small number of VMP stars currently known, their sample size would increase significantly as a result of such a survey.

This sample is currently being used as a test case to see if this is indeed true. Follow-up photometry (Beers et al., 2007a) and medium-resolution spectroscopy (e.g. Beers et al., 2007b, and see Figure 7.1) has been obtained for nearly all of the 403 stars in this sample. High-resolution spectroscopy has been obtained for many of these stars as well. Temperatures, gravities, metallicities, and carbon abundances are being determined based on this data, partially through the use of autoMOOG. Near-infrared observations have also been obtained for a number of these stars (Beers et al., 2007b) to determine $^{12}C/^{13}C$ ratios, in an attempt to understand their changing abundances with evolution.

As we have primarily studied warmer ($T_{eff} > 5000$ K) stars in this analysis, this sample of cooler ($T_{eff} \sim 4000$ K) stars, which have significantly stronger carbon features and thus less obvious continuum levels, have proven somewhat problematic to fit. This is similar to our difficulties with high metallicity stars, seen in §5.2. Once these issues have been resolved, we will be able to identify the most interesting stars within this sample, and potentially verify the use of such a sample in identifying larger numbers of VMP stars.
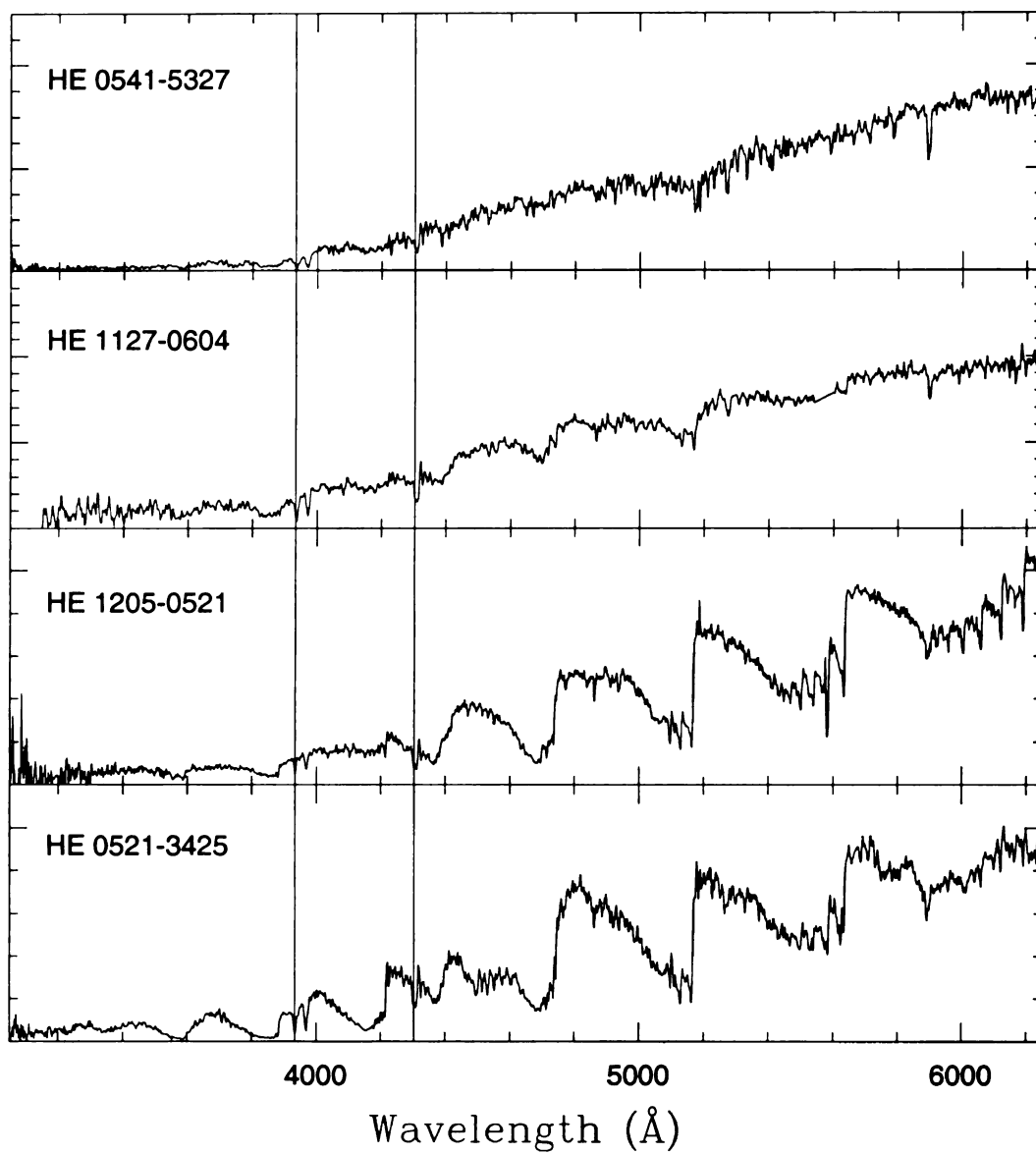
Figure 7.1 Example medium-resolution spectra taken of HESCAR stars, showing stars with larger carbon features towards the bottom.

In addition, while these stars were selected based on the strength of their carbon features, and thus cannot be used for any analysis of the global fraction of CEMP stars, they potentially make an excellent sample for studying the changing fractions of CEMP subclasses as a function of metallicity. At the very least, the identification and measurement of lines of barium or strontium can help to classify stars as possible CEMP-s stars, which can potentially indicate the changing binary fraction at various metallicities.

As they don't span the full range of available carbon-enhancement parameter space, this sample may be biased towards subclasses which contain larger enhancements of carbon. If this is true, we may not be able to get a true measure of the changing relative fractions of such stars, but that would still indicate which mechanisms are the most effecient carbon producers, which is itself interesting.

Clearly, future large samples of stars selected based on their carbon-enhancements will greatly assist in the discovery of the most metal-poor stars and assist in the understanding of the changing nature of CEMP stars with changing metallicity. Such surveys are currently underway, with the observations being conducted as part of the Sloan Extension for Galactic Understanding and Exploration (SEGUE) or the future work of the LAMOST survey.

Now that we have a much better understanding of the global fraction of carbon enhancement with respect to several parameters, it is this subclass fraction which requires our focus. Only with this understanding will we truly be able to determine the origin of CEMP stars, and the importance of the mechanisms which produce them over the history of the galaxy.

APPENDICES

APPENDIX A: autoMOOG FITS

Here we display some examples of the sorts of fits possible through the use of auto-MOOG. In Figures A.1, A.2, A.3, and A.4, examples of cooler stars from the SDSS calibration sample are seen, whereas Figures A.5, A.6, A.6, and A.6 show primarily warmer stars.

In both figures, stars of various metallicity are chosen, with slightly higher metallicity stars being shown near the top of the figure, and lower metallicity stars at the bottom. For each set of metallicity ranges, a carbon-normal and carbon-enhanced star is selected to illustrate the strength of the G band. Note that for several of the G band fits, an upper limit is indicated instead, as a true fit is impossible. This is more true for the warmer stars than the cooler stars, as seen in our earlier analysis.
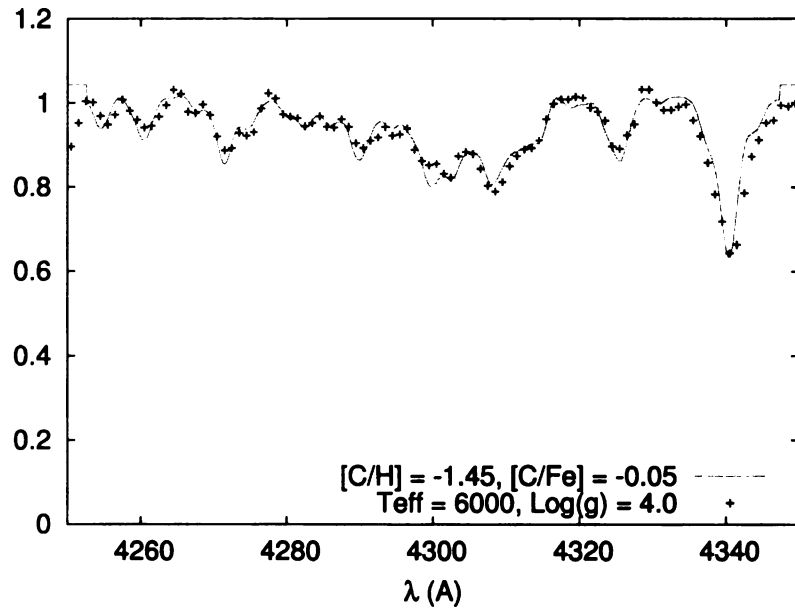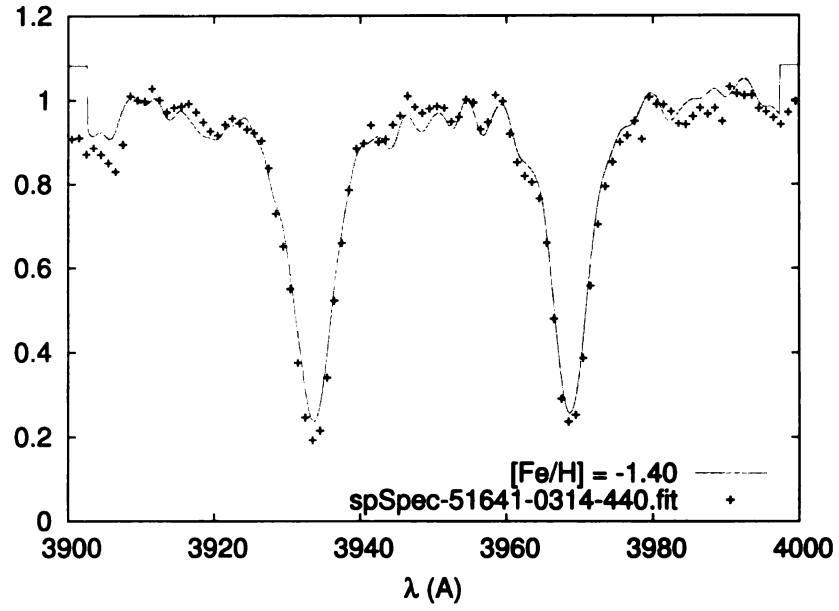
Figure A.1 Example autoMOOG fits of spectra for a cool, metal-rich, carbon-normal star in our sample of the Ca K region (top) and the G band (bottom).
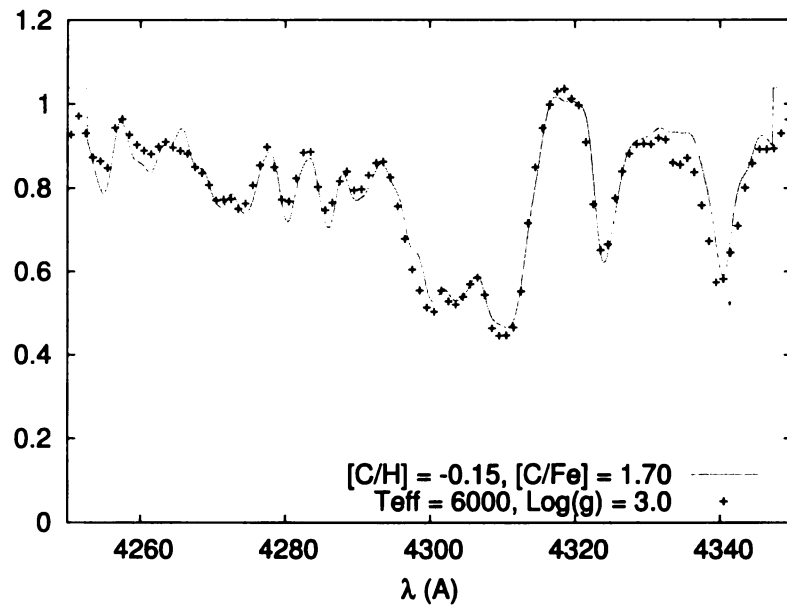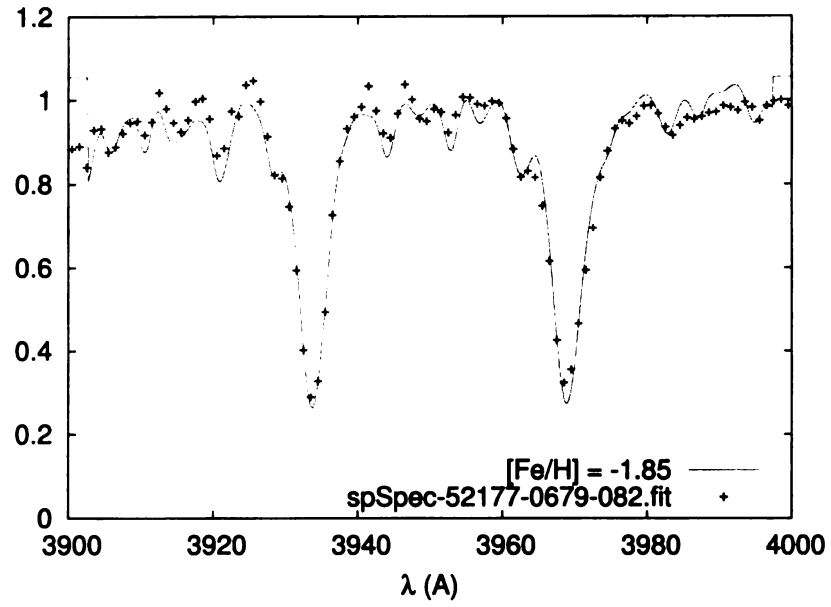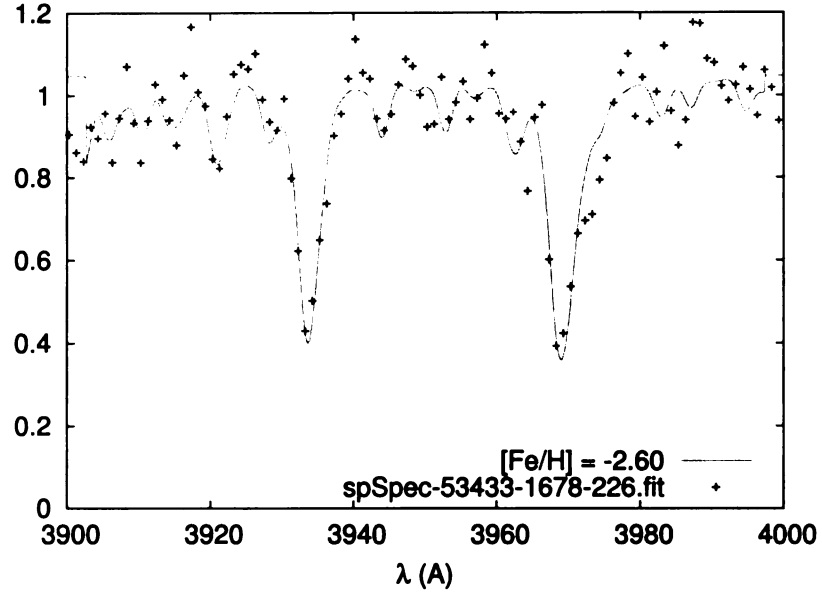
Figure A.2 Example autoMOOG fits of spectra for a cool, metal-rich, carbon-enhanced star in our sample of the Ca K region (top) and the G band (bottom).
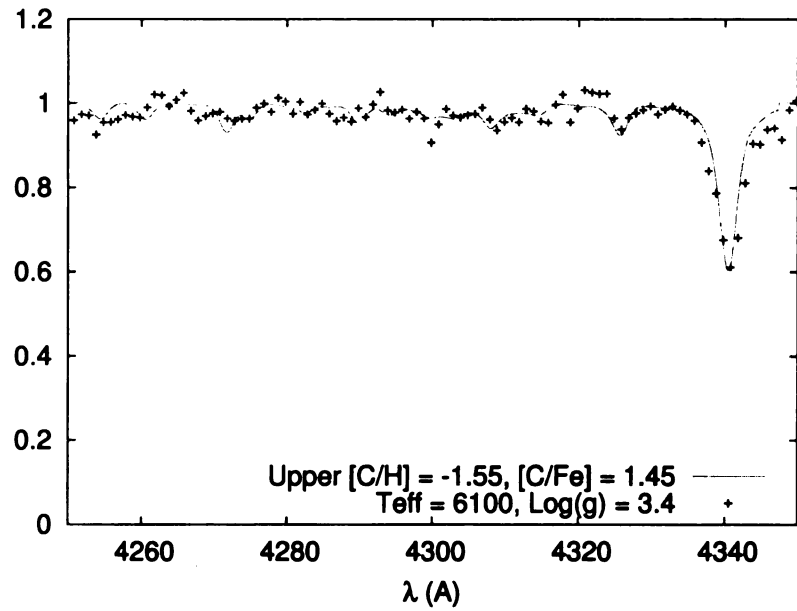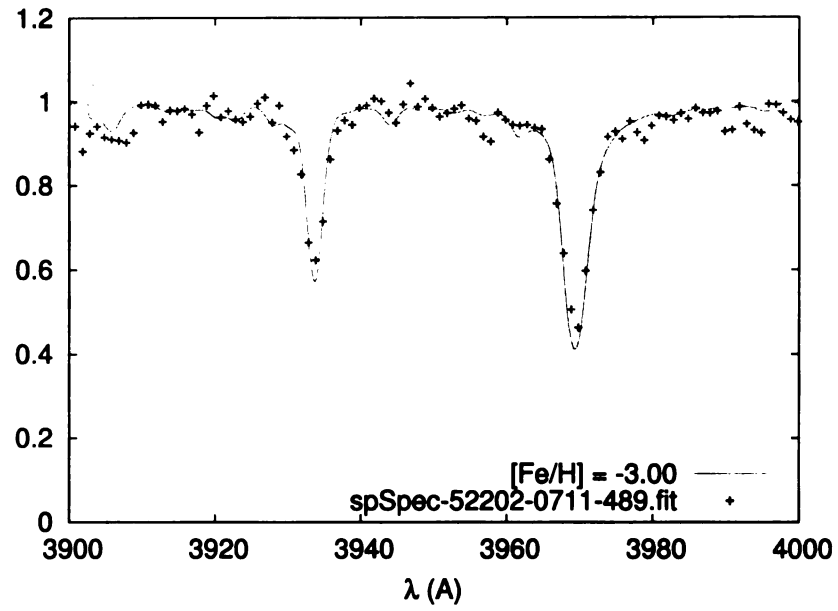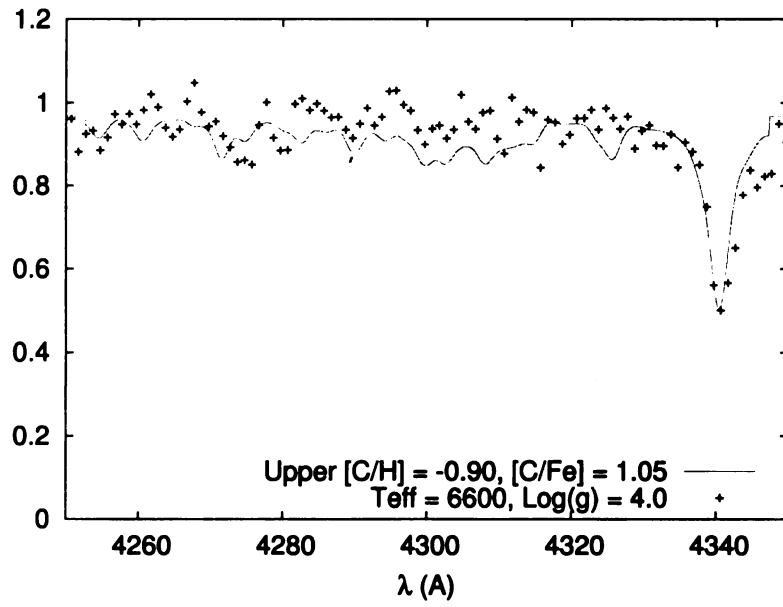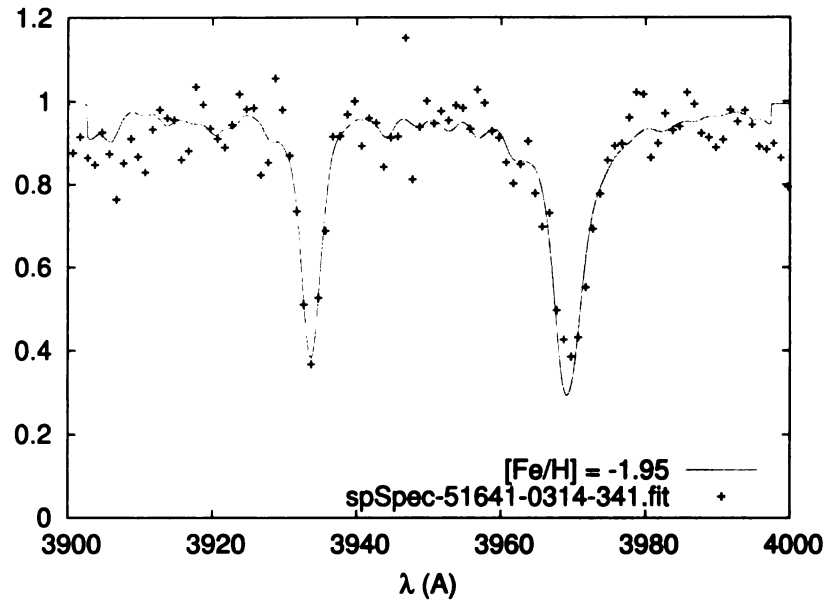
Figure A.3 Example autoMOOG fits of spectra for a cool, metal-poor, carbon-normal star in our sample of the Ca K region (top) and the G band (bottom).
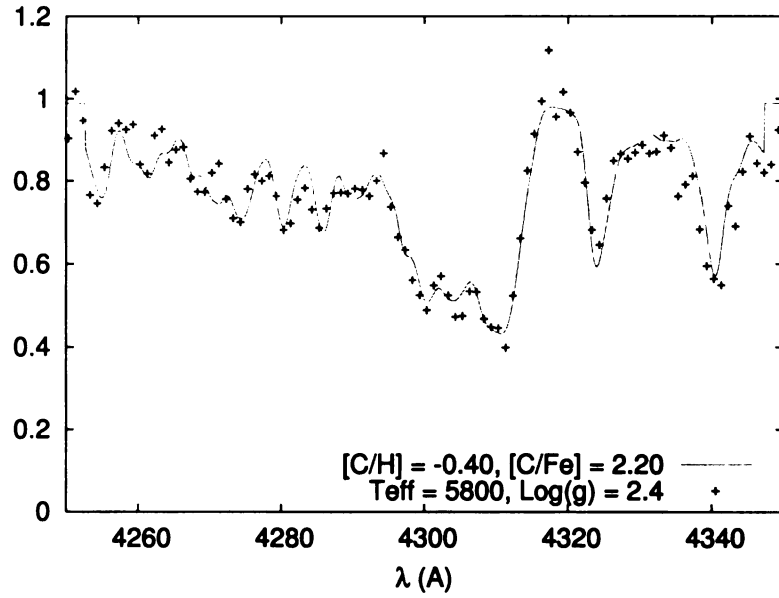
Figure A.4 Example autoMOOG fits of spectra for a cool, metal-poor, carbon-enhanced star in our sample of the Ca K region (top) and the G band (bottom).
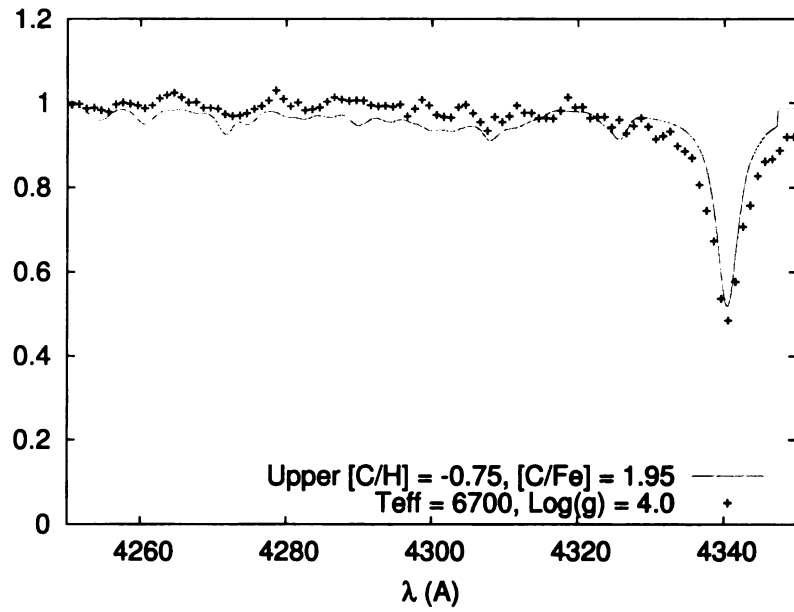
Figure A.5 Same as Figure A.1 but for a warmer star in our sample.
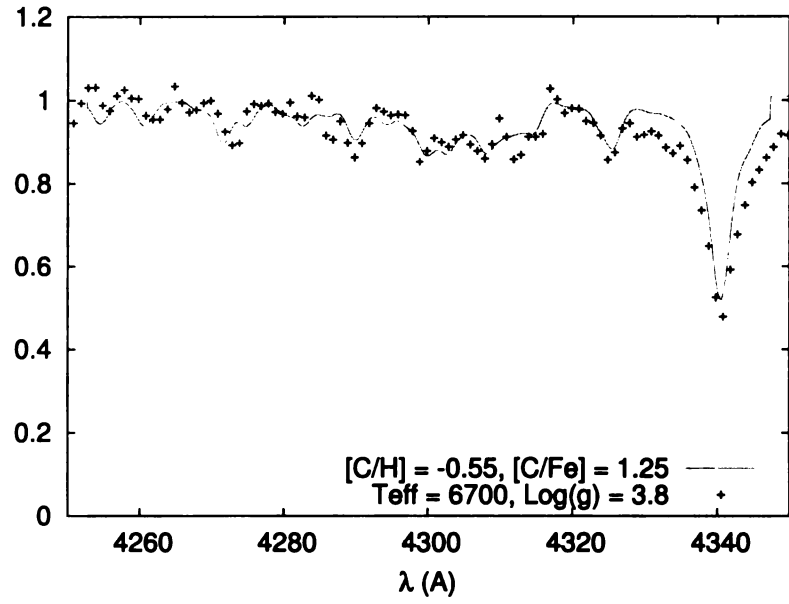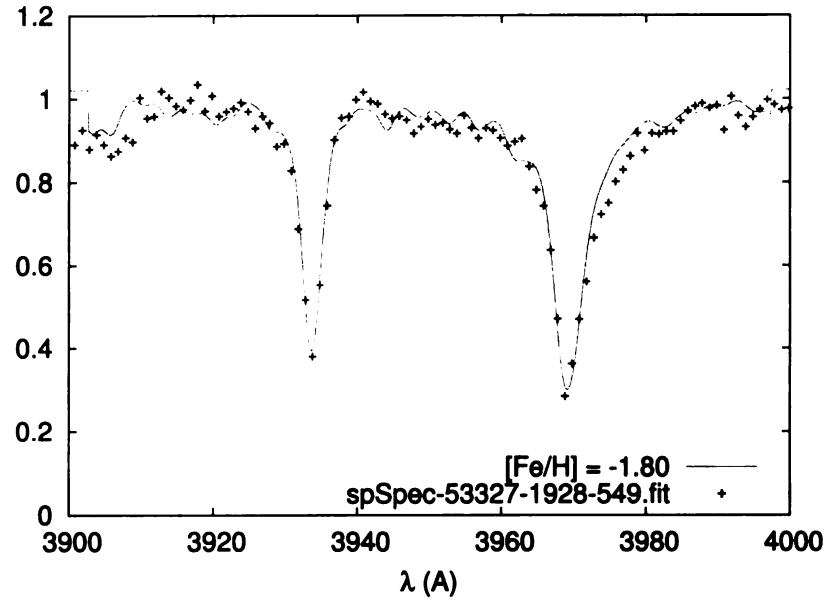
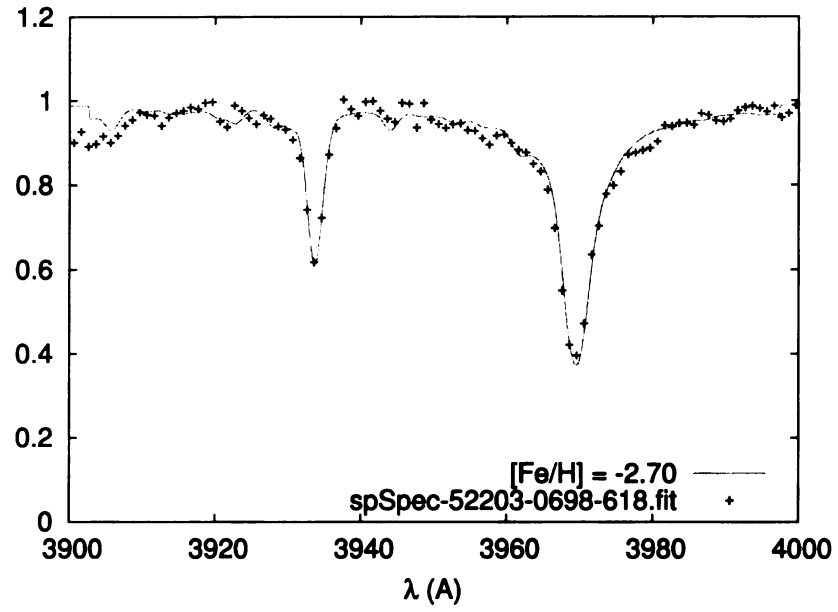Figure A.6 Same as Figure A.2 but for a warmer star in our sample.

Figure A.7 Same as Figure A.3 but for a warmer star in our sample.
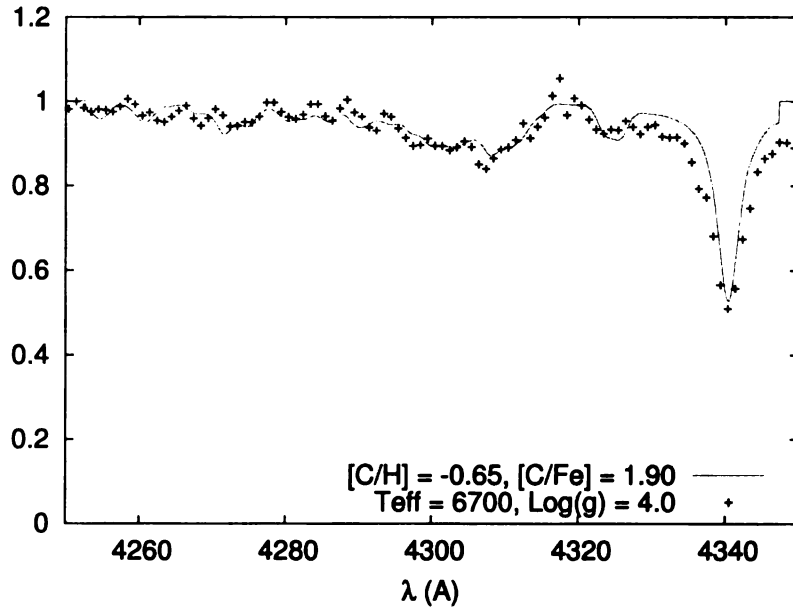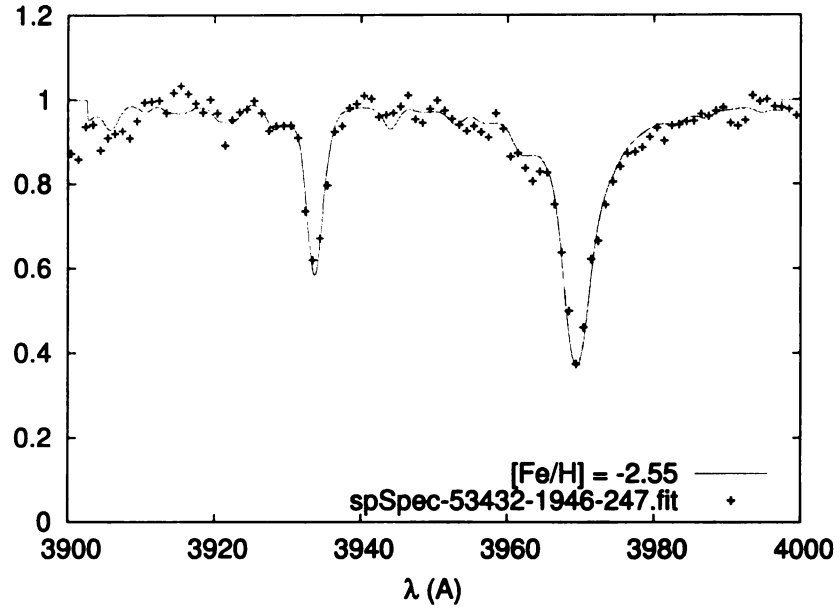
Figure A.8 Same as Figure A.4 but for a warmer star in our sample.

116

BIBLIOGRAPHY

REFERENCES

J. Adelman-McCarthy et al. 2007, ApJ Supplements, in press

Aoki, W., Beers, T. C., Christlieb, N., Norris, J. E., Ryan, S. G., & Tsangarides, S. 2007, ApJ, 655, 492

Aoki, W., et al. 2006, ApJsubmitted

Aoki, W., et al. 2006, ApJ, 639, 897

Aoki, W., Ryan, S. G., Norris, J. E., Beers, T. C., Ando, H., & Tsangarides, S. 2002, ApJ, 580, 1149

Argast, D., Samland, M., Thielemann, F.-K., & Qian, Y.-Z. 2004, A&A, 416, 997

Baikov, I. V., & Chechetkin, V. M. 2004, Astronomy Reports, 48, 229

Barbuy, B., Spite, M., Spite, F., Hill, V., Cayrel, R., Plez, B., & Petitjean, P. 2005, A&A, 429, 1031

Barklem, P. S., et al. 2005, A&A, 439, 129

Beers, T. C., Sivarani, T., Marsteller, B., Lee, Y., Rossi, S., & Plez, B. 2007, AJ, 133, 1193

Beers, T. C., et al. 2007, ApJS, 168, 128

Beers, T. C., & Christlieb, N. 2005, ARA&A, 43, 531

Beers, T. C., Preston, G. W., & Shectman, S. A. 1992, AJ, 103, 1987

Beers, T. C., Preston, G. W., & Shectman, S. A. 1985, AJ, 90, 2089

Beers, T. C., Rossi, S., Norris, J. E., Ryan, S. G., & Shefler, T. 1999, AJ, 117, 981

Bidelman, W. P., & MacConnell, D. J. 1973, AJ, 78, 687

Bidelman, W. P., & Keenan, P. C. 1951, ApJ, 114, 473

Blake, J. B., Woosley, S. E., Weaver, T. A., & Schramm, D. N. 1981, ApJ, 248, 315

Bonifacio, P., Molaro, P., Beers, T. C., & Vladilo, G. 1998, A&A, 332, 672

Bromm, V. 2005, From Lithium to Uranium: Elemental Tracers of Early Cosmic Evolution, 228, 121

Burbidge, E. M., Burbidge, G. R., Fowler, W. A., & Hoyle, F. 1957, Reviews of Modern Physics, 29, 547

Cameron, A. G. W. 2001, ApJ, 562, 456

Carroll, B. W., & Ostlie, D. A. 2006, An introduction to modern astrophysics / B. W. Carroll and D. A. Ostlie. 2nd edition. San Francisco: Pearson, Addison-Wesley, ISBN 0-8053-0402-9. 2007, XVI+1278+A32+I31 pp.

Castelli, F., & Kurucz, R. L. 2003, IAU Symposium, 210, 20P

Cayrel de Strobel, G., Soubiran, C., & Ralite, N. 2001, A&A, 373, 159

Christlieb, N., Green, P. J., Wisotzki, L., & Reimers, D. 2001, A&A, 375, 366

Christlieb, N., et al. 2004, A&A, 428, 1027

Christlieb, N., Gustafsson, B., Korn, A. J., Barklem, P. S., Beers, T. C., Bessell, M. S., Karlsson, T., & Mizuno-Wiedner, M. 2004, ApJ, 603, 708

Cohen, J. G., et al. 2006, AJ, 132, 137

Cohen, J. G., et al. 2005, ApJ, 633, L109

Cohen, J. G., Christlieb, N., Qian, Y.-Z., & Wasserburg, G. J. 2003, ApJ, 588, 1082

Collet, R., Asplund, M., & Trampedach, R. 2006, ApJ, 644, L121

Cowan, J. J., & Thielemann, F.-K. 2004, Physics Today, 57, 47

Cui, W., & Zhang, B. 2006, MNRAS, 368, 305

Frebel, A., Johnson, J. L., & Bromm, V. 2007, ArXiv Astrophysics e-prints, arXiv:astro-ph/0701395

Frebel, A., et al. 2005, ApJ, 652, 1585

Fujimoto, M. Y., Ikeda, Y., & Iben, I. J. 2000, ApJ, 529, L25

Fujimoto, M. Y., Iben, I. J., & Hollowell, D. 1990, ApJ, 349, 580

Gallino, R., Wasserburg, G. J., Busso, M., & Straniero, O. 2005, From Lithium to Uranium: Elemental Tracers of Early Cosmic Evolution, 228, 461

Goriely, S., Demetriou, P., Janka, H.-T., Pearson, J. M., & Samyn, M. 2005, Nuclear Physics A, 758, 587

Goswami, A., Aoki, W., Beers, T. C., Christlieb, N., Norris, J. E., Ryan, S. G., & Tsangarides, S. 2006, MNRAS, 372, 343

Gratton, R. G., & Sneden, C. 1994, A&A, 287, 927

Herwig, F. 2005, ARA&A, 43, 435

Hill, V., et al. 2000, A&A, 353, 557

Iben, I. J. 1967, ARA&A, 5, 571

Ivans, I. I., Sneden, C., Gallino, R., Cowan, J. J., & Preston, G. W. 2005, ApJ, 627, L145

Jonsell, K., Barklem, P. S., Gustafsson, B., Christlieb, N., Hill, V., Beers, T. C., & Holmberg, J. 2006, A&A, 451, 651

Komiya, Y., Suda, T., Minaguchi, H., Shigeyama, T., Aoki, W., & Fujimoto, M. Y. 2007, ApJ, 658, 367

Kratz, K.-L., Pfeiffer, B., Cowan, J. J., & Sneden, C. 2004, New Astronomy Review, 48, 105

Lattimer, J. M., Mackie, F., Ravenhall, D. G., & Schramm, D. N. 1977, ApJ, 213, 225

LeBlanc, J. M., & Wilson, J. R. 1970, ApJ, 161, 541

Lau, H. B., Stancliffe, R. J., & Tout, C. A. 2007, ArXiv Astrophysics e-prints, arXiv:astro-ph/0703685

Lee, Y. S., et al. 2006, American Astronomical Society Meeting Abstracts, 209, #168.15

Lucatello, S., Tsangarides, S., Beers, T. C., Carretta, E., Gratton, R. G., & Ryan, S. G. 2005, ApJ, 625, 825

Lucatello, S., Beers, T. C., Christlieb, N., Barklem, P. S., Rossi, S., Marsteller, B., Sivarani, T., Lee, Y. S., submitted to ApJ Letters

Marsteller, B., Beers, T. C., Rossi, S., Christlieb, N., Bessell, M., & Rhee, J. 2005, Nuclear Physics A, 758, 312

Masseron, T., et al. 2006, A&A, 455, 1059

McSaveney, J. A., Wood, P. R., Scholz, M., Lattanzio, J. C., & Hinkle, K. H. 2007, MNRAS, 378, 1089

Nomoto, K., Tominaga, N., Umeda, H., Kobayashi, C., & Maeda, K. 2006, Nuclear Physics A, 777, 424

Norris, J. E., Ryan, S. G., Beers, T. C., Aoki, W., & Ando, H. 2002, ApJ, 569, L107

Norris, J. E., Ryan, S. G., & Beers, T. C. 1997, ApJ, 489, L169

Norris, J. E., Ryan, S. G., & Beers, T. C. 1997, ApJ, 488, 350

Qian, Y.-Z., & Wasserburg, G. J. 2003, ApJ, 588, 1099

Qian, Y.-Z. 2000, ApJ, 534, L67

Rossi, S., Beers, T. C., Sneden, C., Sevastyanenko, T., Rhee, J., & Marsteller, B. 2005, AJ, 130, 2804

Rosswog, S., Liebendörfer, M., Thielemann, F.-K., Davies, M. B., Benz, W., & Piran, T. 1999, A&A, 341, 499

Ryan, S. G., Aoki, W., Norris, J. E., & Beers, T. C. 2005, ApJ, 635, 349

Ryan, S. G. 2003, Astronomical Society of the Pacific Conference Series, 304, 128

Ryan, S. G., Norris, J. E., & Beers, T. C. 1996, ApJ, 471, 254

Saigo, K., Matsumoto, T., & Umemura, M. 2004, ApJ, 615, L65

Scalo, J. M., Despain, K. H., & Ulrich, R. K. 1975, ApJ, 196, 805

Seeger, P. A., Fowler, W. A., & Clayton, D. D. 1965, ApJS, 11, 121

Sharpee, B., Zhang, Y., Williams, R., Pellegrini, E., Cavagnolo, K., Baldwin, J. A., Phillips, M., & Liu, X.-W. 2007, ApJ, 659, 1265

Sneden, C., et al. 2003, ApJ, 591, 936

Sneden, C., Preston, G. W., McWilliam, A., & Searle, L. 1994, ApJ, 431, L27

Sneden, C., & Pilachowski, C. A. 1985, ApJ, 288, L55

Sneden, C. A. 1973, Ph.D. Thesis,

Spite, M., et al. 2006, A&A, 455, 291

Stancliffe, R. J., Glebbeek, E., Izzard, R. G., & Pols, O. R. 2007, A&A, 464, L57

Stoughton, C., et al. 2002, AJ, 123, 485

Takahashi, K., Witti, J., & Janka, H.-T. 1994, A&A, 286, 857

Thielemann, F.-K., Arnould, M., & Hillebrandt, W. 1979, A&A, 74, 175

Truran, J. W., Cowan, J. J., Pilachowski, C. A., & Sneden, C. 2002, PASP, 114, 1293

Truran, J. W., Cowan, J. J., & Cameron, A. G. W. 1978, ApJ, 222, L63

Tumlinson, J. 2007, ArXiv e-prints, 706, arXiv:0706.2903

Umeda, H., & Nomoto, K. 2005, ApJ, 619, 427

Umeda, H., & Nomoto, K. 2002, ApJ, 565, 385

Van Eck, S., Goriely, S., Jorissen, A., & Plez, B. 2003, A&A, 404, 291

Van Eck, S., Goriely, S., Jorissen, A., & Plez, B. 2001, Nature, 412, 793

Westin, J., Sneden, C., Gustafsson, B., & Cowan, J. J. 2000, ApJ, 530, 783

Woosley, S. E., Wilson, J. R., Mathews, G. J., Hoffman, R. D., & Meyer, B. S. 1994, ApJ, 433, 229

Zhang, B., Ma, K., & Zhou, G. 2006, ApJ, 642, 1075

Zijlstra, A. A. 2004, MNRAS, 348, L23